Journal: ACP
Title: Chemical characterization and source apportionment of submicron aerosols measured in Senegal during the 2015 SHADOW campaign
Author(s): Laura-Hélèna Rivellini et al.
MS No.: acp-2016-1127

The authors want to thank Reviewer #1 for his/her helpful comments. They are addressed below in blue. Changes in the manuscript are written in red.

Anonymous Referee #1

Manuscript is a well-written and organized and it offers important information about the aerosols and their sources in West-Africa, Senegal. I recommend it for publishing in ACP after addressing some comments below.

1. Aerosol acidity approach (Chapter 3.1.3, equation 11?) is valid if the influence of metal ions, as well as organic acids and bases on NH4+ concentration is negligible (Zhang et al., 2007). When the sulfate to NH4+ ratio is high, the amount of atmospheric ammonium is not sufficient to neutralize all SO4, NO3 and Cl anions. In such a case at least a fraction of NO3 and Cl anions must be associated with cations other than NH4+ and Eq. (11) is no longer valid. This should be discussed and clarified in the revised manuscript.

Author's response: 23% of the data are associated to a $NH_{4,meas}/NH_{4,predict}$ ratio inferior to 0.75 and correspond to points under the 1:1 line in Figure S3a. For such points, the amount of NH_4 predicted is overestimated in comparison to the amount measured on site, and considering that NH_4 will preferentially react with SO_4, we agree with Reviewer #1 that other anions like NO_3 and Chl are partially under chemical states other than ammonium nitrate and chloride.
Chloride species have been observed in this study as emitted by local combustion processes (m/z 36, HCl^+). Besides, HNO_3 adsorption on dust as already been reported in the literature (Fairlie et al., 2010; Savoie et al., 1989) and this is consistent with ratio values inferior to 0.75 which are mainly observed while the site is under dust influence (Figure S3b).
If only SO_4 is taken into account in the ion balance as described in Tiitta et al. (2014) who observed a lack of ammonium to fully neutralize the inorganic anions during the wet season, the $NH_{4,meas}/NH_{4,predict}$ ratio increases up to 1.20 (see Figure R1 below). This clearly indicates that sulfates are fully neutralized in our case and that additional NH_4 is available to neutralize at least partially other inorganic anions.

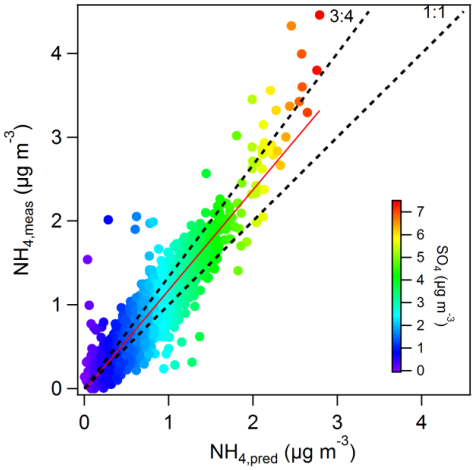

Figure R1. Scatter plot of measured-to-predicted NH_4 using only SO_4 in the ion balance equation. Data points are colored by sulfate concentrations.

Changes in the manuscript: The equation number associated with the neutralization equation has been corrected from (10) to (11), page 12 line 29.

The following paragraph has been added page 13 line 2: "On the other hand, 23% of the data are associated to a $NH_{4,meas}/NH_{4,predict}$ ratio inferior to 0.75 and correspond to points under the 1:1 line in Figure S3a. For such points, the amount of NH_4 predicted is overestimated in comparison to the amount measured on site, and considering that NH_4 will preferentially react with SO_4, other anions like NO_3 and Chl are partially under chemical states other than ammonium nitrate and chloride. As mentioned previously and developed in section 3.2, this can be explained by chloride species emitted by local combustion processes but also by HNO_3 adsorption on dust as already reported in the literature (Fairlie et al., 2010; Savoie et al., 1989) and this is consistent with ratio values inferior to 0.75 which are mainly observed while the site is under dust influence (Figure S3b). Nevertheless these periods also correspond to low levels of inorganic species in PM_1."

2. Recently, it has been demonstrated that some inorganic salts (e.g. (NH4)2SO4) have a positive bias on the CO_2^+ signal through reaction on the aerosol mass spectrometer vaporizer (Pieber et al., 2016). This interference is highly variable between instruments and with measurement history. How big is this interference value for your ACSM and possible impacts on data analyses including PMF.

Author's response: Pieber et al. (2016) have evidenced that the bias is significant when the inorganic fraction is > 50%, 3-10 times more important for ammonium nitrate than for sulfate, and also dependent on the instrument history.
The dataset has been acquired in 2015, when no calibration performed at that time took into account the impact of CO_2^+ from inorganic salts on m/z 44 (using the automated procedure of the instrument). For this reason we are not able to determine the b value for this specific campaign, that would allow to estimate the magnitude of the bias and introduce an appropriate correction into the fragmentation table. Nevertheless, the maximum of possible interferences on m/z 44 (observed when NO_3/OM and SO_4/OM ratios are high) also correspond to lower CO_2^+ mass concentrations (Figure R2, left). Moreover our last ammonium nitrate calibration (performed recently at a site in Northern France after 6-month sampling of air masses showing high levels of ammonium nitrate), led to an estimation of the m/z 44 vs NO_3 ratio of 9% (Figure R2, right).

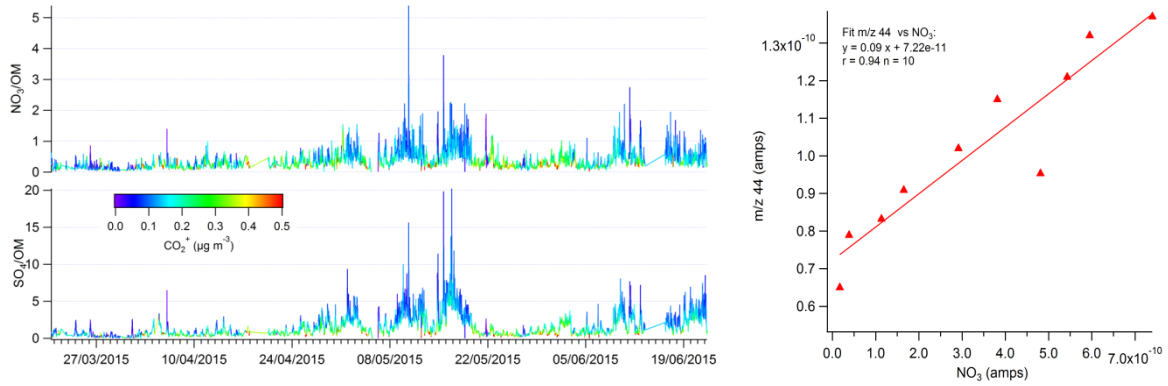

Figure R2. (left) Ratios of NO_3 and SO_4 over OM colored by CO_2^+ signal and (right) m/z 44 vs NO_3 signals (in Amps) obtained during NH_4NO_3 calibration.

Based on this measurement, and considering the rather low levels of NO_3 observed at M'Bour and the predominance of SO_4 in the inorganic fraction, we consider this interference on m/z 44 as likely negligible.

3. How can authors explain high NO3-concentrations in air masses from South-West? The air mass history can be investigated e.g. using backtrajectories calculated with the HYbrid Single-Particle Lagrangian Integrated Trajectory (HYSPLIT).

Author's response: We tend to attribute these NO_3 concentrations from the SW wind sector (oceanic) to NO_x emissions from Dakar which are transported and transformed above the ocean before reaching our sampling site. Adon et al. (2016) have observed an annual average for NO_2 concentrations as high as 32 ppb (60 µg m^{-3}). This regional transport is supported by NO_3 NWR plot and PSCF map now added in the Supplementary Information, Figure S8.

4. What are the following steps for aerosol research in this region of the world? Are these results valuable for policy makers to guide cleanup and decision making for future industry? Please, improve discussion.

Author's response: We have added some additional comments in the Conclusion section regarding Reviewer #1's request.

Changes in the manuscript: The following paragraph has been added page 19 line 31: "As shown during this field campaign, at least half of the organic aerosols measured in the submicron fraction are from anthropogenic origins (HOA + COA + LCOA) and we were able to attribute them to specific sources. On the contrary, little is known about the oxygenated fraction – often associated to secondary organic aerosols, which constitutes the other half of OA and therefore efforts should be directed toward better characterizing SOA precursors (anthropogenic and biogenic) and their concentration levels in West Africa. Moreover, the specific LCOA source puts an emphasis on open waste burning, which is highly problematic in terms of health issues, and should be addressed through the implementation of waste disposal facilities and an effective waste collection infrastructure."

References cited in this reply

Adon, M., Yoboué, V., Galy-Lacaux, C., Liousse, C., Diop, B., Doumbia, E. H. T., Gardrat, E., Ndiaye, S. A. and Jarnot, C.: Measurements of NO_2, SO_2, NH_3, HNO_3 and O_3 in West African urban environments, Atmos. Environ., 135, 31–40, doi:10.1016/j.atmosenv.2016.03.050, 2016.

Fairlie, T. D., Jacob, D. J., Dibb, J. E., Alexander, B., Avery, M. A., van Donkelaar, A. and Zhang, L.: Impact of mineral dust on nitrate, sulfate, and ozone in transpacific Asian pollution plumes, Atmos Chem Phys, 10(8), 3999–4012, doi:10.5194/acp-10-3999-2010, 2010.

Savoie, D. L., Prospero, J. M. and Saltzman, E. S.: Non-sea-salt sulfate and nitrate in trade wind aerosols at Barbados: Evidence for long-range transport, J. Geophys. Res. Atmospheres, 94(D4), 5069–5080, doi:10.1029/JD094iD04p05069, 1989.

Journal: ACP
Title: Chemical characterization and source apportionment of submicron aerosols measured in Senegal during the 2015 SHADOW campaign
Author(s): Laura-Hélèna Rivellini et al.
MS No.: acp-2016-1127

The authors want to thank Reviewer #2 for his/her helpful comments. They are addressed below in blue. Changes in the manuscript are written in red.

Anonymous Referee #2

1. Please consider revising the calculated Fe concentrations and/or the PM1 concentrations and/or the ACSM concentrations (RF for NO3). These data together have inconsistencies that need to be addressed or commented and the possible sources of uncertainty should be stated. The authors report a mean value of 4.6% for the Fe/PM1 ratio. This means 16% for the Fe/RefractoryPM1, since 71% of PM_1 is NR-PM1. (Or 20% for the ratio Fe/(PM1-ACSM-BC) according to Figure S2, considering 5% of Fe and 25% of PM1-ACSM-BC). Hence, it is this 16% (or 20%) which should be compared to the data in the literature, given that the literature data that the authors quote make reference to Dust (and not total PM, regardless of the size fraction). Please see some additional comments related to this one below.

Author's response:
The reviewer is correct in stating that comparison to literature data should be made considering the iron content in dust (and not in total PM_1). The dust amount in our case corresponds to the sum of the unaccounted fraction (assuming negligible influence of sea salt), and Fe obtained by deconvolving absorption measurements, that is to say 25% (Figure S2). The Fe/(Fe + Unacc.) ratio is therefore 20% on average (varying between 12% for marine and 23% for continental days on average, Figures R1a-c).
Table R1 below summarizes the iron content determined in Saharan samples, which shows that the relative contribution of iron determined in this work is in the same order of magnitude but still significantly higher. However iron oxides can be found mostly (for ~2/3) in the clay fraction (~$PM_{2.5}$) and ~1/3 in the silt (coarse) fraction (Journet et al., 2014; Kandler et al., 2009), which is consistent with increased ratios in the submicron fraction compared to larger ones. It is also worth noting that Val et al. (2013) measured the iron content in the ultrafine and fine fractions (corresponding to PM_1) of particles collected in Dakar, and measured a ratio in the upper range of those already reported in the literature, even in the absence of dust event.

Table R1. Comparison of iron content (in %) determined in Saharan dust and soil samples

Reference	Location	Method [a]	Size fraction	%Fe [b]
Dust samples				
(Lafon et al., 2004)	Banizoumbou (Niger)	XRF; CBD	TSP	6.3; 7.8
(Lafon et al., 2006)	Banizoumbou,	XRF; CBD	TSP	4.3 – 6.1
(Lafon et al., 2006)	Cape Verde	XRF; CBD	TSP	5.3 – 6.0
(Formenti et al., 2008)	Banizoumbou	CBD	40 µm	5.8
(Val et al., 2013)	Dakar (Senegal)	ICP-MS	1 µm	7.8
This work	M'Bour	cf. text	1 µm	23 (continental) 21 (sea breeze) 16 (marine)
Soil samples				
(Moreno et al., 2006)	Saharan region (9 samples)	ICP-AES/ ICP-MS	TSP	2.0 – 4.7
(Lafon et al., 2006)	Banizoumbou,	XRF; CBD	10.2 µm [*] 2.5 µm [*]	5.3 5.8
(Joshi et al., 2017)	M'Bour, Bordj (Algeria), Nefta (Tunisia)	XRD	100 µm	< 0.5

[a] XRF: X-ray Fluorescence (XRF) Spectrometry for elemental analysis; CBD: chemical method based on citrate-bicarbonate-dithionite (CBD) reagent for quantification of iron oxides adapted from soil analysis (Mehra and Jackson, 1960)

[b] Percentages of iron relative to the mass of all oxides, classically taking into account Na_2O, MgO, Al_2O_3, SiO_2, K_2O, CaO, TiO_2 and Fe_2O_3.

[*] Soil samples resuspended using wind tunnel and collected with a 13-stage impactor

The uncertainties in the calculation of the Fe/(Fe + Unacc.) ratio can come from the measurements themselves (those for the ACSM, in particular regarding RF(NO_3), are detailed in the reply to comment 4 and will influence the determination of the unaccounted fraction); but are mostly related to the BC and dust absorption Angström exponents (AAE) corresponding to α and β values, respectively, in the deconvolution method. This method is indeed highly sensitive to even small variations of these parameters, with values quite well known for BC from fossil fuel ranging from 0.8 to 1.1 (Hansen, 2005; Zotter et al., 2017) but not so much for dust. In the manuscript, we chose to use β = - 4, according to Fialho et al. (2006) values determined at the Azores Islands for samples influenced by Saharan dust events. But other values can be found in the literature (Table R2), ranging from -1.6 to -6.5 and largely influenced by the wavelength range as well as dust origins and size fractions since the iron content differ depending on emission sources and particle size (Journet et al., 2014). Even during the SAMUM campaign (May to June 2006 in Morocco), a wide range of AAE values have been reported from 1.6 up to 5.1 for ground-based measurements in the same size fraction, as shown in Table R2.

Table R2. Mineral dust AAE values reported from field campaigns around the Saharan region.

Reference	Location / Period	Wavelengths (nm)	Fraction	β
Fialho et al. (2006) [a]	Azores Islands Jul. 2001 – Jun. 2005	370-950	-	-4
Müller et al. (2009) [a]	Tinfou, Morocco (SAMUM) Summer 2006	467/660	PM_{10}	-2.25 to -5.13
Petzold et al. (2009) [b]	South-East Morocco (SAMUM) Summer 2006	467/660	$PM_{2.5}$	-2 to -6.5
Schladitz et al. (2009) [a]	Tinfou, Morocco (SAMUM) Summer 2006	537/637	PM_{10}	-1.6 to -4.73
(Linke et al., 2006) [c]	Morocco Egypt	266/532	~PM_4	-4.2 -5.3
(Caponi et al., 2017) [c]	Morocco Lybia Algeria Mali	375-850 375-532 375-850 375-532	$PM_{2.5}$ ($PM_{10.6}$)	-2.6 -4.1 (-3.2) -2.8 (-2.5) -3.4

[a] In situ ground-based measurements; [b] Airborne measurements through dust plumes; [c] Laboratory experiments with resuspended soil samples

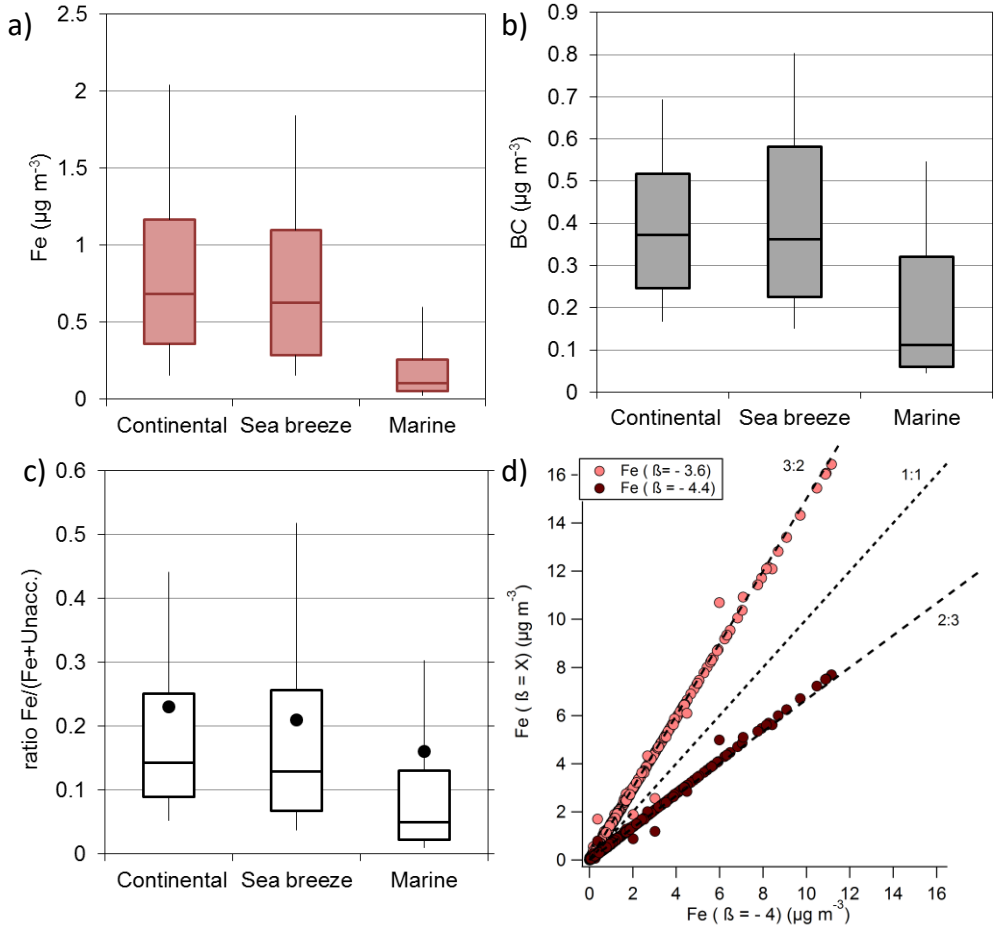

Figure R1. Box plots of (a) Fe, (b) BC concentrations and (c) Fe/(Fe+Unacc.) ratio for continental, sea breeze and marine days. (d) Scatter plot of iron concentrations (in µg m^{-3}) obtained from Fialho's deconvolution method using an AAE value of ± 10% compared to the one from the literature and used in the manuscript.

Applying a relatively small increase (resp. decrease) of 10% on the value of β for our dataset led to a 33% decrease (resp. 50% increase) of iron concentrations, as shown in Figure R1d, but no change in the temporal behavior.

In conclusion, the approach used here leads to an estimate of the absolute concentrations of iron, although with high uncertainties given all the necessary assumptions and the empirical algorithm used to deconvolve BC and Fe from absorption measurements. However the temporal profiles, non-parametric wind regression (NWR) plots and potential source contribution function (PSCF) maps (now provided in Figures S5b and S5c, respectively) are all consistent with the expected behavior of such a desert dust tracer and show that it can be useful in determining the contribution of dust to absorption measurements (see also reply to comment 24). We nonetheless agree with reviewer #2 that there is quite some room for improvement, in particular for a better estimation of the AAE value for dust similar to the efforts carried out to determine the AAE values for BC from fossil fuel and wood burning (Zotter et al., 2017). We strongly believe the lack of information for submicron particles in terms of chemical composition of refractory species and optical properties should be better addressed, but is beyond the scope of this work.

Changes in manuscript:
A new appendix (S2) in the Supplementary Information now includes the whole discussion above. Changes in the main text have been also done page 8, line 18 with a new sentence added: "Applying the propagation for uncertainties approach on the values of K_{Fe} (10%) and the slope b (39%, calculated using a variability of 0.2 for α and β (Fialho et al., 2006)) gives an overall uncertainty of ~40% for iron concentrations. However the deconvolution algorithm is highly sensitive to the values of the Angström absorption exponents (α and β) and a more detailed discussion can be found in Appendix S2."

2. The sampling period is actually 3 months (20 March to 22 June), and not 4 as stated.

Author's response: Page 1 line 27, this mistake has been corrected.

3. Please homogenize the dry and wet period definition: in the introduction it says that the dry season extends from November to May; in section 2.1 it says that the dry season is from December to March; in section 2.3.1 it says that dry season is generally defined from November to April; in the same section 2.3.1 it is coherent within the section and it says that "Our study taking place from March to June allowed for the observation of both the late part of the dry season (March-April) and the beginning of the wet season (May-June)"; in the conclusions section it says "during four months of the 2015 dry season". Given that precipitation data for the specific campaign is available, according to section 2.2.3, could you please provide this data, or make the classification based on these data? (Although the info in literature about the usual dry-wet periods can still be included).

Author's response:
We understand our wording can be confusing. The two contrasted dry and wet seasons observed around the Equator originate from the closeness of the Intertropical Convergence Zone (ITCZ), which brings moist air masses and heavy precipitations. Kaly et al. (2015), based on 5 years of observations (2006-2010) at M'Bour, defined the dry season as the period during which no precipitation occurs from November to April and the wet season from May to October, where significant precipitation is measured, with a transition during April/May.
In Mortier et al. (2016), who analyzed data from 2006 to 2012 at M'Bour, the seasons are defined based on RH levels: from December to March/April (RH < 40%) for the dry season and from June to September (RH ~ 80%) for the wet season. They also observed different wind patterns at the ground level, that is to say trade winds coming mostly from the North-East during the dry season, whereas the wet season was characterized by winds from the west. During the AMMA field campaign in the Sahelian belt, Haywood et al. (2008) defined the period from May to June as the monsoon onset. Finally, Slingo et al. (2008) also mentioned "*large interannual variability in the seasonal progression of humidity, with no clearly reproducible pattern from year-to-year*" in Niamey, Niger.

Therefore we based the definition of the dry and wet seasons in this work on the observed weather parameters during the field campaign. Since absolutely no precipitation was observed during the whole period, but differences in RH levels (Figure R2) – though not as pronounced as reported by Mortier et al. (2016) – and wind patterns were clearly visible, we considered March and April to belong to the dry season and May-June to the transition period.

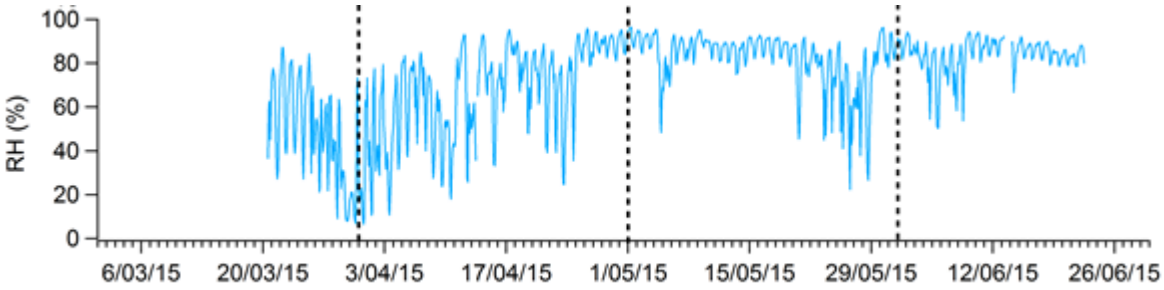

Figure R2. Time series of relative humidity (in %; 2-hour averages).

Changes in manuscript:

Complementary information concerning the distinction between dry and wet seasons has been added in section 2.3.1 "Classification of air masses", and some sentences have been simplified to hopefully make things clearer.

Page 2 lines 26-27, sentence modified: "During the months of January-February (dry season)"

Page 3 lines 30-31, sentence modified: "the dry season", with no mention of the month range.

Page 6 lines 16 - 24, paragraph modified: "The station of M'Bour is under the influence of a typical Sahelian climatic cycle composed of two contrasted dry and wet seasons observed around the Equator, which originate from the closeness of the Intertropical Convergence Zone (ITCZ), bringing moist air masses and heavy precipitations. Kaly et al. (2015), based on 5 years of observations (2006-2010) at M'Bour, defined the dry season as the period during which no precipitation occurs from November to April and the wet season from May to October, where significant precipitation is measured, with a transition during April/May. In Mortier et al. (2016), who analyzed data from 2006 to 2012 at M'Bour, the seasons are defined based on RH levels: from December to March/April (RH < 40%) for the dry season and from June to September (RH ~ 80%) for the wet season. They also observed different wind patterns at the ground level, that is to say trade winds coming mostly from the North-East during the dry season, whereas the wet season was characterized by winds from the west. During the AMMA field campaign in the Sahelian belt, Haywood et al. (2008) defined the period from May to June as the monsoon onset. Finally, Slingo et al. (2008) also mentioned large inter-annual variability in the seasonal progression of moisture, with no clearly reproducible pattern from year-to-year in Niamey, Niger.

Therefore we based the definition of the dry and wet seasons in this work on the observed weather parameters during the field campaign. Since absolutely no precipitation was observed during the whole period, but differences in RH levels – though not as pronounced as reported by Mortier et al. (2016) – and wind patterns were clearly visible (Figure 2a), we considered March (RH = 49%) and April (68%) to belong to the dry season, and May (82%) and June (84%) to the transition period."

4. Section 2.2.1. Please confirm that no major changes (such as filament replacement) occurred to the ACSM during the time between Feb 2014 and Jan 2015, for which the calibration constants were taken. This is necessary to be able to take the average of all calibrations. Especially between Dec 2014 and Jan 2015 there is a big difference for the RF of NO3 (Fig S1). This is a source of uncertainty that should be acknowledged in the manuscript, especially considering that the absolute concentrations are used and that the differences with the bulk PM1 concentrations are taken as very valid and interpreted.

Author's response:

We confirm that no major changes that could impact RF(NO_3) calibration occurred between Feb. 2014 and Jan. 2015. In particular, we have operated our ACSM with the same filament since its purchase in

2013. Additional calibrations performed since the end of the SHADOW field campaign have confirmed the stability of this value with an average of $(3.75 \pm 0.67) \times 10^{-11}$ Amps / (µg m^{-3}). It must be noted however that the uncertainties on mass concentrations with aerosol mass spectrometers are estimated at 20-35% (2σ) for the total mass (Bahreini et al., 2009). Furthermore, Crenn et al. (2015) reported reproducibility expanded uncertainties of Q-ACSM concentration measurements of 9, 15, 19, 28, and 36% for NR-PM_1, nitrate, organic matter, sulfate, and ammonium, respectively, during an intercomparison that involved 13 Q-ACSM in the Paris area during springtime.

Changes in the manuscript:
Page 5 lines 9 - 12, the text now reads: "It must be noted however that the uncertainties on mass concentrations with aerosol mass spectrometers are estimated at 20-35% (2σ) for the total mass (Bahreini et al., 2009). Furthermore, Crenn et al. (2015) reported reproducibility expanded uncertainties of Q-ACSM concentration measurements of 9, 15, 19, 28, and 36% for NR-PM_1, nitrate, organic matter, sulfate, and ammonium, respectively, during an intercomparison that involved 13 Q-ACSM in the Paris area during springtime."

5. Section 2.3.1. "During IOP-1 two main prevailing directions were found (Fig. 2a). The first one [...] and North-West to South-West (315-225_, dominant in May-June)"
Maybe you could indicate which wind direction prevails for the first and second periods (Mar-Apr and May-Jun), since the wind directions for the periods are given based on literature info, but the data for the specific campaign is available and then the wind roses are commented for the entire period.

Author's response:
The period from end of March to April was dominated by winds coming from NW to NE (~62%) with some occurrences (~33%) of Western winds during the sea breezes, while from May to June winds were mainly originating from the West (72%).

Changes in the manuscript:
Figure 2 has been modified to include wind frequency rose plots for March-April (dry season) and May-June (transition period). Besides, the following sentence has been added page 6, lines 30-31: "The period from end of March to April was dominated by winds coming from NW to NE (~62%) with some occurrences (~33%) of Western winds during the sea breezes, while from May to June winds were mainly originating from the West (72%)."

6. Section 2.3.1. "In summary, among the 91 days of IOP-1, 19% were classified as continental days, 32% as sea breeze days and 49% as marine days". You could say these percentages for the dry and wet periods? Or the rain for each of the 3 types of days? Somehow the info of the day types and the info on rain (dry-wet) should be linked. This is related to Fig 2 as well.

Author's response:
As indicated in reply to comment #3, no precipitation was observed during the whole campaign. Nonetheless, we provide in Table R3 below the number of days associated with the dry season (March-April) and the transition period (May-June).

Table R3. Number of days (relative contribution in parenthesis) associated with the continental, sea breeze and marine influences for the dry season, the transition period and the whole IOP-1.

	Continental	Sea breeze	Marine	Total
Mar-Apr.	13 (32%)	19 (48%)	8 (20%)	40 (100%)
May-Jun.	4 (8%)	10 (20%)	37 (73%)	51 (100%)
IOP-1	17 (19%)	29 (32%)	45 (49%)	91 (100%)

Changes in the manuscript:
Figure 2 in the manuscript now includes the wind roses for the dry season (March-April) and the transition period (May-June).

7. Section 3.1.1. "the fraction of unaccounted material therefore corresponded to DD and SS contributions". Note that if Fe is 2-5% of DD, then according to Fe concentrations, DD>unaccounted mass.

Author's response: As correctly pointed out in comment #1 by this reviewer and discussed in our reply, the Fe contribution to DD is 20% on average in PM_1, and not 2-5%.

8. Section 3.1.1. "The unaccounted fraction (determined as the difference between the gravimetrically measured PM_1 mass concentration and the sum of chemical species from ACSM and aethalometer measurements) corresponds to 27%, 26% and 16% of the PM1 mass for continental, sea breeze and marine days, respectively (see Figure S2)". Please specify that for these numbers you already applied the model from Fialho for this calculation, so that you derived already BC and Fe concentrations from the aethalometer measurements.

Changes in the manuscript:
Page 8 line 18, now added in the methodology section: "In the rest of the paper, when BC and Fe concentrations are mentioned, it corresponds to the deconvolved values based on the above-mentioned method."
Page 10 lines 4-7: "The unaccounted fraction was determined as the difference between the gravimetrically measured PM_1 mass concentration and the sum of chemical species from ACSM (Org, NO_3, SO_4, NH_4, Chl) and aethalometer (BC, Fe) measurements. It corresponded to 27%, 26% and 16% of the PM_1 mass for continental, sea breeze and marine days, respectively (see Figure S3)."

9. Section 3.1.1. Related with comment 4, please comment on the uncertainty of ACSM measurements since you took RF of NO3 as an average of previous calibrations and not determined on site.

Author's response:
Indeed we were not able to perform calibrations on site due to technical and regulatory constraints (for instance shipping our SMPS with a radioactive source to Senegal would have been nearly impossible). As indicated in the reply to comment #4, additional calibrations performed since the end of the SHADOW field campaign have confirmed the stability of the averaged value used for this campaign. Another (indirect) way to confirm that the calibrations are not too far off is the slope close to unity of Figure S4a that shows NH_4 measured vs. NH_4 predicted since these two parameters depend on both RF(NO3) and RIE values (at least of the main inorganic species that neutralize NH_4), as mentioned page 12 lines 32-34.

10. Section 3.1.2. "Although a weak correlation (r = 0.55) was found between Fe and total PM1 concentrations, Fe concentrations showed higher correlations with PM_{10} (r = 0.70, see Figure 4)". You could check the correlation between Fe and PM1-ACSM-BC.

Author's response: The correlation observed between Fe and the unaccounted PM_1 is even worse for the whole IOP-1 (r = 0.47). It is partly due to the absence of TEOM-FDMS PM_1 measurements during the periods with major dust events (whereas TEOM PM_{10} measurements were available), that leads to excluding Fe concentrations above 4 µg m^{-3}.

Changes in the manuscript:
Page 10 lines 32-35 now reads: "Although weak correlations were found between Fe and total PM_1 concentrations (r = 0.55) and unaccounted PM_1 (r = 0.47), Fe concentrations showed higher

correlations with PM_{10} (r = 0.70, see Figure 4). This could be explained by the lack of PM_1 mass concentration measurements during intense dust events, as well as DD domination in the coarse fraction, while the fine fraction is mainly driven by NR and BC species during most of the IOP-1 (Figure 3c)."

11. Section 3.1.2. "the highest Fe concentrations (> 8.0 µg m-3) are generally associated with continental and sea breeze days. These maxima also coincide with PM10 highest concentrations (> 400 µg m-3)". Note that 8 µg m-3 of Fe corresponds to 160 µg m-3 of DD (if Fe is 5% of DD on average according to literature values). Even if we assume a high percentage of refractory PM1 for this data point (higher than the average 29% according to data in page 9, line 24), let's estimate 60% of PM1 is refractory, this would mean that the PM1 is 267 _g m-3. If PM10 is 400 _g m-3, then the ratio PM1/PM10 for this event would be 67%, much higher than the average 10% reported.
Is this the case? Please check for consistency. Either Fe is overestimated, or PM1 is underestimated, or both.

Author's response: During the whole IOP-1, the PM_1/PM_{10} ratio average was indeed 10% but it varied between 2 and 55% for 2-hour averages. We expect it to be closer to the lower values during dust events (according to Figure 3b), for which unfortunately we had to invalidate PM_1 mass concentrations. Additionally, we recalculated the percentage of {Fe + Unacc.} in PM_1 for the highest PM_{10} concentrations (> 400 µg m^{-3}) and found an average value of 0.77 ± 0.04, slightly higher than the 60% used in the reviewer's calculations.
Therefore, using our corrected ratio of 20% of Fe in submicron DD (see comment 1), 8 µg m^{-3} of Fe corresponds to 40 µg m^{-3} of DD, 52 µg m^{-3} of PM_1 and a PM_1/PM_{10} ratio of 13%, consistent with the values presented in the manuscript. Note that this is an upper value since the concentrations of PM_{10} reached 950 µg m^{-3} at the site, while the highest Fe concentration was 11.2 µg m^{-3}.

12. Section 3.1.2. Last paragraph. "Fe contributions to PM10 estimated in M'Bour (average Fe/PM_{10} ratio of 0.51% over IOP-1 and 0.89% for continental days)". The Fe concentrations determined in this study correspond to PM1, since the aethalometer was equipped with a PM_1 inlet. If this is correct, then the authors are taking the Fe in PM_1 with respect to bulk PM_{10}, whereas the Fe concentration in PM_{10} corresponding to the Fe concentrations in PM1 determined in the present study would be much higher. Hence the comparisons with the ratios of Fe/DD or Fe/soil in the literature are not direct. Regarding the sentence "Nonetheless they (Formenti et al in PM_{40}) measured for the same samples an averaged iron concentration of 10 µg m^{-3}, in the same order of magnitude as our maximum concentration of 11.2 µg m^{-3} in PM_1"; this is not directly comparable, Fe in PM40 with Fe in PM_1.

Author's response: As mentioned in reply to comment 1 (Table 1), we only found one study that determined the iron content in PM_1 DD, leading to a value of 7.8% in the absence of dust events, which is within the same order of magnitude with the one found here, i.e. 20%.
We agree with reviewer #2 that our wording is confusing in this paragraph since the Fe/PM_{10} ratio refers indeed to Fe_{PM1} / PM_{10} and not to the proportion of Fe in the PM_{10} size fraction.
Direct comparisons with other size fractions cannot be straightforward since it would assume that the contribution of Fe is constant whatever the particle size, although literature has shown that, as mentioned above (comment 1), iron oxides belong mostly (for ~2/3) to the clay fraction (~$PM_{2.5}$) and ~1/3 to the silt (coarse) fraction (Journet et al., 2014; Kandler et al., 2009), which is consistent with increased ratios in the submicron fraction compared to larger ones.

Changes in the manuscript:
Page 11 lines 3-13: "From the only study in the literature focusing on iron concentrations in the submicron fraction in West Africa (Val et al., 2013), we could infer an elemental iron contribution of 7.8% to PM_1 dust, in Dakar, in the absence of dust events. Other studies focused on dust gave the iron contribution for size fractions higher than PM_1, thus no straightforward comparisons can be made with our average ratios of Fe/DD_{PM1} (20, 23, 21 and 16% for respectively IOP-1, continental, sea breeze

and marine days). It can nevertheless be interesting to have in mind values retrieved within the same region as it is known that iron oxides mainly belong to the finest fraction (Journet et al., 2014; Kandler et al., 2009) and therefore the elemental iron contribution should be lower for larger sizes, which is consistent with values reported in Table S2.2."

13. Section 3.1.2. To compare with % determined in DD or soil samples, the ratios that should be taken from this study are the Fe/(PM1-ACSM-BC), assuming PM1-ACSMBC a proxy for DD if we disregard sea salt, as DD or soil samples do not have the NR components that we have in the PM1 in this study. This ratio (Fe/(PM1-ACSM-BC)) is 20% approx for IOP-1 and about 23% for continental days (according to Figure S2).

Author's response: See response to comment 1.

14. Section 3.1.3. "regional background sites such as MontSec, Spain". Consider replacing regional by continental, since Montsec site is defined as continental back-ground site in Ripoll et al, 2015.

Changes in the manuscript:
Page 11 line 25: "continental background sites such as MontSec"

15. Section 3.1.4. The wind is always from the North (NW-NE), so the variation along the day cannot be explained by transport only, since the transport takes place the entire daytime (during the night the wind velocity is lower, so this can partially explain some variation).

Author's response: We agree with the reviewer that for continental days, the wind is always blowing from the NW to NE, whereas during sea breeze days, part of the afternoon is under the influence of marine air masses, and for marine days western winds dominate.
We have indeed highlighted several times in that section that for continental days the observed temporal variations are also coming from the temporal variability of local emissions.
For instance, page 13 lines 13-14: "*suggesting an influence linked to emissions by rather local anthropogenic activities rather than long-range transport sources*"; page 13, line 28: "*probably combining local emissions and reduced dispersion*"; page 13, lines 34-35: "*These peaks are measured for air masses coming from the continent and correspond to traffic and/or cooking hours*"; page 14, line 1: "*(…) tend to confirm combustion sources for these species*".

16. Section 3.2.2. "The HOA rose plot shows marked peaks in the directions of the two open waste burning areas and of the fish-smoking area located northeast of the site in the outskirts of M'Bour". Can you please give a tentative explanation for this?

Author's response: HOA rose plot and NWR plot both show higher concentrations in these directions. As for the open waste burning areas, a possible explanation could be the formation of organic compounds which present molecular structures that, when fragmented by electron impact ionization, are very similar to the HOA mass spectrum for m/z below 100. This is for instance the case for phthalate esters (Wienecke et al., 1992), whose mass spectrum is shown below.

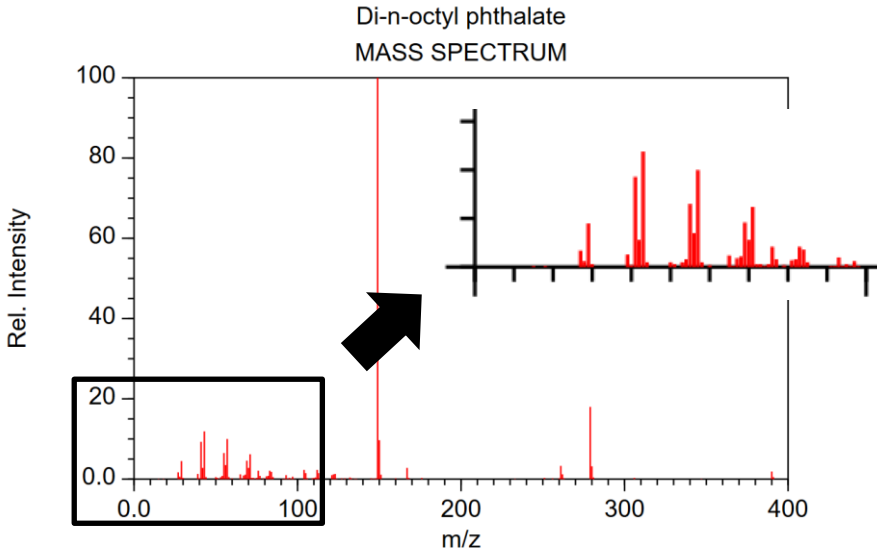

Figure R3. Mass spectrum of di-n-octyl phthalate obtained by electron impact ionization

It is less obvious why HOA points out also to the fish-smoking area. We have not been able to observe the process of fish-smoking but were told that they used millet flour as fuel. Since it is extracted from the grains, it should contain almost no cellulose (0.7-1.8% according to Wankhede et al. -1979)), contrary to the stems of plants where it amounts to ~40% (Ververis et al., 2004). This could explain why we do not see any biomass burning tracer, since levoglucosan is formed by the pyrolysis of cellulose. Finally, we cannot exclude higher traffic emissions at this location during the hours when the fish is smoked, since it has to be transported from the harbour to the fish-smoking area.

17. Section 3.2.2. Could you comment on the 5-factors solution constraining HOA and COA? Do you get LCOA and 2 different OOA factors? If this is the case, you could see different origins for OOA, ideally locally formed versus transported? Or is the 5-factors solution resulting in a mix LCOA-OOA factor not well defined?

Author's response: The 5-factor solution presented in Appendix S6 of the submitted manuscript (now Appendix S8) was obtained with m/z 36 in the PMF input in addition to the "classical" organics matrix. This mass was consistently attributed to the LCOA factor, as mentioned in the Appendix discussion. Besides, strong constraints on the different POA factors (using profiles of HOA, COA and LCOA obtained with unconstrained solutions) were applied. In these conditions only, two different kinds of OOA factors could be deconvolved: one more oxidized (MO-OOA; 76.5% of OOA) and considered from a more regional origin (mostly marine as highlighted by its NWR plot and PSCF map in Figure R4 below) and the other less oxidized (LO-OOA; 23.5% of OOA), locally emitted as per its NWR plot. Nonetheless, without using m/z 36 as input and literature profiles for constraining HOA and COA none of the solution leads to two completely distinct OOA profiles. If considering MO-OOA only, most of it could be rather due to the oxidation of ship emissions along the Western African coast, which would also explain the better correlation observed with NO_3 from NO_x emission processing despite the predominance of this regional oxidized factor over the local one.

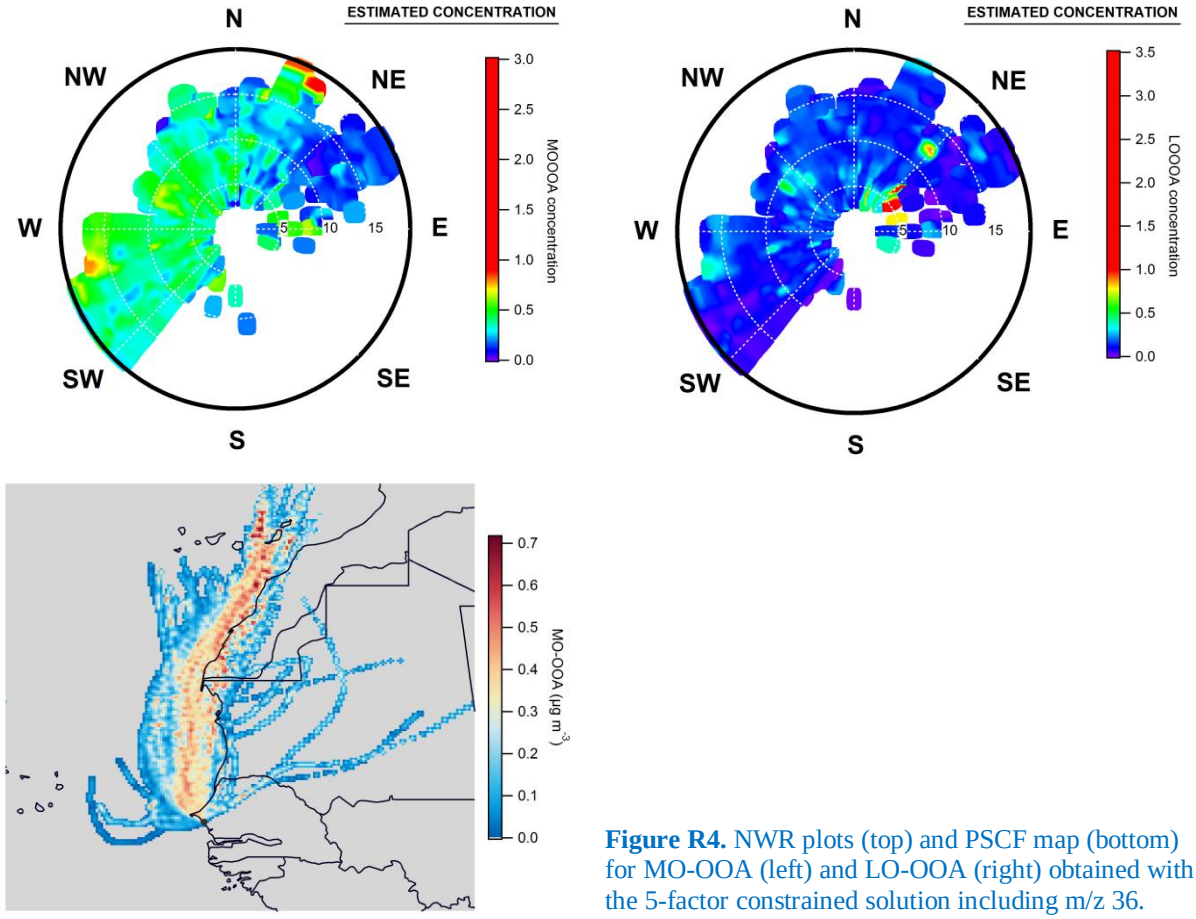

Figure R4. NWR plots (top) and PSCF map (bottom) for MO-OOA (left) and LO-OOA (right) obtained with the 5-factor constrained solution including m/z 36.

Changes in the manuscript:

Abstract, page 2 lines 4-6: "The remaining fraction was identified as oxygenated organic aerosols (OOA), a factor that prevailed regardless of the day type (45%) and was representative of regional (~3/4) but also local (~1/4) sources due to enhanced photochemical processes."

Page 15 lines 34-36: "Since the behavior of Chl had also been suspected to come from the same sources, PMF solutions adding the m/z 36 signal in the input matrix were investigated, and a solution is presented in Appendix S8, where regional OOA accounts for ~3/4 of the OOA and local OOA ~1/4."

Page 18 line 21: "The OOA PSCF map (Figure S5c) seems to trace back its origin along the entire Western African coast, where shipping emissions could be a major source of organic aerosols."

18. Section 3.2.2. The COA profile does not meet the 41>43 characteristic of the COA. Do you have any comment on this?

Author's response: HOA and COA profiles were quite difficult to separate over the whole period when running unconstrained PMF, as has been shown in previous studies with Q-ACSM (Fröhlich et al., 2015 and references therein). When applying strong constraints on the primary profile, part of the m/z 43 fragment goes to HOA and OOA, as observed in the 5-factor constrained solution (Appendix S8). However this does not change significantly the contribution of this factor to the total OA.

19. Section 3.2.2. “Our measurements over a large period of four months”. Please re-write to state the 3 months period. Maybe 3 months cannot be considered a large period (true it is larger than typical 3 weeks campaign for AMS, but it is not very large).

Changes in the manuscript:
Page 18 line 30: “over a period of three months”

20. Conclusions section. “during four months of the 2015 dry season”. Please revise if you wanted to say dry season, or dry+wet. Please correct the duration to 3 months.

Changes in the manuscript:
Page 18 lines 35-36: “during three months encompassing the end of the dry season and the transition period toward the wet season of 2015”

21. Conclusions section. “This factor (LCOA), although minor on average, could represent as high as 7% on a 30-minute time period when the air masses were blowing from the waste burning areas”. Isn’t it even more as a maximum? The average contribution of LCOA for marine events is 7%, so there must be some individual 30-min data points with a higher contribution. Or are these points you mention when air masses blow from the waste burning areas not taking place during marine-classified days? Maybe worth to clarify this. Moreover, maybe worth to clarify also the differences in absolute contributions, although the percentage is higher for marine days (by a factor of 2 or 3 with respect to other days), the absolute contribution is not so much higher. Still the absolute contribution for marine is higher (continental: 5.98 µg m^{-3} x 36% of OA x 2% of LCOA= 0.04 µg m^{-3} of LCOA; sea breeze: 6.29 µg m^{-3} x 40% of OA x 3% of LCOA=0.08 _g m-3 of LCOA; marine: 6.09 µg m^{-3} x 25% of OA x 7% of LCOA=0.11 µg m^{-3} of LCOA) (calculations to be improved with the corresponding decimals and not rounded values taken from the plots). Why the absolute average contribution of LCOA is higher for marine days even that during marine days the wind is never coming from the identified waste burning sources, according to map and wind rose in Figs 1 and 2?

Author’s response: Overall the concentration of LCOA is 0.05 (11%), 0.06 (17%) and 0.07 (34%) µg m^{-3} on average (maximum contribution) for continental, sea breeze and marine days, respectively. Days during which air masses were coming from the identified open waste burning areas of Gandigal or/and Saly Douté were classified either as continental or sea-breeze days. Some strong events also appear during marine days at an average distance from the site (see LCOA NWR plot in Figure S5b) and may be related to air masses carried over Dakar where similar massive anthropogenic emissions from waste burning could be expected from Mbeubeuss, the largest dumpsite in Senegal located 25 km north-east of Dakar along the coast, which receives 250,000 tons of garbage per year from the Dakar region (Cissé, 2012). In the absence of strictly controlled waste regulations, it is however quite likely there are other unidentified open waste burning sites along the coast that could also contribute to this factor. The more regional influence seen in the NWR plot may also be due to chlorine-driven photo-oxidation processes occurring off the coast of Senegal (Hossaini et al., 2016).

Changes in the manuscript: The dumpsite of Mbeubeuss in Dakar is now identified in Figure 1.

Page 17 line 29: “Besides, the NWR plots of Chl (local influence) and LCOA (both local and regional) rather suggest the presence of chlorinated organics. The PSCF maps identify two possible origins, one clearly from the ocean that could be related to chlorine-driven photo-oxidation processes (Hossaini et al., 2016) and the other linked to air masses carried over Dakar where similar massive anthropogenic emissions from waste burning could be expected from Mbeubeuss, the largest dumpsite in Senegal located 25 km north-east of Dakar along the coast, which receives 250,000 tons of garbage per year from the Dakar region (Cissé, 2012).

Page 19 lines 19-26: “Three primary OA linked to anthropogenic activities from nearby sources were also identified: HOA (22%), COA (28%) and a new factor LCOA (3%) related to local combustion sources (emissions from open-waste burning and fish smoking areas), for which a good correlation with particulate chloride (m/z 36) was consistently found. Non-refractory chloride fragments from waste burning or fish smoking areas were suggested to originate from local plastic smoldering/flaming processes (for the former) and/or sea salt (for both) submitted to high temperatures under continental influence. This factor, although minor on average, could represent as high as 7% on a 30-minute time period when the air masses were blowing from the local waste burning areas, and very likely resulted in the concomitant emissions of highly-toxic compounds such as dioxins that would require further investigation. Back-trajectories also suggest possible distant sources of combustion, with part of LCOA, OOA and BC associated to processed oceanic air masses which could be influenced by Dakar traffic emissions and waste burning activities, as well as shipping emissions along the West African coast.”

22. Figure 5. Maybe choose a different color for Fe (in print it looks same as sulfate).

Changes in the manuscript: Figure 5 has been modified as suggested using dark brown for iron.

23. Figure 7a. Consider choosing a different scale for OM and (SO4, NH4, NO3 and Chl) to help seeing the variations, not very evident now for components different from OM.

Changes in the manuscript: Figure 7a has been modified as suggested, plotting OM on the right axis and all the other concentrations on the left one.

24. Figure 7b. Fe correlates with BC. This is an indication that the Fe calculation should be revised. The explanation of the co-transport of BC and Fe may not explain completely this parallel behavior. You could isolate the dust events and see the differences in Fe and BC ratios.

Author’s response: A correlation coefficient of 0.55 between Fe and BC was calculated for the whole IOP-1. Both species show quite distinctive origins (Figure S5b and S5c), iron sources pointing toward the Saharan desert (PSCF map) but also attributed to more local emissions most probably caused by traffic resuspension (NWR plot). BC appeared to be emitted both by cities located along the Western African coast especially Dakar (PSCF) and by local sources and attributable to diesel combustion from traffic which could explain the common peaks encountered in the morning and the evening by the two compounds.

25. Figure S6. Should legend in first plot read LCOA instead of WCOA?

Changes in the manuscript: The legend of Figure S8 (formerly Fig. S6) has been corrected.

References cited in this reply

Bahreini, R., Ervens, B., Middlebrook, A. M., Warneke, C., de Gouw, J. A., DeCarlo, P. F., Jimenez, J. L., Brock, C. A., Neuman, J. A., Ryerson, T. B., Stark, H., Atlas, E., Brioude, J., Fried, A., Holloway, J. S., Peischl, J., Richter, D., Walega, J., Weibring, P., Wollny, A. G. and Fehsenfeld, F. C.: Organic aerosol formation in urban and industrial plumes near Houston and Dallas, Texas, J. Geophys. Res. Atmospheres, 114(D7), D00F16, doi:10.1029/2008JD011493, 2009.

Caponi, L., Formenti, P., Massabó, D., Di Biagio, C., Cazaunau, M., Pangui, E., Chevaillier, S., Landrot, G., Andreae, M. O., Kandler, K., Piketh, S., Saeed, T., Seibert, D., Williams, E., Balkanski, Y., Prati, P. and Doussin, J.-F.: Spectral- and size-resolved mass absorption efficiency of mineral dust

aerosols in the shortwave: a simulation chamber study, Atmos Chem Phys Discuss, 2017, 1–39, doi:10.5194/acp-2017-5, 2017.

Cissé, O.: Les décharges d'ordures en Afrique - Mbeubeuss à Dakar au Sénégal, Karthala., 2012.

Crenn, V., Sciare, J., Croteau, P. L., Verlhac, S., Fröhlich, R., Belis, C. A., Aas, W., Äijälä, M., Alastuey, A., Artiñano, B., Baisnée, D., Bonnaire, N., Bressi, M., Canagaratna, M., Canonaco, F., Carbone, C., Cavalli, F., Coz, E., Cubison, M. J., Esser-Gietl, J. K., Green, D. C., Gros, V., Heikkinen, L., Herrmann, H., Lunder, C., Minguillón, M. C., Močnik, G., O'Dowd, C. D., Ovadnevaite, J., Petit, J.-E., Petralia, E., Poulain, L., Priestman, M., Riffault, V., Ripoll, A., Sarda-Estève, R., Slowik, J. G., Setyan, A., Wiedensohler, A., Baltensperger, U., Prévôt, A. S. H., Jayne, J. T. and Favez, O.: ACTRIS ACSM intercomparison – Part 1: Reproducibility of concentration and fragment results from 13 individual Quadrupole Aerosol Chemical Speciation Monitors (Q-ACSM) and consistency with co-located instruments, Atmos Meas Tech, 8(12), 5063–5087, doi:10.5194/amt-8-5063-2015, 2015.

Fialho, P., Freitas, M. C., Barata, F., Vieira, B., Hansen, A. D. A. and Honrath, R. E.: The Aethalometer calibration and determination of iron concentration in dust aerosols, J. Aerosol Sci., 37(11), 1497–1506, doi:10.1016/j.jaerosci.2006.03.002, 2006.

Formenti, P., Rajot, J. L., Desboeufs, K., Caquineau, S., Chevaillier, S., Nava, S., Gaudichet, A., Journet, E., Triquet, S., Alfaro, S., Chiari, M., Haywood, J., Coe, H. and Highwood, E.: Regional variability of the composition of mineral dust from western Africa: Results from the AMMA SOP0/DABEX and DODO field campaigns, J. Geophys. Res. Atmospheres, 113(D23), D00C13, doi:10.1029/2008JD009903, 2008.

Fröhlich, R., Crenn, V., Setyan, A., Belis, C. A., Canonaco, F., Favez, O., Riffault, V., Slowik, J. G., Aas, W., Aijälä, M., Alastuey, A., Artiñano, B., Bonnaire, N., Bozzetti, C., Bressi, M., Carbone, C., Coz, E., Croteau, P. L., Cubison, M. J., Esser-Gietl, J. K., Green, D. C., Gros, V., Heikkinen, L., Herrmann, H., Jayne, J. T., Lunder, C. R., Minguillón, M. C., Močnik, G., O'Dowd, C. D., Ovadnevaite, J., Petralia, E., Poulain, L., Priestman, M., Ripoll, A., Sarda-Estève, R., Wiedensohler, A., Baltensperger, U., Sciare, J. and Prévôt, A. S. H.: ACTRIS ACSM intercomparison – Part 2: Intercomparison of ME-2 organic source apportionment results from 15 individual, co-located aerosol mass spectrometers, Atmos Meas Tech, 8(6), 2555–2576, doi:10.5194/amt-8-2555-2015, 2015.

Hansen, A. D. A.: Aethalometer Operations Manual, Magee scientifique, Berkeley, CA, USA., 2005.

Haywood, J. M., Pelon, J., Formenti, P., Bharmal, N., Brooks, M., Capes, G., Chazette, P., Chou, C., Christopher, S., Coe, H., Cuesta, J., Derimian, Y., Desboeufs, K., Greed, G., Harrison, M., Heese, B., Highwood, E. J., Johnson, B., Mallet, M., Marticorena, B., Marsham, J., Milton, S., Myhre, G., Osborne, S. R., Parker, D. J., Rajot, J.-L., Schulz, M., Slingo, A., Tanré, D. and Tulet, P.: Overview of the Dust and Biomass-burning Experiment and African Monsoon Multidisciplinary Analysis Special Observing Period-0, J. Geophys. Res. Atmospheres 1984–2012, 113(D23), doi:10.1029/2008JD010077, 2008.

Hossaini, R., Chipperfield, M. P., Saiz-Lopez, A., Fernandez, R., Monks, S., Feng, W., Brauer, P. and von Glasow, R.: A global model of tropospheric chlorine chemistry: Organic versus inorganic sources and impact on methane oxidation, J. Geophys. Res. Atmospheres, 121(23), 2016JD025756, doi:10.1002/2016JD025756, 2016.

Joshi, N., Romanias, M., Riffault, V. and Thévenet, F.: Investigating water adsorption on natural mineral dust particles: A DRIFT and BET theory study, under press, Aeolian Research, 2017.

Journet, E., Balkanski, Y. and Harrison, S. P.: A new data set of soil mineralogy for dust-cycle modeling, Atmos Chem Phys, 14(8), 3801–3816, doi:10.5194/acp-14-3801-2014, 2014.

Kaly, F., Marticorena, B., Chatenet, B., Rajot, J. L., Janicot, S., Niang, A., Yahi, H., Thiria, S., Maman, A., Zakou, A., Coulibaly, B. S., Coulibaly, M., Koné, I., Traoré, S., Diallo, A. and Ndiaye, T.: Variability of mineral dust concentrations over West Africa monitored by the Sahelian Dust Transect, Atmospheric Res., 164–165, 226–241, doi:10.1016/j.atmosres.2015.05.011, 2015.

Kandler, K., SchÜTz, L., Deutscher, C., Ebert, M., Hofmann, H., JÄCkel, S., Jaenicke, R., Knippertz, P., Lieke, K., Massling, A., Petzold, A., Schladitz, A., Weinzierl, B., Wiedensohler, A., Zorn, S. and Weinbruch, S.: Size distribution, mass concentration, chemical and mineralogical composition and derived optical parameters of the boundary layer aerosol at Tinfou, Morocco, during SAMUM 2006, Tellus B, 61(1), 32–50, doi:10.1111/j.1600-0889.2008.00385.x, 2009.

Lafon, S., Rajot, J.-L., Alfaro, S. C. and Gaudichet, A.: Quantification of iron oxides in desert aerosol, Atmos. Environ., 38(8), 1211–1218, doi:10.1016/j.atmosenv.2003.11.006, 2004.

Lafon, S., Sokolik, I. N., Rajot, J. L., Caquineau, S. and Gaudichet, A.: Characterization of iron oxides in mineral dust aerosols: Implications for light absorption, J. Geophys. Res. Atmospheres, 111(D21), D21207, doi:10.1029/2005JD007016, 2006.

Linke, C., Möhler, O., Veres, A., Mohácsi, Á., Bozóki, Z., Szabó, G. and Schnaiter, M.: Optical properties and mineralogical composition of different Saharan mineral dust samples: a laboratory study, Atmos Chem Phys, 6(11), 3315–3323, doi:10.5194/acp-6-3315-2006, 2006.

Moreno, T., Querol, X., Castillo, S., Alastuey, A., Cuevas, E., Herrmann, L., Mounkaila, M., Elvira, J. and Gibbons, W.: Geochemical variations in aeolian mineral particles from the Sahara–Sahel Dust Corridor, Chemosphere, 65(2), 261–270, doi:10.1016/j.chemosphere.2006.02.052, 2006.

Mortier, A., Goloub, P., Derimian, Y., Tanré, D., Podvin, T., Blarel, L., Deroo, C., Marticorena, B., Diallo, A. and Ndiaye, T.: Climatology of aerosol properties and clear-sky shortwave radiative effects using Lidar and Sun photometer observations in the Dakar site, J. Geophys. Res. Atmospheres, 121(11), 2015JD024588, doi:10.1002/2015JD024588, 2016.

Müller, T., Schladitz, A., Massling, A., Kaaden, N., Kandler, K. and Wiedensohler, A.: Spectral absorption coefficients and imaginary parts of refractive indices of Saharan dust during SAMUM-1, Tellus B, 61(1), 79–95, doi:10.1111/j.1600-0889.2008.00399.x, 2009.

Petzold, A., Rasp, K., Weinzierl, B., Esselborn, M., Hamburger, T., Dörnbrack, A., Kandler, K., Schütz, L., Knippertz, P., Fiebig, M. and Virkkula, A.: Saharan dust absorption and refractive index from aircraft-based observations during SAMUM 2006, Tellus B, 61(1), 118–130, doi:10.1111/j.1600-0889.2008.00383.x, 2009.

Schladitz, A., Müller, T., Kaaden, N., Massling, A., Kandler, K., Ebert, M., Weinbruch, S., Deutscher, C. and Wiedensohler, A.: In situ measurements of optical properties at Tinfou (Morocco) during the Saharan Mineral Dust Experiment SAMUM 2006, Tellus B, 61(1), 64–78, doi:10.1111/j.1600-0889.2008.00397.x, 2009.

Slingo, A., Bharmal, N. A., Robinson, G. J., Settle, J. J., Allan, R. P., White, H. E., Lamb, P. J., Lélé, M. I., Turner, D. D., McFarlane, S., Kassianov, E., Barnard, J., Flynn, C. and Miller, M.: Overview of observations from the RADAGAST experiment in Niamey, Niger: Meteorology and thermodynamic variables, J. Geophys. Res. Atmospheres, 113(D13), D00E01, doi:10.1029/2008JD009909, 2008.

Val, S., Liousse, C., Doumbia, E. H. T., Galy-Lacaux, C., Cachier, H., Marchand, N., Badel, A., Gardrat, E., Sylvestre, A. and Baeza-Squiban, A.: Physico-chemical characterization of African urban aerosols (Bamako in Mali and Dakar in Senegal) and their toxic effects in human bronchial epithelial cells: description of a worrying situation, Part Fibre Toxicol, 10(10), 2013.

Ververis, C., Georghiou, K., Christodoulakis, N., Santas, P. and Santas, R.: Fiber dimensions, lignin and cellulose content of various plant materials and their suitability for paper production, Ind. Crops Prod., 19(3), 245–254, doi:10.1016/j.indcrop.2003.10.006, 2004.

Wankhede, D. B., Shehnaj, A. and Rao, M. R. R.: Carbohydrate composition of finger millet (Eleusine coracana) and foxtail millet (Setaria italica), Qual. Plant., 28(4), 293–303, doi:10.1007/BF01095511, 1979.

Wienecke, J., Kruse, H. and Wassermann, O.: Organic compounds in the waste gasification and combustion process, Chemosphere, 25(4), 437–447, doi:10.1016/0045-6535(92)90277-X, 1992.

Zotter, P., Herich, H., Gysel, M., El-Haddad, I., Zhang, Y., Močnik, G., Hüglin, C., Baltensperger, U., Szidat, S. and Prévôt, A. S. H.: Evaluation of the absorption Ångström exponents for traffic and wood burning in the Aethalometer-based source apportionment using radiocarbon measurements of ambient aerosol, Atmos Chem Phys, 17(6), 4229–4249, doi:10.5194/acp-17-4229-2017, 2017.

Journal: ACP
Title: Chemical characterization and source apportionment of submicron aerosols measured in Senegal during the 2015 SHADOW campaign
Author(s): Laura-Hélèna Rivellini et al.
MS No.: acp-2016-1127

The authors want to thank Reviewer #3 for his/her helpful comments. They are addressed below in blue. Changes in the manuscript are written in red.

Anonymous Referee #3

Overview:

This manuscript presented the highly-time resolved chemical characterization and source apportionment of atmospheric submicron aerosol particles (PM1) in West Africa, along with field on-line measurements (including an ACSM and a 7-wavelength aethalometer) and offline model analysis. The campaign was deployed under the environment affected by anthropogenic emissions (e.g., traffic, cooking, and biomass burning) and natural sources (e.g., desert dust and marine air masses), etc.. The results showed that the ten times lower average concentrations of NR-PM1 were observed here compared to the results from other megacities with persistent air pollution issues, i.e., Beijing and Paris. Sea breeze phenomena and Saharan desert dust outbreaks may lead to pollution events with high concentrations of PM10 (up to 900 µg/m3). Organic matter (OM) and sulfate could dominate the major fraction of aerosol particles when air massed could be associated to different influences, i.e., continental and sea breeze and oceanic region related. The authors also estimated the mass concentrations of particulate Fe from the Aethalometer data, for which an average contribution (4.6%) of Fe to PM1 was obtained. A new organic aerosol factor (LCOA), Local Combustion Organic Aerosol, was resolved by PMF analysis, with relatively low contribution (3%). Both regional and local photochemistry processes could contribute the formation of oxygenated organic aerosols in this area. The results seem to be interesting. The manuscript is well written and organized. I would recommend this paper could consider to be published in ACP once the following comments are addressed.

Specific comments:

1. Page 4, line 30: Should keep the same abbreviations for those species throughout the manuscript. For example, what's the different between "NO3-" and "NO3" (Page 5 and line 5), and somewhere else "SO42-" and "SO4", "Cl-", "Cl" and "Chl", etc.. If they are different for the discussion in this manuscript, please the authors give the related text to explain them.

Author's response: As suggested we have harmonized the nomenclature regarding the sum of nitrate (NO_x, ONO_x…), ammonium (NH_x), sulfate (SO_x, H_ySO_x) and chloride (Cl, HCl) related fragments. The SO_4^{2-}, NO_3^- and Cl^- ions are only used in the neutralization equation.

Changes in the manuscript:

Page 4 lines 29-31: "Non-refractory species, such as organic matter (OM), sulfate (SO_4), nitrate (NO_3), ammonium (NH_4) and non-refractory chloride (Chl), are vaporized at this temperature and then ionized by electron impact (70 eV). The abovementioned names of the different NR species correspond to the sum of all m/z fragments related to one given species in the fragmentation table (Allan et al., 2004), that is to say $H_{0\leq x\leq 2}S_{0\leq y\leq 1}O_{0\leq z\leq 4}$ for sulfate, $NH_{0\leq x\leq 2}$ for ammonium, $NO_{0\leq x\leq 2}$ and HNO_3 for nitrate, and $H_{0\leq x\leq 1}Cl$ for chloride."

2. Page 5, line 3: It was interesting to perform the chloride calibration with ammonium chloride particles. Could the authors also present the related calibration results in supporting information, as showing in Fig. S1, since your RIEChl is much higher than the default value (1.3). In addition, did the authors try to validate chloride data based on your calibration results? It's also interesting to know how it works about the chloride calibration.

Author's response: Chloride RIE calibrations (relative to nitrate) were performed using the same methodology as for ammonium nitrate and sulfate calibrations. A monodisperse aerosol at 300 nm was generated from an aqueous solution of NH_4Cl (> 99.8%, Merck) at 5×10^{-3} mol L^{-1}. The fragments at m/z 15, 16 and 17 were taken into account to determine the concentration of NH_4 whereas those at 35, 36, 37 and 38 were used for Chl.
Chl concentrations (in µg m^{-3}) were then calculated using the following equation:

$$\mathrm{Chl} = N_{CPC} \times \mathrm{S} \times \mathrm{V_{part}} \times \rho \times \frac{\mathrm{M}(Cl^-)}{\mathrm{M}(\mathrm{NH_4Cl})}$$

where N_{CPC} is the number concentration given by the CPC in particles per cm^3, S the shape factor (taken as 1), V_{part} the particle volume (in cm^3) corresponding to 300 nm and assuming spherical shape, ρ the ammonium chloride density (1.53 g cm^{-3}), M(X) the molar mass in g mol^{-1}.
Using the ratio of the slopes obtained by plotting the sum of Chl signals vs Cl mass, and the similar plot for NH_4, combined with RIE(NH_4), allows to retrieve RIE(Chl) through the following equation:

$$\mathrm{RIE}(Chl) = \mathrm{RIE}(Chl/NH_4) \times \mathrm{RIE}(NH_4/NO_3)$$

with RIE(Chl/ NH_4) and RIE(NH_4/NO_3) mean values of 0.39 ± 0.04 and 5.72 ± 0.55, respectively, we obtained RIE(Chl) = 2.26 ± 0.02.
Comparing this value with external chloride calibrations is tricky since only non-refractory chloride can be detected by AMS/ACSM techniques, whereas most chloride ambient analyses (using ion chromatography for instance) would be dominated by (refractory) sea-salt chloride. Furthermore, NR-Chl tend to be rather low at most sites and therefore has not been a major concern in the AMS/ACSM community so far.

Changes in the manuscript: An example of chloride calibration with NH_4Cl has been added in the supplementary (Figure S1e). Page 5 line 7 now reads: "S1(a-e)".

3. Page 7, line 32: Would it be possible that the authors could give uncertainties of estimated Fe concentrations with this method for your study?

Author's response: Indeed the uncertainties on estimated Fe concentrations can be calculated by applying the propagation for uncertainties on the values of K_{Fe} (10%) and the slope b (39%, calculated using a variability of 0.2 for β and α (Fialho et al., 2006)), which gives an overall uncertainty of ~40%. However this method is highly sensitive to even small variations of α (BC) and β (DD), with values quite well known for BC from fossil fuel ranging from 0.8 to 1.1 (Hansen, 2005; Zotter et al., 2017 and references therein) but not so much for dust. In the manuscript, we chose to use β = - 4, according to Fialho et al. (2006) values determined at the Azores Islands for samples influenced by Saharan dust events. But other values can be found in the literature (Table R1), ranging from -1.6 to -6.5 and largely influenced by the wavelength range as well as dust origins and size fractions since the iron content differ depending on emission sources and particle size (Journet et al., 2014). Even during the SAMUM campaign (May to June 2006 in Morocco), a wide range of AAE values have been reported from 1.6 up to 5.1 for ground-based measurements in the same size fraction, as shown in Table R1.

Table R1. Mineral dust AAE values reported from field campaigns around the Saharan region.

Reference	Location / Period	Wavelengths (nm)	Fraction	β
Fialho et al. (2006) [a]	Azores Islands Jul. 2001 – Jun. 2005	370-950	-	-4
Müller et al. (2009) [a]	Tinfou, Morocco (SAMUM) Summer 2006	467/660	PM_{10}	-2.25 to -5.13
Petzold et al. (2009) [b]	South-East Morocco (SAMUM) Summer 2006	467/660	$PM_{2.5}$	-2 to -6.5
Schladitz et al. (2009) [a]	Tinfou, Morocco (SAMUM) Summer 2006	537/637	PM_{10}	-1.6 to -4.73
(Linke et al., 2006) [c]	Morocco Egypt	266/532	~PM_4	-4.2 -5.3
(Caponi et al., 2017) [c]	Morocco Lybia Algeria Mali	375-850 375-532 375-850 375-532	$PM_{2.5}$ ($PM_{10.6}$)	-2.6 -4.1 (-3.2) -2.8 (-2.5) -3.4

[a] In situ ground-based measurements; [b] Airborne measurements through dust plumes; [c] Laboratory experiments with resuspended soil samples

Therefore applying a relatively small increase (resp. decrease) of 10% on the value of β for our dataset led to a 33% decrease (resp. 50% increase) of iron concentrations, as shown in Figure R1, but no change in the temporal behavior.

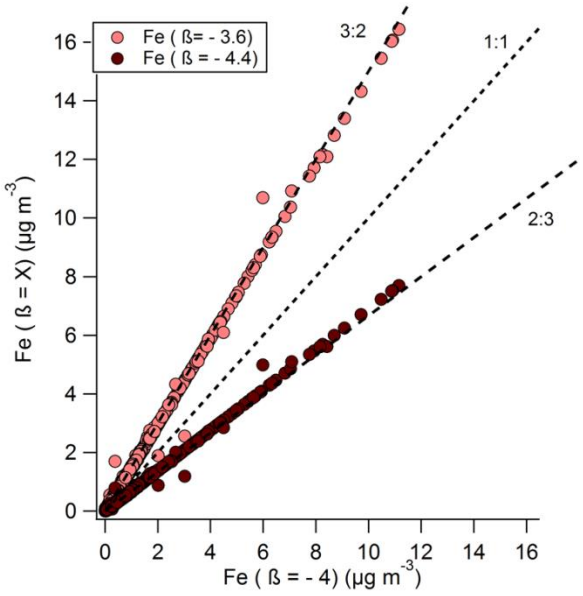

Figure R1. Scatter plot of iron concentrations (in µg m^{-3}) obtained from Fialho's deconvolution method using an AAE value of ± 10% compared to the one from the literature and used in the manuscript.

Changes in the manuscript:

A new appendix (S2) in the Supplementary Information now includes this whole discussion. Changes in the main text have been also done page 8, line 18 with a new sentence added: "Applying the propagation for uncertainties approach on the values of K_{Fe} (10%) and the slope b (39%, calculated using a variability of 0.2 for α and β (Fialho et al., 2006)) gives an overall uncertainty of ~40% for iron concentrations. However the deconvolution algorithm is highly sensitive to the values of the Angström absorption exponents (α and β) and a more detailed discussion can be found in Appendix S2."

4. Page 8, line 19: In this paragraph, I suggest that the authors could consider to also mention some brief information about ME-2 algorithm how it works for constraining organic aerosol factors (Canonaco et al., 2013), since this will be helpful and easier for readers to quickly understand the SoFi how it works in this study.

Changes in the manuscript: Page 9 lines 4, sentence added at the end of the paragraph: "In case of mixed (known) factors, the solution can be furthermore constrained by imposing reference factor profiles (F, from the literature) as inputs. The user can apply those constraints with a certain degree of freedom defined by a scalar a-value ranging from 0 (no degree of freedom) up to 1 (totally unconstrained)."

5. Page 10, line 20: The authors should consider to explain which kind of combustion sources for the ACSM m/z 57 tracer is. When I am reading here, I immediately realized that why the authors did not perform the source apportionment of black carbon by using the Aethalometer model (Sandradewi et al., 2008). As described in Section 2.1, there are both traffic and biomass-burning emissions that would potentially contribute the ambient black carbon burden at this sampling site. So, is it possible to identify blackcarbon aerosols related to traffic and biomass-burning emissions here? This will be very helpful for the source apportionment of organic aerosol.

Author's response: m/z 57 is mostly the $C_4H_9^+$ fragment, which has been linked to combustion sources, and is one of the key fragments in HOA and COA spectra but appears as well in the BBOA one without being the main tracer (Ng et al., 2011a).
As to the second part of the comment, although biomass burning (BB) events can sometimes be observed in the region, no BB aerosols were detected during IOP-1 as mentioned in section 2.3.2. That was in fact the first condition required to apply the deconvolution method from Fialho et al. between BC from fossil fuel and Fe from mineral dust. Using this method does assume that no brown carbon (BrC) is present since the Angström absorption exponent (AAE) for BC is taken as the one from fossil fuel (AAE ~ 1).
On the other hand, the method proposed by Sandradewi et al. (2008) assumes that absorbing particles are only BC from fossil fuel or wood burning sources, and that there is no significant absorption from dust, which we know to be untrue at the M'Bour site. Therefore, as both dust and BC from wood burning absorb in the shortest wavelengths, the two models cannot be applied at the same time unless we could have constrained the time profile of each source with external tracers. In the absence of external data, a three-factor deconvolution has been tried but would still be highly hypothetical and therefore is not presented here.
Anyway, during the campaign, mineral dust was clearly present, sometimes at high concentrations, whereas sources of BrC were almost unsignificant. Therefore we chose to exclude the very few periods when BrC could be suspected to influence our measurements (1% of the data) and therefore the empirical deconvolution using Fialho's algorithm.

Changes in the manuscript:
Page 10 lines 19-20, sentence modified: "The higher concentrations can be attributed to local anthropogenic combustion processes as BC concentrations present a significant correlation (r = 0.79) with the ACSM m/z 57 tracer of all types of combustion."

Page 7 line 36 – page 8 line 1, sentence now reads: "As mentioned by Fialho et al. (2014), this method allows to estimate elemental iron concentrations only in the absence of brown carbon since an absorption Angström exponent of 1 (which correspond to fossil fuel BC) is applied. Therefore, other methods, such as the one proposed by Sandradewi et al. (2008) to deconvolve BC from fossil fuel and biomass burning, cannot be used in our conditions."

6. Page 11, line 3: Here is a little bit confusion about the ratio of Fe/PM10, since your Fe concentrations were estimated by the PM1 aethalometer, but not PM10 Fe. Is this the case? If yes, the

authors could consider to add "PM1" in front of "Fe" when you discuss this ratio in the main text of the manuscript.

Author's response: Indeed Fe was deconvolved from PM_1 absorption measurements and we agree that using the Fe/PM_{10} ratio was confusing. We have now removed these direct comparisons and focused on the only available study for which we could derive Fe/DD_{PM1} in Dakar, Senegal, although in the absence of significant dust events. We only use the Fe/DD ratios found in the literature to emphasize the influence of the size fraction on the iron contribution to DD since most of it can be found in the clay fraction (~$PM_{2.5}$; Journet et al., 2014; Kandler et al., 2009), as part of Appendix S2.

Changes in the manuscript:
Page 11 lines 3-13: "From the only study in the literature focusing on iron concentrations in the submicron fraction in West Africa (Val et al., 2013), we could infer an elemental iron contribution of 7.8% to PM_1 dust, in Dakar, in the absence of dust events. Other studies focused on dust gave the iron contribution for size fractions higher than PM_1, thus no straightforward comparisons can be made with our average ratios of Fe/DD_{PM1} (20, 23, 21 and 16% for respectively IOP-1, continental, sea breeze and marine days). It can nevertheless be interesting to have in mind values retrieved within the same region as it is known that iron oxides mainly belong to the finest fraction (Journet et al., 2014; Kandler et al., 2009) and therefore the elemental iron contribution should be lower for larger sizes, which is consistent with values reported in Table S2.2."

Table S2.2: Comparison of iron content (in %) determined in Saharan dust and soil samples

Reference	Location	Method [a]	Size fraction	%Fe [b]
Dust samples				
(Lafon et al., 2004)	Banizoumbou (Niger)	XRF; CBD	TSP	6.3; 7.8
(Lafon et al., 2006)	Banizoumbou,	XRF; CBD	TSP	4.3 – 6.1
(Lafon et al., 2006)	Cape Verde	XRF; CBD	TSP	5.3 – 6.0
(Formenti et al., 2008)	Banizoumbou	CBD	40 µm	5.8
(Val et al., 2013)	Dakar (Senegal)	ICP-MS	1 µm	7.8
This work	M'Bour	cf. text	1 µm	23 (continental) 21 (sea breeze) 16 (marine)
Soil samples				
(Moreno et al., 2006)	Saharan region (9 samples)	ICP-AES/ ICP-MS	TSP	2.0 – 4.7
(Lafon et al., 2006)	Banizoumbou,	XRF; CBD	10.2 µm [*] 2.5 µm [*]	5.3 5.8
(Joshi et al., 2017)	M'Bour, Bordj (Algeria), Nefta (Tunisia)	XRD	100 µm	< 0.5

[a] XRF: X-ray Fluorescence (XRF) Spectrometry for elemental analysis; CBD: chemical method based on citrate-bicarbonate-dithionite (CBD) reagent for quantification of iron oxides adapted from soil analysis (Mehra and Jackson, 1960)
[b] Percentages of iron relative to the mass of all oxides, classically taking into account Na_2O, MgO, Al_2O_3, SiO_2, K_2O, CaO, TiO_2 and Fe_2O_3.
[*] Soil samples resuspended using wind tunnel and collected with a 13-stage impactor

7. Page 11, lines 27-28: Why didn't the authors consider to give the contribution of chloride to total NR-PM1? I suggest the authors could also mention it.

Changes in the manuscript: The contribution of chloride (~1%) was added page 11 line 28.

8. Page 11, lines 32-34: Is there evidence to support this discussion? Otherwise, the authors should give related reference(s).

Author's response: We have now lengthened the discussion on that point, plus corrected a typo (SO_4 and not SO_2).

Changes in the manuscript:
Page 11 line 30: "In our case these differences could be explained both by the semi-volatile nature of NH_4NO_3 combined with the limited use of fertilizers that prevent NH_3 emissions and ammonium nitrate formation, and more sources of non sea salt(nss)-SO_4 such as marine DMS oxidation processes. The first point can be assessed by emission inventories that provide annual NH_3 emissions (in 2010) of 53 kT in Senegal against 870 kT in France and 204 kT in the Netherlands (source EC-JRC/PBL. EDGAR version 4.2. http://edgar.jrc.ec.europa.eu/, 2011). nss-SO_4 comes from secondary origin and has been investigated in PM_{10} at the Cape Verde Atmospheric Observatory (Fomba et al., 2014). This study showed increased concentrations of nss-SO_4 during dust events, linked to the oxidation of anthropogenic SO_2 transported by continental air masses. They also evidenced a seasonal variability of nss-SO_4 for marine air masses, increasing during summer, which was attributed to increased photochemistry and changes in the emission of dimethyl sulfide (DMS) due to higher biological activities in the ocean. This activity can be traced back using satellite data from AQUA/MODIS, in particular the algae concentrations along the Senegalese coast (Ocean biology processing group, 2003)."

9. Page 14, Section 3.2.1: It would be more convinced about the discussion on geographical origins, if the authors would also combine with some modeling methods, e.g., potential source contribution function (PSCF) that might be easily performed on highly-time resolved data (Petit et al., 2017). In addition, it could be also interesting to perform PSCF on organic aerosol factors.

Author's response: Indeed we have hopefully improved the discussion on geographical origins by adding a supplementary figure (Figures S5a-c) that presents: (i) back-trajectory clusters for the entire period and the different day categories (continental, sea breeze, marine); (ii) non-parametric wind regression (NWR) plots, which combine atmospheric concentrations with measured wind speed and direction for the different species and PMF factors; (iii) probability source contribution function (PSCF) maps for the variables presenting a regional origin according to the NWR plots.

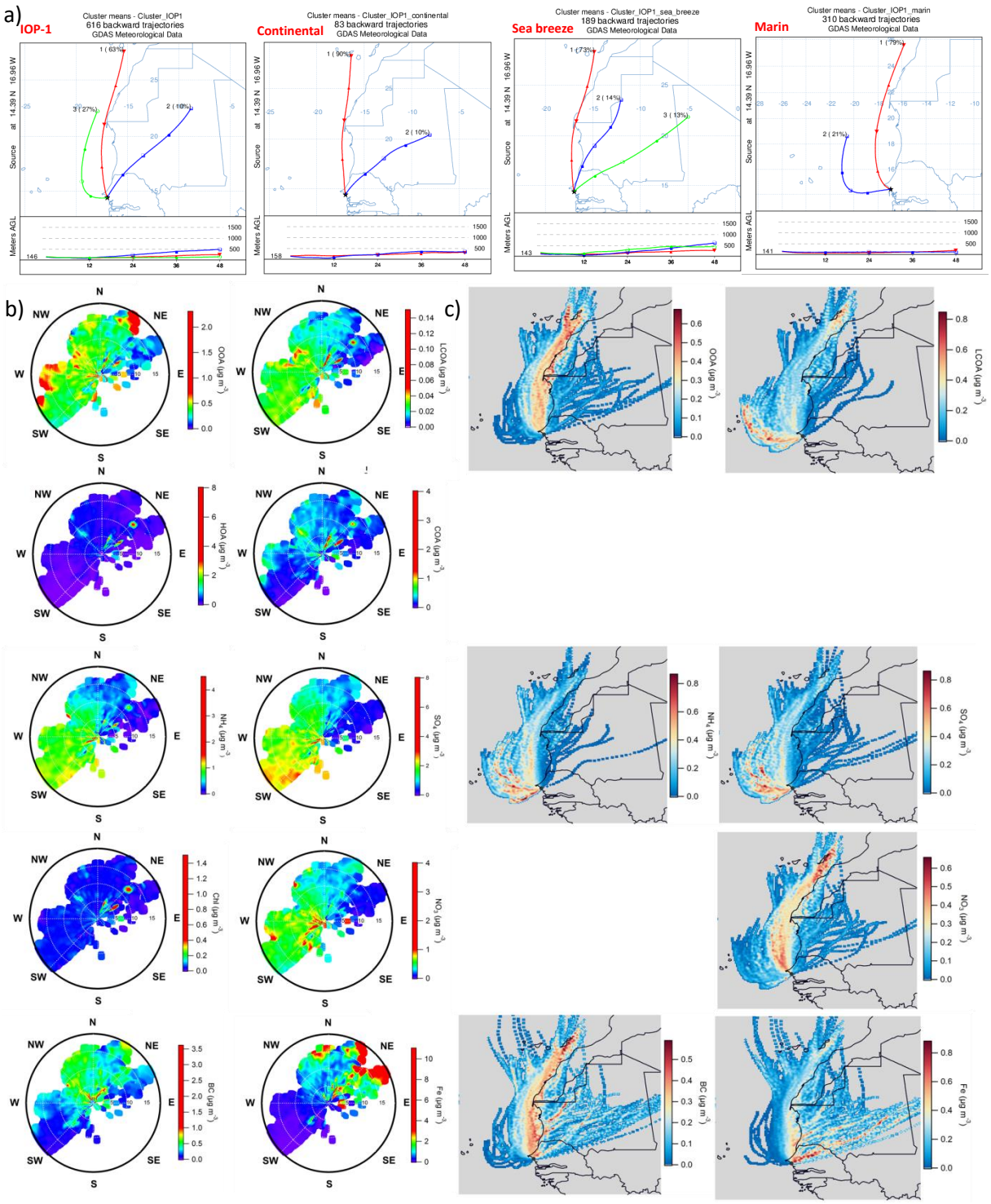

Figure S5. (a) 48-hour back trajectory clusters for (from left to right) IOP-1, continental, sea breeze and marine days. (b) NWR plots (input parameters: angular and radial resolution: 0.1, angle smoothing: 2, radial smoothing: 1; upper limit of the color scale: 75th percentile) for PMF factors and NR-PM$_1$, BC and Fe species and corresponding (c) PSCF maps for species showing regional influence (threshold: 75th percentile) during IOP-1.

Changes in the manuscript:

A new sub-section was added in the methodology section to introduce back-trajectory calculations, NWR plots and PSCF maps page 9 line 4:

"2.3.4. Geographical origins of air masses and chemical species

Air masses reaching the site were characterized through 48-hour back-trajectories (every 3 hours) retrieved from the computer version of the Hybrid Single-Particle Lagrangian Integrated Trajectory model (HYSPLIT; Draxler and Hess (1998)), for an altitude set at one half of the mixed layer depth and coupled with the GDAS (1 degree) meteorological database. Note that sea breeze phenomena, which occur at short time and spatial scales, cannot be satisfactorily reproduced by this type of model. However given the dynamics of sea breezes, only back-trajectories arriving on site at 3 pm and eventually at 6 pm during sea breeze days (< 8.2%) could not be representative of the ground dynamic observations. Therefore all the back-trajectories available for IOP-1 were kept and could be statistically grouped into clusters according to the variation of the total spatial variance, for the whole period and also by day type.

We also used pollution roses to identify local wind directions leading to high concentrations for each species or PMF factors, but also two additional tools provided by the ZeFir Igor-based package developed by Petit et al. (2017):
(i) Non-parametric regression (NWR, Henry et al. (2009)) plots, which combine smoothed surface concentrations and local wind speed and direction, to discriminate between local and more distant/regional sources;
(ii) Potential Source Contribution Function (PSCF, (Polissar et al., 2001)) maps for regional sources, which couple time series of one variable with air mass back-trajectories to redistribute the concentrations observed at the site into geographical emission parcels."

Page 14 line 28: "From back-trajectory analysis (Figure S5a) three different clusters were encountered during the whole period. The prevailing one (77% for the whole IOP-1; 91, 80 and 43% for continental, sea breeze and marine days, respectively) evidences air masses transported along the Western African coast and over Dakar. A second cluster corresponds to air masses purely originating from the ocean (19% of the total back-trajectories) and appeared as two clusters during marine days. A last cluster coming from the Saharan desert contributes only 4% of the IOP-1 air masses but reaches 9 and 10% for the continental and sea breeze days, respectively."

Page 14 line 31: "NWR plots and PSCF maps can be found in Figure S5b and S5c, respectively."

Page 14 line 34: "BC and NO_3 both exhibit local and regional influences, as suggested by their NWR plots (Figure S5b). The corresponding PSCF maps (Figure S5c) indicate regional background concentrations could come from anthropogenic emissions from Dakar (~1 million inhab. within city limits and ~3 in the metropolitan area) and possibly from maritime traffic along the Western African coast."

Page 15 line 5: "These species may also be released by anthropogenic activities in distant cities like Dakar, whose emissions may be carried toward the ocean and brought back to M'Bour by western winds. This hypothesis is also supported by back-trajectory analysis (Figure S5a)."

Page 15 line 10: "Regarding the iron pollution rose and NWR plots reported in Figure 8 and Figure S5b, maxima are measured when the site is under the influence of NE winds. The NWR plot evidences both local emissions possibly linked to traffic resuspension of DD and a regional component, that the Fe PSCF map clearly attributes to the Saharan region."

Page 16 line 34: "The HOA rose plot shows marked peaks in the directions of the two open waste burning areas and of the fish-smoking area located northeast of the site in the outskirts of M'Bour. HOA and Chl NWR plots are very similar, which suggests either common sources or a mixture of both compounds in the air masses which resulted into a correlation of 0.64 between these two variables."

Page 17 line 29: "Besides the NWR plots of Chl (local influence) and LCOA (both local and regional) rather suggest the presence of chlorinated organics. The PSCF maps identify two possible origins, one clearly from the ocean that could be related to chlorine-driven photo-oxidation processes (Hossaini et

al., 2016) and the other linked to air masses carried over Dakar where similar massive anthropogenic emissions from waste burning could be expected from Mbeubeuss, the largest dumpsite in Senegal located 25 km north-east of Dakar along the coast, which receives 250,000 tons of garbage per year from the Dakar region (Cissé, 2012)."

Page 17 line 21: "whereas LCOA pollution rose and NWR plots clearly point out toward the local combustion areas already mentioned previously"

Page 18 line 11: "OOA might not be only emitted by long distant sources, as also suggested by its NWR plot (Figure S5b)"

Page 18 line 14: "(Figures 8 and S5b)"

Page 18 line 23: "As shown by the PSCF map (Figure S5c), higher OOA concentrations are associated to air masses that moved along the coast and could transport oxidized anthropogenic species to the receptor site."

10. Page 15, lines 24-25: Should "CnH2n-1" and "CnH2n+1" be "CnH2n-1+" and "CnH2n+1+", respectively?

Changes in the manuscript: The "+" charges have been added page 15 lines 24-25.

11. Page 15, line 13: Change "Source apportionment" to "Source apportionment of OM".

Changes in the manuscript: Page 15 line 13: the title has been changed.

12. Page 15, Section 3.2.2: The biggest question I have in this manuscript is about the PMF-OA solution.
1) Page 15, lines 15-17: Please the authors could also present the results of 3 – 10 factors from the PMF-free runs in supporting information.

Changes in the manuscript: The results of 3-10 factors from the PMF unconstrained runs are now available in Supporting Information (Figure S6.1).

A sentence has been added page 15 line 21: "This factor appeared constantly above 4 factors in the unconstrained runs from 3 to 10 factors (Appendix S6, Figure S6.1) and was associated with one of the OOA for the continental, sea breeze and marine 4-factor unconstrained solutions (Figure S6.2)".

(a) 3-factor solution

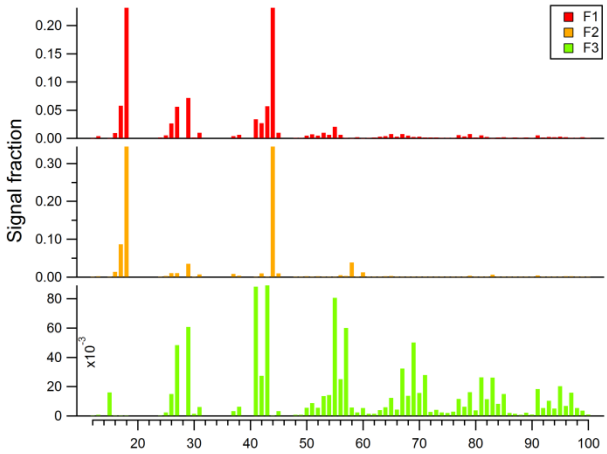

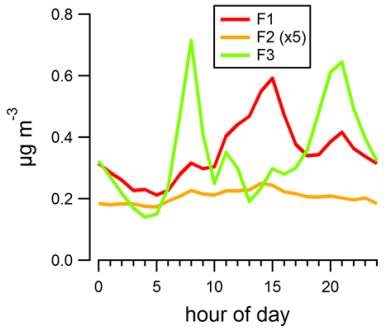

(b) 4-factor solution

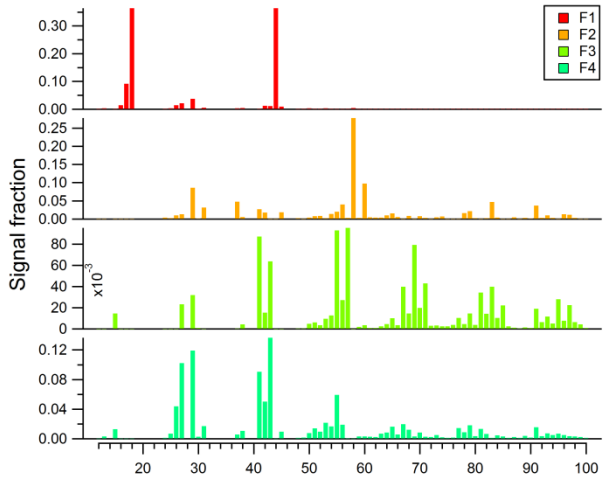

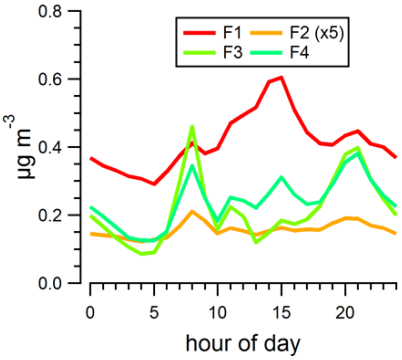

(c) 5-factor solution

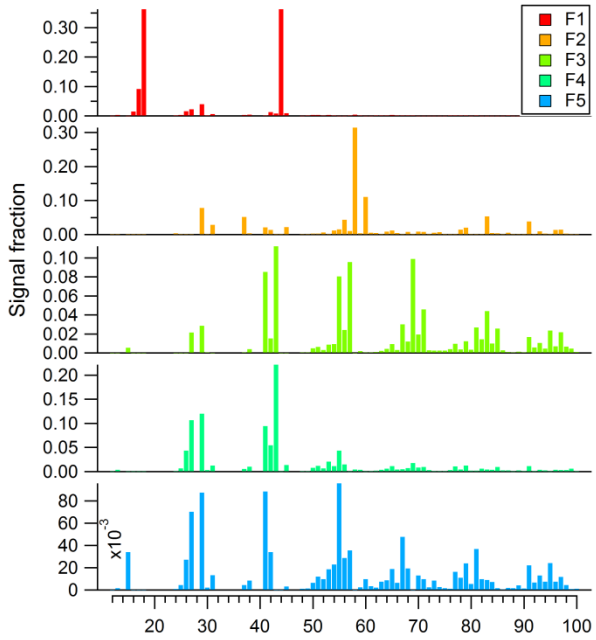

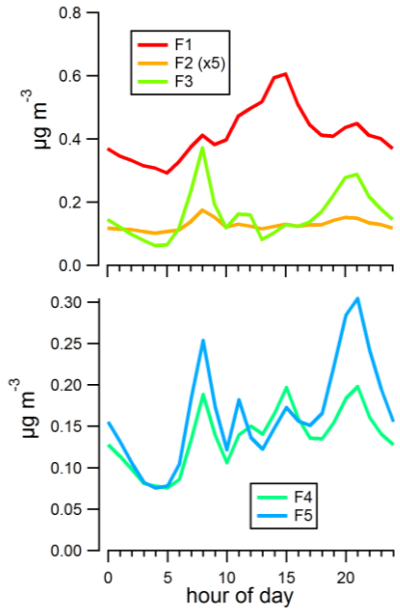

(d) 6-factor solution

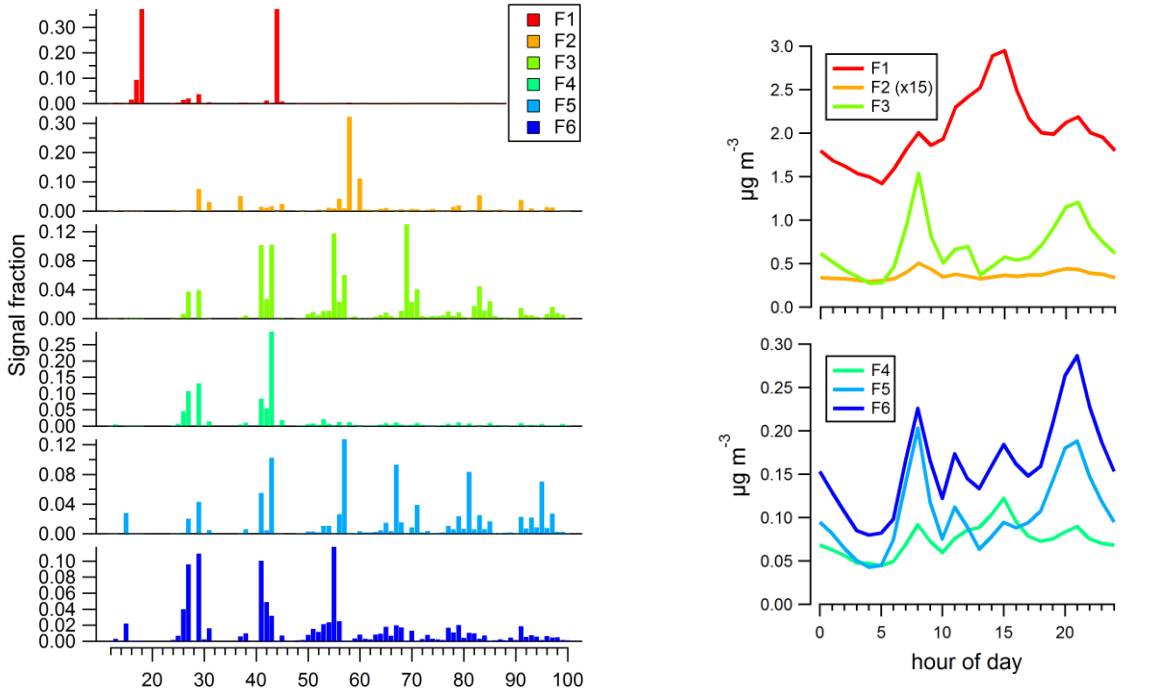

(e) 7-factor solution

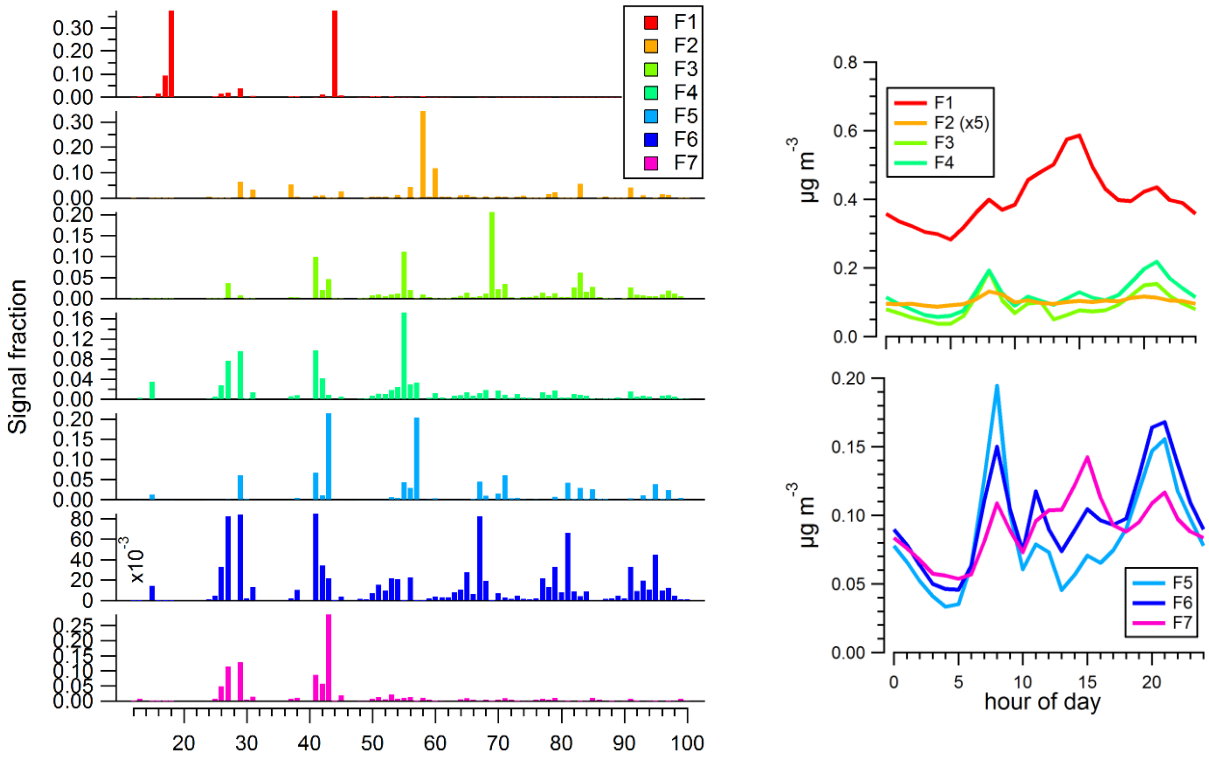

(f) 8-factor solution

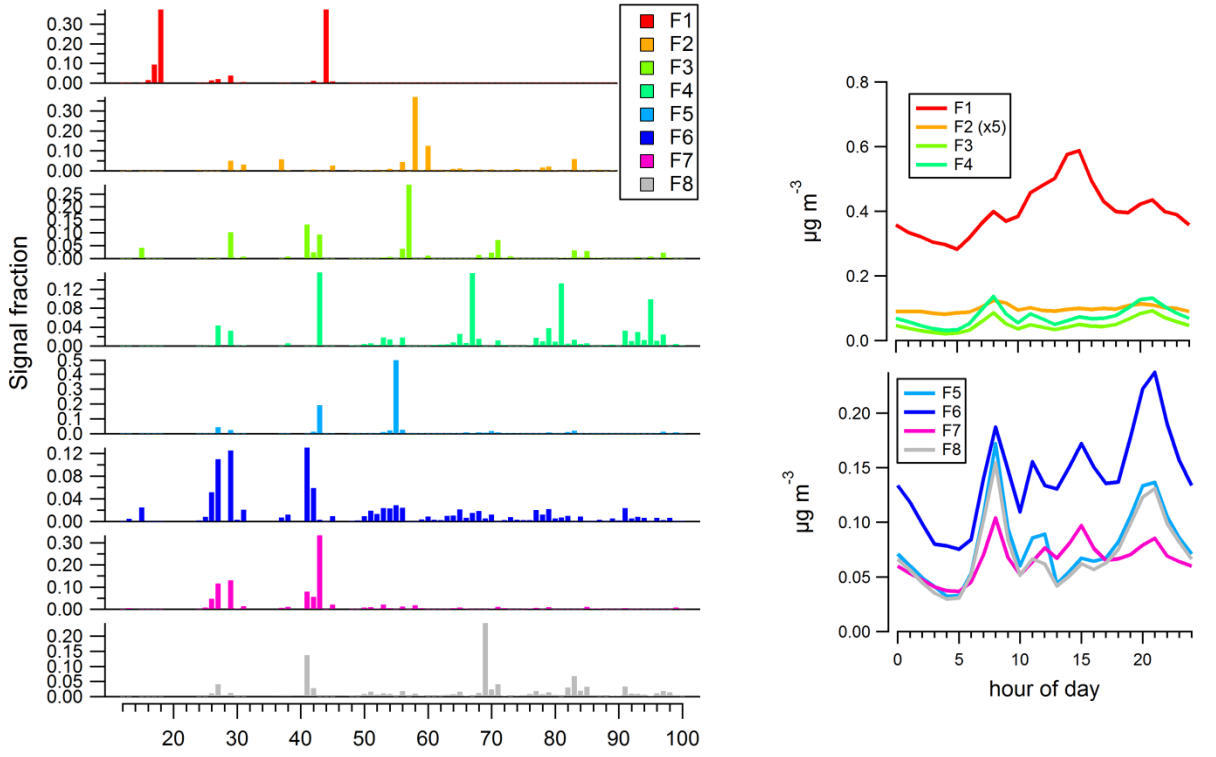

(g) 9-factor solution

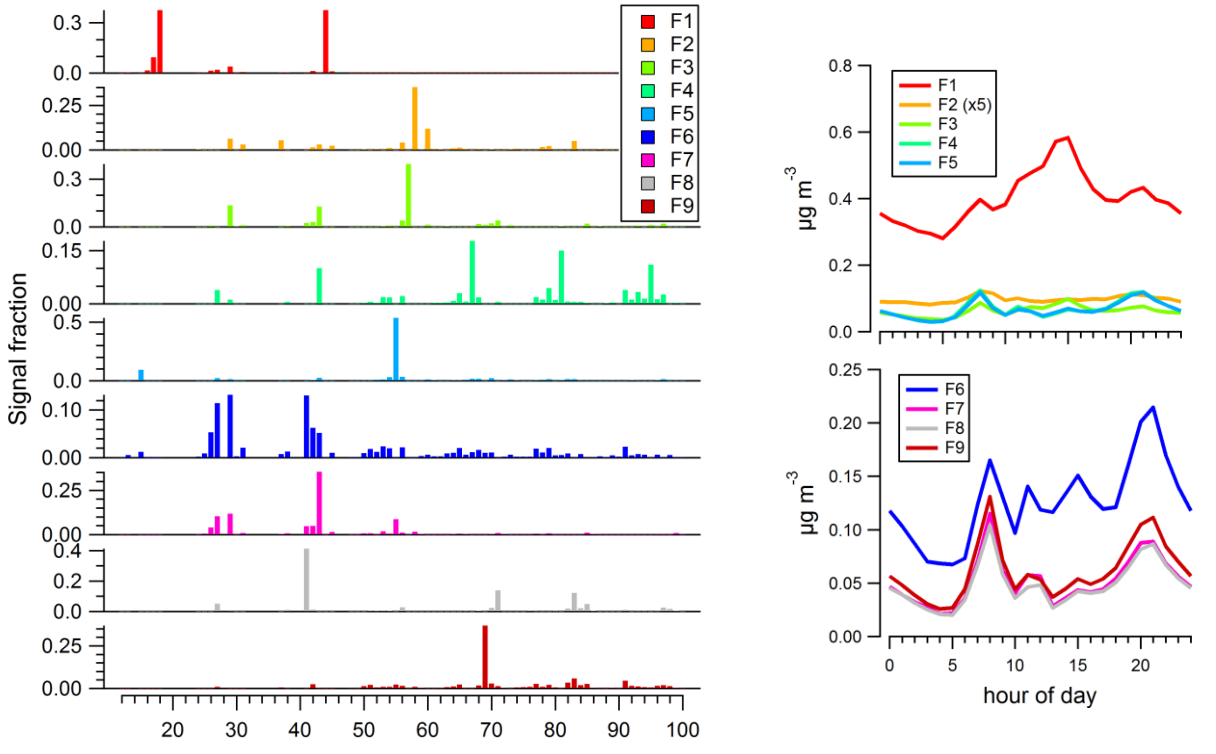

(h) 10-factor solution

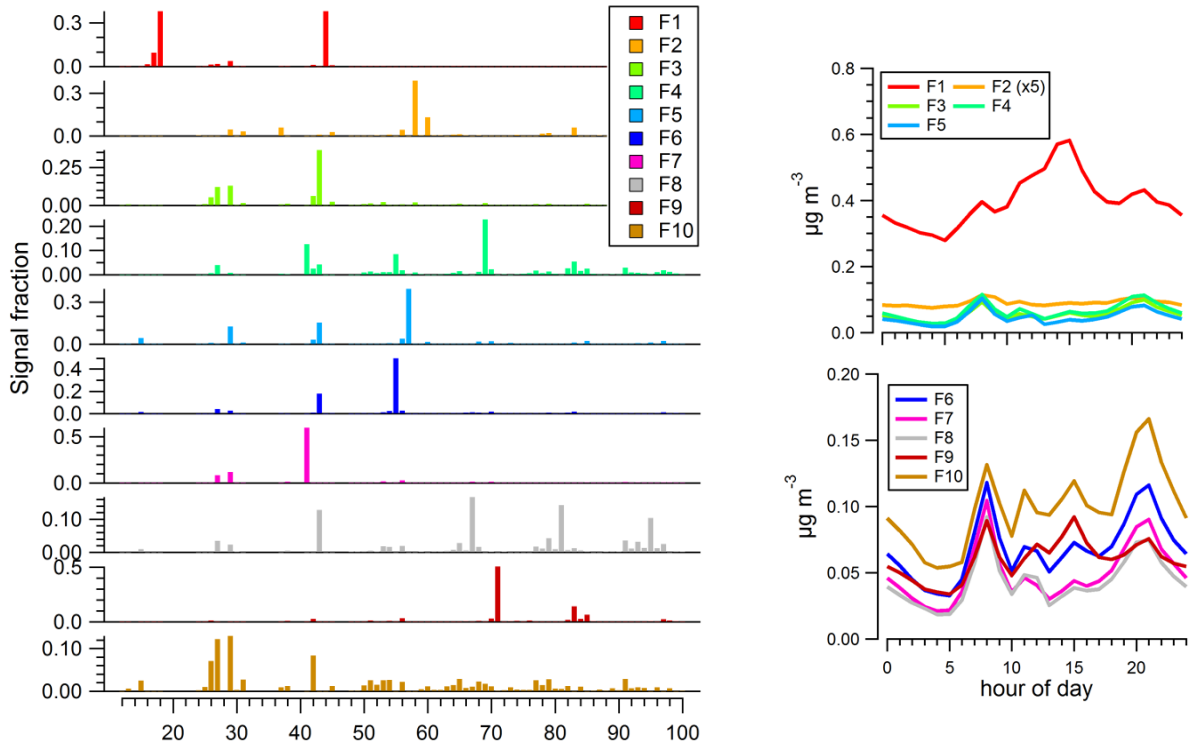

Figure S6.1. PMF unconstrained solutions from 3 to 10 factors, with (left) factor profiles and (right) corresponding daily cycles.

2) About the LCOA factor related to local open waste-burning emissions, did the authors try to compare it with any tracers? For example, please try to do some correlation analysis between LCOA with f60 (an AMS/ACSM biomass-burning tracer), f36 (as mentioned by the authors), and black-carbon aerosols from different sources, etc..

Author's response:

LCOA was compared with some tracers, as mentioned in section 3.2.2 (page 17 lines 14-16), namely Chl (r = 0.44), m/z 36 (r = 0.55) and 58 (r = 0.84).

LCOA correlation with m/z 60 remains moderate (r = 0.52), and when considering f_{36} (= mz36 / OA) and f_{60} (= mz60 / OA), correlations drop down to 0.16 and 0.25, respectively. No correlation is observed with BC (r = -0.02). We have also compared LCOA with m/z 39 (r = 0.29), which is commonly attributed to potassium ion K^+ but can be emitted by various sources including biomass burning, industrial processes and waste incineration (Olmez et al., 1988; Riffault et al., 2015; Simoneit, 2002; Vassilev et al., 2010).

The following figure shows scatter plots related to the above-mentioned correlations between LCOA and tracers.

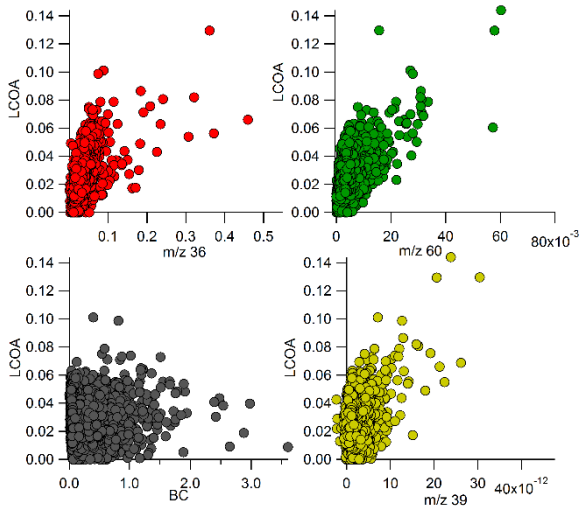

Figure R2. Scatter plots of LCOA vs. m/z 36, 60, BC (units are in μg m^{-3}) and m/z 39 (unit Amps).

At the same time, the authors did not find any reasonable BBOA profile instead of LCOA factor. Did the authors try to compare the LCOA profile with any BBOA related profiles? What's different from them?

Author's response: Figure R3 compares our LCOA profile from the 4-factor constrained solution with two BBOA profiles from the literature (Crippa et al., 2013; Ng et al., 2011b). The LCOA factor remains atypical with higher signals at m/z 37, 56, 60, 83, 91; and lower signals at m/z 15, 27, 41, 43, 55.

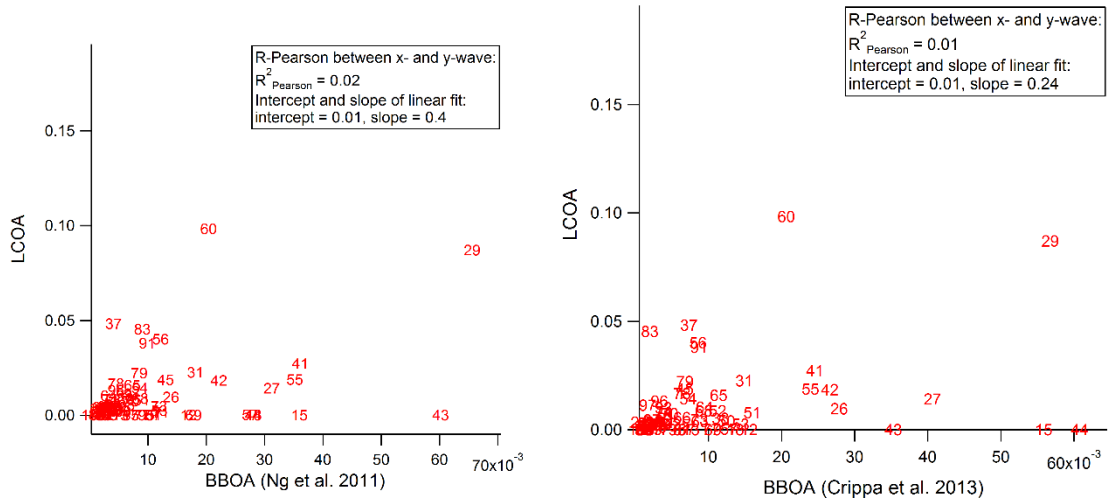

Figure R3. Scatter plots of LCOA m/z profile from the 4-factor constrained solution vs. two BBOA literature profiles, with marker symbols as m/z numbers.

And did the authors find any similar such mass spectrum of LCOA during your unconstrained runs and/or constrained HOA and COA runs, respectively? I am thinking whether the LCOA factor is a kind of splitted factors due to constrained HOA and COA? Could the authors give those results from your 3-10 factor runs and make comparison with your LCOA profiles.

Author's response: The 3-10 factor unconstrained solutions are now provided in Appendix S6 Figure S6.1 (cf. reply to comment 12). The LCOA factor consistently appears without constraints as a stable factor (F2) from 4 factors and more as shown in Figure S6.1.

Based on the results of Fig. S6, the constrained five-factor solution seems also good. Why didn't the authors choice this one for the finally PMF-factors solution?

Author's response: First, it should be emphasized that both solutions (the 4-factor mildly constrained one and the 5-factor strongly constrained one) lead to physically realistic modelling of the observations. As for any statistical source receptor model, there is no unique solution and therefore it is the responsibility of the user (based on one's modelling expertise and knowledge of the field site) that generally guides toward one solution over the other. This feature can indeed be a weakness since the user can drive the solution toward his/her preconceived expectations. Therefore the constraints should be ideally as low as possible and always consistent with other available information.
In order for our PMF solution to be comparable to other studies in the literature, we chose to present the 4 factor solution in the main text, for which more conventional model input data (that is to say only the organics matrix) were used with (i) profiles from the literature and (ii) mild constraints on the factor profiles. The 5-factor solution was obtained by using m/z 36 (HCl^+) as an additional input for the PMF m/z matrix, and strong constraints on all the primary OA profiles (HOA, COA and LCOA all taken from unconstrained runs and not from the literature). It nevertheless gives an interesting insight into the use of non-refractory Chloride species or fragments as possible tracers of specific activities not observed so far in previous studies, as well as an estimation of the attribution of a more oxidized (and therefore more regional) OOA (MO-OOA), and one that is rather locally formed due to enhanced photochemical processes (LO-OOA) and that is why we decided to present it in the Supplementary Information as well.

Did the authors also try to constrain all BBOA, COA, and HOA factors together to check the five-factor solution? And the authors could also try to just constrain BBOA and HOA factors to check the results. There is in factor that the BBOA factor/profile could be affected when HOA and COA factors were constrained together.

Author's response: The BBOA factor was constrained for different a-values, either alone or in combination with other primary factors (HOA/COA/LCOA) as mentioned in section 3.2.2 (page 15 line 36 to page 16 line 16) but no realistic profile or solution could be found.
Page 8, lines 1-5, we also reported the average f_{60} signal (0.3%) highlighting the absence of significant BBOA at the site.

3) In addition, could the authors explain why the median mass concentrations of COA and HOA show relatively similar diurnal variations (Fig. 9), and the similarly high peaks of HOA, COA, and LCOA around 8 am? I suggest that the authors could also make correlation analysis among HOA, COA, and LCOA each other in supporting information. In addition, the authors should also consider to perform the source apportionment of black carbon as mentioned above. It will be very useful to evaluate the PMF solution by checking the relationships between HOA, COA, and LCOA with black carbon from fossil fuel combustion and biomass burning, respectively.

Author's response: Weak correlations were obtained between HOA vs. LCOA and COA vs. LCOA with respectively r =0.20 and 0.38 while HOA vs. COA present a higher correlation (r=0.77). Indeed the morning wind conditions were really stable from day-to-day for continental and sea breeze days so air masses arriving at the site around 8 am were likely loaded with the three types of POA from the different combustion sources encountered in the NE direction. We have added some pictures of the three different sites identified as possible sources for the LCOA factor in Figure 1.
It can be noted also that the HOA and COA factors were hard to deconvolve because of this repetitive temporal dynamic pattern on continental days (as has already been shown for other datasets, e.g. Fröhlich et al., 2015) but they appeared without any constraints when running the PMF on sea breeze days (see Figure S6.2c, formerly Fig S4.1c) and were further used as anchors for the constrained PMF solutions. HOA was compared with BC (estimated using α = - 1 so mainly resulting from fossil fuel combustion) but we are not able to compare our factors with BC_{bb} (not retrievable using Fialho's

deconvolution, see reply to comment 5) and chose instead to use other tracers like m/z 36 or 58 for LCOA.

Changes to the manuscript: Pictures of three sites identified as contributing to the LCOA factor (Gandigal and Saly Douté open waste burning areas and a suburban fish-smoking site in M'Bour) were added to Figure 1.

Page 15 line 33: "(Figure 1 and Appendix S6, Figure S6.3)"

Page 18 line 6: "The hot temperatures and intense solar irradiation encountered in the region enhance these processes and can explain the major contribution (45%) observed for the OOA factor during IOP-1, and the predominance (~3/4) of the more-oxidized fraction in the solution presented in Appendix S8."

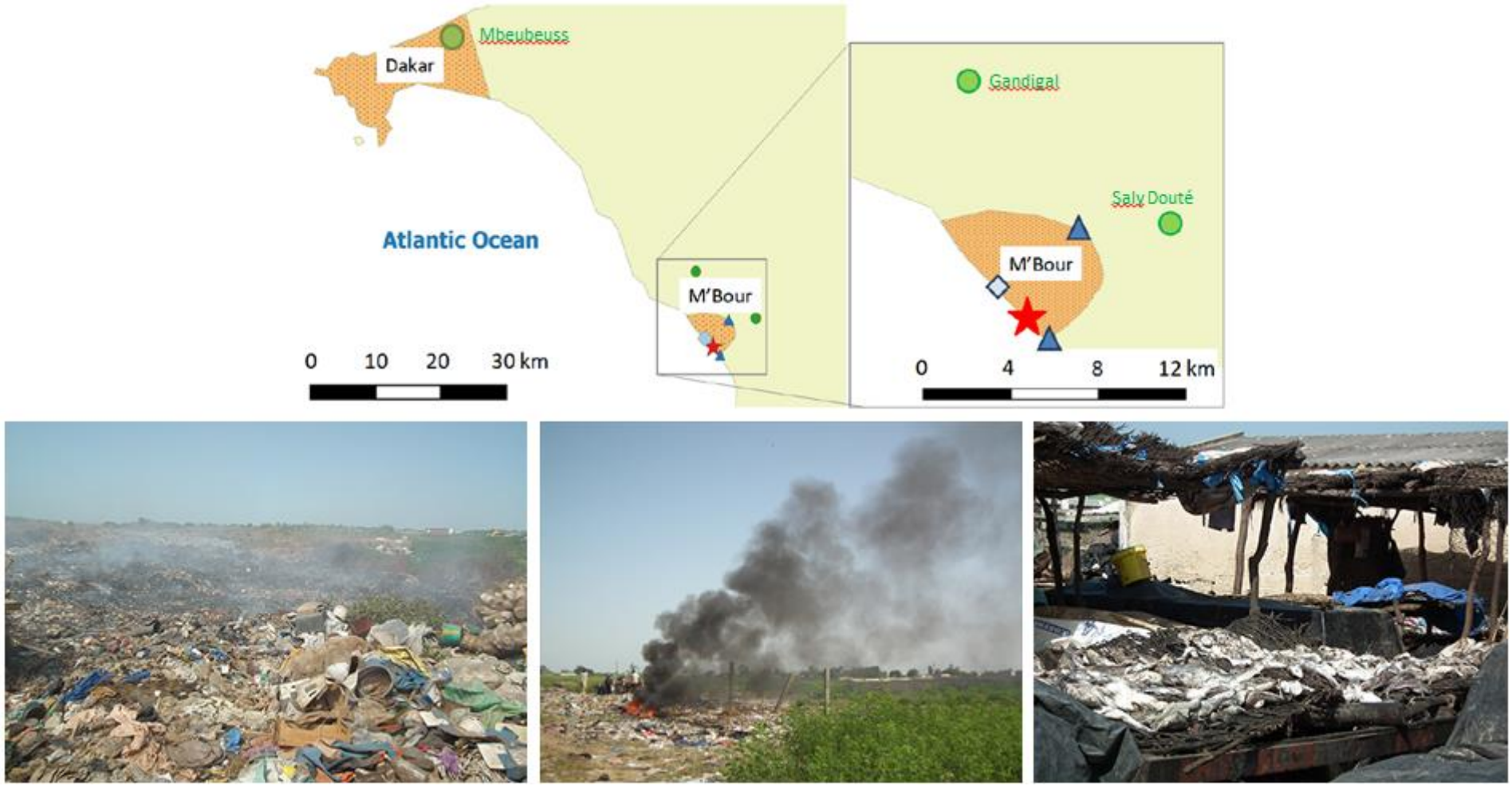

Figure1. (top left) Dakar and M'Bour locations with city delimitations in orange and (top right) local sources located around the IRD sampling site (red star), with open waste burning areas (green circles), fish-smoking sites (blue triangles) and the M'Bour port (light blue diamond). (bottom) Photographs of (from left to right) smoldering fire in the Gandigal open waste burning area; flaming fire in the Saly Douté open waste burning area; fish-smoking location (drying stage) in the suburb of M'Bour.

4) Why did the authors select a-value = 0.6 for both HOA and COA factors (Fig. 9)? I suggest that the authors could also perform the sensitivity test of a-values (e.g., from 0 to 1, with delta a = 0.1/0.05) on HOA and COA factors for your data sets. And why did the authors apply the reference mass spectrum of COA from HR-AMS (Crippa et al., 2013) for ME-2 constraining runs, but not from the ACSMs (Fröhlich et al., 2015;Ng et al., 2011)?

Author's response: We applied different combinations of a-values based on the approach described in Elser et al. (2016); the value of 0.6 was the one offering the best solution without using too strong constraints (in order not to drive the solution to what we are expecting). We also used this approach when constraining 1, 2, 3 or 4 primary factors at a time (LCOA, HOA, COA and BBOA). There were not many differences between both the Ng et al. (2011b) and Crippa et al. (2013) COA profiles especially as we used a-values between 0.3 and 0.9. It must be noted that in the intercomparison study of Fröhlich et al. (2015) mentioned by referee #3, the COA factor could not be deconvolved by Q-ACSMs without constraints and therefore the Crippa et al. (2013) factor obtained in a previous field campaign in Paris was used as the reference profile as well.

Please check "Ng et al., 2016" in the plot?

Changes in the manuscript: Fig 9 corrected from "Ng et al., 2016" to "Ng et al., 2011".

5) Page 18, lines 3-23: It would be also interesting to discuss the different types of OOA factor, i.e., LO-OOA and MO-OOA, as showing in Fig. S6. Why didn't the authors keep both them for OOA factors in the final PMF solution? The authors would consider to try to take a look at the relationship between OOA and Fe concentrations. This might make sense to find something new.

Author's response: In the 5-factor constrained solution presented in Appendix S6 of the submitted manuscript (now Appendix S8), two different kinds of OOA were obtained: one more oxidized (MO-OOA; 76.5% of OOA) and considered from a more regional origin (mostly marine as highlighted by its NWR plot and PSCF map in Figure R4 below) and the other less oxidized (LO-OOA; 23.5% of OOA), locally emitted as per its NWR plot. Nonetheless, without using m/z 36 as input and literature profiles for constraining HOA and COA none of the solution leads to two completely distinct OOA profiles. When comparing both LO-OOA and MO-OOA with Fe and BC, only low correlations ($r < 0.4$) were found between the different variables, except for LO-OOA and BC ($r = 0.64$; $n=3854$) which might underline common sources for these species. Iron and OOA have completely different origins as also shown in the NWR plots and PSCF maps now presented in Figure S5 (see comment 9). If considering MO-OOA only, most of it could be rather due to the oxidation of ship emissions along the Western African coast, which would also explain the better correlation observed with NO_3 from NO_x emission processing despite the predominance of this regional oxidized factor over the local one.

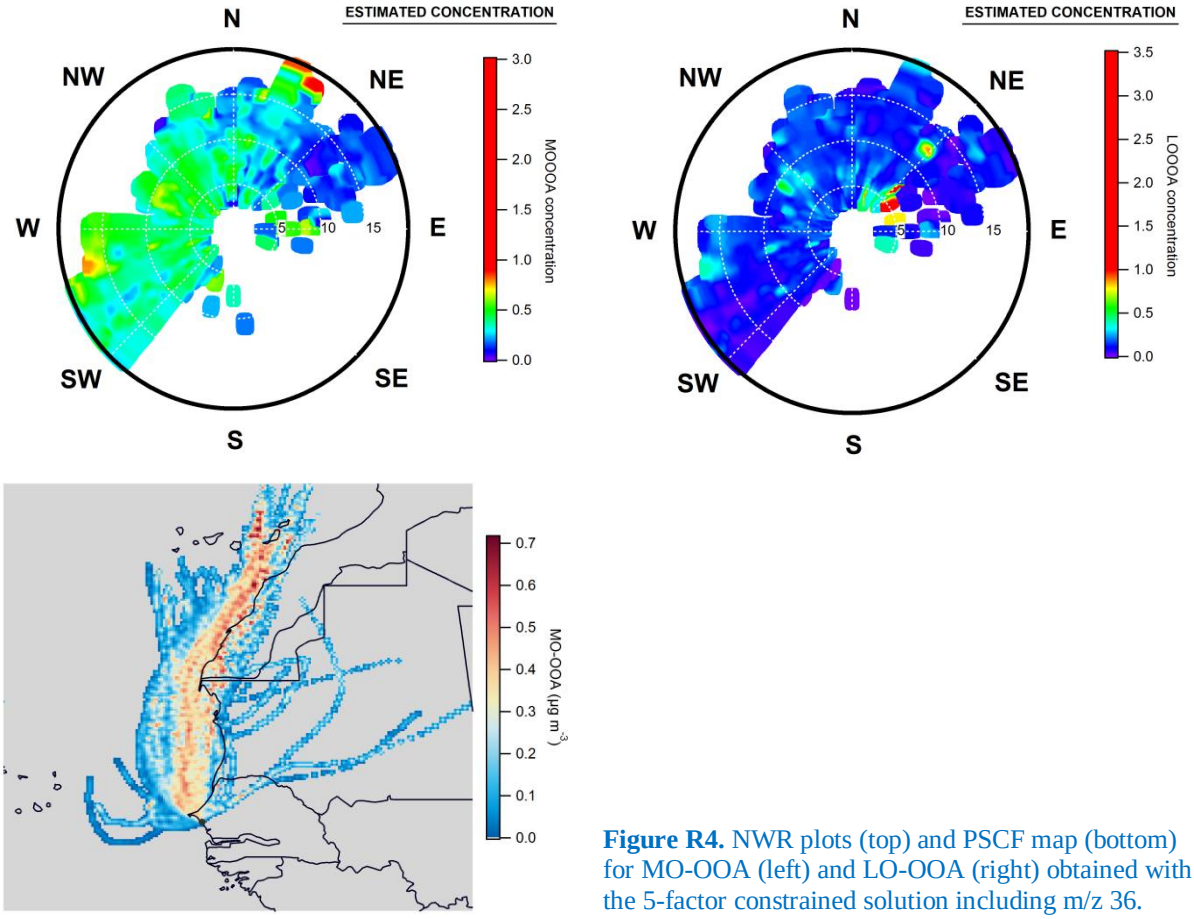

Figure R4. NWR plots (top) and PSCF map (bottom) for MO-OOA (left) and LO-OOA (right) obtained with the 5-factor constrained solution including m/z 36.

Changes in the manuscript:

Abstract, page 2 lines 4-6: "The remaining fraction was identified as oxygenated organic aerosols (OOA), a factor that prevailed regardless of the day type (45%) and was representative of regional (~3/4) but also local (~1/4) sources due to enhanced photochemical processes."

Page 15 lines 34-36: "Since the behavior of Chl had also been suspected to come from the same sources, PMF solutions adding the m/z 36 signal in the input matrix were investigated, and a solution is presented in Appendix S8, where regional OOA accounts for ~3/4 of the OOA and local OOA ~1/4."

Page 18 line 21: "The OOA PSCF map (Figure S5c) seems to trace back its origin along the entire Western African coast, where shipping emissions could be a major source of organic aerosols."

References cited in this reply

Allan, J. D., Bower, K. N., Coe, H., Boudries, H., Jayne, J. T., Caragaratna, M. R., Millet, D. B., Goldstein, A. H., Quinn, P. K., Weber, R. J. C. G. L. and Worsnop, D. R.: Submicron aerosol composition at Trinidad Head, California, during ITCT 2K2: Its relationship with gas phase volatile organic carbon and assessment of instrument performance, J. Aerosol Sci., 35, 909–922, doi:10.1016/j.jaerosci.2004.02.007, 2004.

Caponi, L., Formenti, P., Massabó, D., Di Biagio, C., Cazaunau, M., Pangui, E., Chevaillier, S., Landrot, G., Andreae, M. O., Kandler, K., Piketh, S., Saeed, T., Seibert, D., Williams, E., Balkanski, Y., Prati, P. and Doussin, J.-F.: Spectral- and size-resolved mass absorption efficiency of mineral dust aerosols in the shortwave: a simulation chamber study, Atmos Chem Phys Discuss, 2017, 1–39, doi:10.5194/acp-2017-5, 2017.

Cissé, O.: Les décharges d'ordures en Afrique - Mbeubeuss à Dakar au Sénégal, Karthala., 2012.

Crippa, M., DeCarlo, P., Slowik, J., Mohr, C., Heringa, M., Chirico, R., Poulain, L., Freutel, F., Sciare, J. and Cozic, J.: Wintertime aerosol chemical composition and source apportionment of the organic fraction in the metropolitan area of Paris, Atmospheric Chem. Phys., 13(2), 961–981, 2013.

Draxler, R. R. and Hess, G. D.: An overview of the HYSPLIT_4 modeling system of trajectories, dispersion, and deposition, Aust. Meteorol. Mag., 47, 295–308, 1998.

Elser, M., Huang, R.-J., Wolf, R., Slowik, J. G., Wang, Q., Canonaco, F., Li, G., Bozzetti, C., Daellenbach, K. R., Huang, Y., Zhang, R., Li, Z., Cao, J., Baltensperger, U., El-Haddad, I. and Prévôt, A. S. H.: New insights into PM2.5 chemical composition and sources in two major cities in China during extreme haze events using aerosol mass spectrometry, Atmos Chem Phys, 16(5), 3207–3225, doi:10.5194/acp-16-3207-2016, 2016.

Fialho, P., Freitas, M. C., Barata, F., Vieira, B., Hansen, A. D. A. and Honrath, R. E.: The Aethalometer calibration and determination of iron concentration in dust aerosols, J. Aerosol Sci., 37(11), 1497–1506, doi:10.1016/j.jaerosci.2006.03.002, 2006.

Fomba, K. W., Müller, K., van Pinxteren, D., Poulain, L., van Pinxteren, M. and Herrmann, H.: Long-term chemical characterization of tropical and marine aerosols at the Cape Verde Atmospheric Observatory (CVAO) from 2007 to 2011, Atmospheric Chem. Phys., 14(17), 8883–8904, doi:10.5194/acp-14-8883-2014, 2014.

Formenti, P., Rajot, J. L., Desboeufs, K., Caquineau, S., Chevaillier, S., Nava, S., Gaudichet, A., Journet, E., Triquet, S., Alfaro, S., Chiari, M., Haywood, J., Coe, H. and Highwood, E.: Regional variability of the composition of mineral dust from western Africa: Results from the AMMA SOP0/DABEX and DODO field campaigns, J. Geophys. Res. Atmospheres, 113(D23), D00C13, doi:10.1029/2008JD009903, 2008.

Fröhlich, R., Cubison, M. J., Slowik, J. G., Bukowiecki, N., Canonaco, F., Croteau, P. L., Gysel, M., Henne, S., Herrmann, E., Jayne, J. T., Steinbacher, M., Worsnop, D. R., Baltensperger, U. and Prévôt, A. S. H.: Fourteen months of on-line measurements of the non-refractory submicron aerosol at the Jungfraujoch (3580 m a.s.l.) – chemical composition, origins and organic aerosol sources, Atmos Chem Phys, 15(19), 11373–11398, doi:10.5194/acp-15-11373-2015, 2015.

Hansen, A. D. A.: Aethalometer Operations Manual, Magee scientifique, Berkeley, CA, USA., 2005.

Henry, R., Norris, G. A., Vedantham, R. and Turner, J. R.: Source Region Identification Using Kernel Smoothing, Environ. Sci. Technol., 43(11), 4090–4097, doi:10.1021/es8011723, 2009.

Hossaini, R., Chipperfield, M. P., Saiz-Lopez, A., Fernandez, R., Monks, S., Feng, W., Brauer, P. and von Glasow, R.: A global model of tropospheric chlorine chemistry: Organic versus inorganic sources and impact on methane oxidation, J. Geophys. Res. Atmospheres, 121(23), 2016JD025756, doi:10.1002/2016JD025756, 2016.

Joshi, N., Romanias, M., Riffault, V. and Thévenet, F.: Investigating water adsorption on natural mineral dust particles: A DRIFT and BET theory study, under press, Aeolian Research, 2017.

Journet, E., Balkanski, Y. and Harrison, S. P.: A new data set of soil mineralogy for dust-cycle modeling, Atmos Chem Phys, 14(8), 3801–3816, doi:10.5194/acp-14-3801-2014, 2014.

Kandler, K., SchÜTz, L., Deutscher, C., Ebert, M., Hofmann, H., JÄCkel, S., Jaenicke, R., Knippertz, P., Lieke, K., Massling, A., Petzold, A., Schladitz, A., Weinzierl, B., Wiedensohler, A., Zorn, S. and Weinbruch, S.: Size distribution, mass concentration, chemical and mineralogical composition and derived optical parameters of the boundary layer aerosol at Tinfou, Morocco, during SAMUM 2006, Tellus B, 61(1), 32–50, doi:10.1111/j.1600-0889.2008.00385.x, 2009.

Lafon, S., Rajot, J.-L., Alfaro, S. C. and Gaudichet, A.: Quantification of iron oxides in desert aerosol, Atmos. Environ., 38(8), 1211–1218, doi:10.1016/j.atmosenv.2003.11.006, 2004.

Lafon, S., Sokolik, I. N., Rajot, J. L., Caquineau, S. and Gaudichet, A.: Characterization of iron oxides in mineral dust aerosols: Implications for light absorption, J. Geophys. Res. Atmospheres, 111(D21), D21207, doi:10.1029/2005JD007016, 2006.

Linke, C., Möhler, O., Veres, A., Mohácsi, Á., Bozóki, Z., Szabó, G. and Schnaiter, M.: Optical properties and mineralogical composition of different Saharan mineral dust samples: a laboratory study, Atmos Chem Phys, 6(11), 3315–3323, doi:10.5194/acp-6-3315-2006, 2006.

Moreno, T., Querol, X., Castillo, S., Alastuey, A., Cuevas, E., Herrmann, L., Mounkaila, M., Elvira, J. and Gibbons, W.: Geochemical variations in aeolian mineral particles from the Sahara–Sahel Dust Corridor, Chemosphere, 65(2), 261–270, doi:10.1016/j.chemosphere.2006.02.052, 2006.

Müller, T., Schladitz, A., Massling, A., Kaaden, N., Kandler, K. and Wiedensohler, A.: Spectral absorption coefficients and imaginary parts of refractive indices of Saharan dust during SAMUM-1, Tellus B, 61(1), 79–95, doi:10.1111/j.1600-0889.2008.00399.x, 2009.

Ng, N. L., Herndon, S. C., Trimborn, A., Canagaratna, M. R., Croteau, P. L., Onasch, T. B., Sueper, D., Worsnop, D. R., Zhang, Q., Sun, Y. L. and Jayne, J. T.: An Aerosol Chemical Speciation Monitor (ACSM) for Routine Monitoring of the Composition and Mass Concentrations of Ambient Aerosol, Aerosol Sci. Technol., 45(7), 780–794, doi:10.1080/02786826.2011.560211, 2011a.

Ng, N. L., Canagaratna, M. R., Jimenez, J. L., Zhang, Q., Ulbrich, I. M. and Worsnop, D. R.: Real-Time Methods for Estimating Organic Component Mass Concentrations from Aerosol Mass Spectrometer Data, Environ. Sci. Technol., 45(3), 910–916, doi:10.1021/es102951k, 2011b.

Ocean biology processing group: MODIS Aqua Level 3 Global Daily Mapped 4 km Chlorophyll a. Ver. 6. PO.DAAC, CA, USA., [online] Available from: https://neo.sci.gsfc.nasa.gov/view.php?datasetId=MY1DMM_CHLORA&year=2015 (Accessed 14 June 2017), 2003.

Olmez, I., Sheffield, A. E., Gordon, G. E., Houck, J. E., Pritchett, L. C., Cooper, J. A., Dzubay, T. G. and Bennett, R. L.: Compositions of Particles from Selected Sources in Philadelphia for Receptor Modeling Applications, JAPCA, 38(11), 1392–1402, doi:10.1080/08940630.1988.10466479, 1988.

Petit, J.-E., Favez, O., Albinet, A. and Canonaco, F.: A user-friendly tool for comprehensive evaluation of the geographical origins of atmospheric pollution: Wind and trajectory analyses, Environ. Model. Softw., 88, 183–187, doi:10.1016/j.envsoft.2016.11.022, 2017.

Petzold, A., Rasp, K., Weinzierl, B., Esselborn, M., Hamburger, T., Dörnbrack, A., Kandler, K., Schütz, L., Knippertz, P., Fiebig, M. and Virkkula, A.: Saharan dust absorption and refractive index from aircraft-based observations during SAMUM 2006, Tellus B, 61(1), 118–130, doi:10.1111/j.1600-0889.2008.00383.x, 2009.

Polissar, A. V., Hopke, P. K. and Poirot, R. L.: Atmospheric Aerosol over Vermont: Chemical Composition and Sources, Environ. Sci. Technol., 35(23), 4604–4621, doi:10.1021/es0105865, 2001.

Riffault, V., Arndt, J., Marris, H., Mbengue, S., Setyan, A., Alleman, L. Y., Deboudt, K., Flament, P., Augustin, P., Delbarre, H. and Wenger, J.: Fine and Ultrafine Particles in the Vicinity of Industrial Activities: A Review, Crit. Rev. Environ. Sci. Technol., 45(21), 2305–2356, doi:10.1080/10643389.2015.1025636, 2015.

Sandradewi, J., Prévôt, A. S. H., Szidat, S., Perron, N., Alfarra, M. R., Lanz, V. A., Weingartner, E. and Baltensperger, U.: Using Aerosol Light Absorption Measurements for the Quantitative Determination of Wood Burning and Traffic Emission Contributions to Particulate Matter, Environ. Sci. Technol., 42(9), 3316–3323, doi:10.1021/es702253m, 2008.

Schladitz, A., Müller, T., Kaaden, N., Massling, A., Kandler, K., Ebert, M., Weinbruch, S., Deutscher, C. and Wiedensohler, A.: In situ measurements of optical properties at Tinfou (Morocco) during the Saharan Mineral Dust Experiment SAMUM 2006, Tellus B, 61(1), 64–78, doi:10.1111/j.1600-0889.2008.00397.x, 2009.

Simoneit, B. R. T.: Biomass burning — a review of organic tracers for smoke from incomplete combustion, Appl. Geochem., 17(3), 129–162, doi:10.1016/S0883-2927(01)00061-0, 2002.

Val, S., Liousse, C., Doumbia, E. H. T., Galy-Lacaux, C., Cachier, H., Marchand, N., Badel, A., Gardrat, E., Sylvestre, A. and Baeza-Squiban, A.: Physico-chemical characterization of African urban aerosols (Bamako in Mali and Dakar in Senegal) and their toxic effects in human bronchial epithelial cells: description of a worrying situation, Part Fibre Toxicol, 10(10), 2013.

Vassilev, S. V., Baxter, D., Andersen, L. K. and Vassileva, C. G.: An overview of the chemical composition of biomass, Fuel, 89(5), 913–933, doi:10.1016/j.fuel.2009.10.022, 2010.

Zotter, P., Herich, H., Gysel, M., El-Haddad, I., Zhang, Y., Močnik, G., Hüglin, C., Baltensperger, U., Szidat, S. and Prévôt, A. S. H.: Evaluation of the absorption Ångström exponents for traffic and wood burning in the Aethalometer-based source apportionment using radiocarbon measurements of ambient aerosol, Atmos Chem Phys, 17(6), 4229–4249, doi:10.5194/acp-17-4229-2017, 2017.

Chemical characterization and source apportionment of submicron aerosols measured in Senegal during the 2015 SHADOW campaign

Laura-Hélèna Rivellini[1,2,*], Isabelle Chiapello[2], Emmanuel Tison[1], Marc Fourmentin[3], Anaïs Féron[4], Aboubacry Diallo[5], Thierno N'Diaye[5], Philippe Goloub[2], Francesco Canonaco[6], André Stephan Henry Prévôt[6], and Véronique Riffault[1 *]

[1]IMT Lille Douai, Univ. Lille, SAGE - Département Sciences de l'Atmosphère et Génie de l'Environnement, 59000 Lille, France
~~[1]Département Sciences de l'Atmosphère et Génie de l'Environnement, IMT Lille Douai, Douai, 59508, France~~
[2]Univ. Lille, CNRS, UMR8518 – LOA – Laboratoire d'Optique Atmosphérique, F-59000 Lille, France~~Laboratoire d'Optique Atmosphérique, Université de Lille - CNRS, Villeneuve d'Ascq, 59655, France~~
[3]Laboratoire de Physico-Chimie de l'Atmosphère, Université du Littoral Côte d'Opale, Dunkerque, 59140, France
[4]Laboratoire Interuniversitaire des Systèmes Atmosphériques, CNRS - Université Paris Est Créteil - Université Paris Diderot, Créteil, 94010, France
[5]Institut de Recherche pour le Développement, M'Bour, Senegal
[6]Laboratory of Atmospheric Chemistry, Paul Scherrer Institute, 5232 Villigen, Switzerland

[*] *Correspondence to*:

Véronique Riffault
Tel.: +33 327 712 604, Fax: +33 327 712 914, e-mail: veronique.riffault@imt-lille-douai.fr

Laura-Hélèna Rivellini
e-mail: laura.rivellini@imt-lille-douai.fr

Abstract. The present study offers the first chemical characterization of the submicron (PM_1) fraction in West Africa at a high time resolution, thanks to collocated measurements of non-refractory (NR) species with an Aerosol Chemical Speciation Monitor (ACSM), black carbon and iron concentrations derived from absorption coefficient measurements with a 7-wavelength aethalometer, and total PM_1 determined by a TEOM-FDMS for mass closure. The field campaign was carried out during ~~four~~ three months (March to June 2015) as part of the SHADOW (SaHAran Dust Over West Africa) project at a coastal site located in the outskirts of the city of M'Bour, Senegal. With an averaged mass concentration of 5.4 µg m^{-3}, levels of NR-PM_1 in M'Bour were three to ten times lower than those generally measured in urban and suburban polluted environments.~~With an average mass concentration of 5.4 µg m^{-3}, levels of NR-PM_1 in M'Bour were three to ten times lower than cities like Paris or Beijing.~~ Nonetheless the first half of the observation period was marked by intense but short pollution events (NR-PM_1 concentrations higher than 15 µg m^{-3}), sea breeze phenomena and Saharan desert dust outbreaks (PM_{10} up to 900 µg m^{-3}). During the second half of the campaign, the sampling site was mainly under the influence of marine air masses. The air masses on days under continental and sea breeze influences were dominated by organics (36-40%), whereas sulfate particles were predominant (40%) for days under oceanic influence. Overall, measurements showed that about 3/4 of the total PM_1 were explained by NR-PM_1, BC and Fe (a proxy for dust) concentrations, leaving ~1/4 for other refractory

species. A mean value of 4.6% for the Fe/PM_1 ratio was obtained. Source apportionment of the organic fraction, using Positive Matrix Factorization (PMF) highlighted the impact of local combustion sources, such as traffic and residential activities, which contribute on average to 52% of the total organic fraction. A new organic aerosol (OA) source, representing on average 3% of the total OA fraction, showed similar variation as non-refractory particulate chloride. Its rose plot and daily pattern pointed out to local combustion processes, that is to say two open waste burning areas located about 6 and 11 km away from the receptor site and to a lesser extent a traditional fish smoking place. The remaining fraction was identified as oxygenated organic aerosols (OOA), a factor that prevailed regardless of the day type (45%) and was representative of regional (~3/4) but also local (~1/4) sources due to enhanced photochemical processes.~~The remaining fraction was identified as oxygenated organic aerosols (OOA), a factor that prevailed regardless of the day type (45%) and was representative of regional but also local sources due to enhanced photochemical processes.~~

1 Introduction

Atmospheric aerosols play a key role in the Earth's radiative forcing, by interacting with incoming solar and outgoing terrestrial radiations (direct effect) and influencing cloud formation, growth and lifetime (indirect effects). Important uncertainties related to such effects remain, as reported in the IPCC reports (IPCC, 2007, 2013). Besides, several epidemiological and toxicological studies (Brook et al., 2004; Kelly and Fussell, 2012) also highlight the sanitary impacts of particulate matter (PM) depending on their size, chemical composition and exposure time. In 2012, around 3.7 million deaths were attributed to cardiovascular and respiratory diseases caused by outdoor PM exposure (Brauer et al., 2012). As a response, the World Health Organization (WHO) established in 2006 air quality thresholds for PM: a daily average of 25 (respectively 50) µg m^{-3} and a mean annual limit of 10 (respectively 20) µg m^{-3} for $PM_{2.5}$ (PM with diameter < 2.5 µm) (PM_{10}) (WHO, 2006). During past decades, high-time resolution monitoring instruments have been implemented in Europe within the ACTRIS (Aerosols, Clouds, and Trace gases Research Infrastructure network) program, in America with the IMPROVE (Interagency Monitoring of Protected Visual Environments) network (Prenni et al., 2016; Schurman et al., 2015) or more recently in Asia, in order to better characterize fine particles. Yet, the African continent remains poorly documented in terms of particulate pollution.

Several studies in West Africa (mostly sub-Saharan regions) have focused on the coarse fraction, since this area is strongly influenced by natural sources, especially the Sahara desert that injects high amounts of mineral aerosols into the atmosphere (e.g Chiapello et al., 1995). Among field campaigns, a large effort was performed on aerosol measurements during the AMMA (African Monsoon Multidisciplinary Analysis) program carried out between 2002 and 2010, with intensive observation periods in 2006 (Redelsperger et al., 2006). During the months of January-February (dry season) ~~(extending from November to May)~~ the transport of desert dust (DD) and biomass burning (BB) aerosols were observed to occur into two layers, one dominated by DD close to the surface (< 1 km), the one containing BB aerosols being located at a higher altitude, between 2 and 4 km (Haywood et al., 2008; Osborne et al., 2008). During one of the AMMA special observing periods (SOP) (February 2006), a chemical characterization of particles at the ground level was performed near M'Bour (Senegal) using filter sampling and individual particle

analysis (Deboudt et al., 2010; Flament et al., 2011). The analysis evidenced both internal and external mixing of DD, sea salt (SS) and carbonaceous aerosols (Deboudt et al., 2010) within the surface layer. The compositions of the coarse (2-10 µm) and fine (< 2 µm) fractions were established at the surface; DD dominated the coarse fraction while organic matter was the major constituent of the fine one. Similar analysis were performed on samples collected during aircraft flights (Formenti et al., 2008a) to determine the chemical composition of aerosols at different altitudes. The altitude layer was mainly composed of BB and DD external mixture (Chou et al., 2008; Hand et al., 2010). From January to March 2006 (AMMA SOP-0), several types of events from mixtures of DD and BB aerosols to pure mineral dust events were identified based on column aerosol retrievals from AERONET sun/sky photometer measurements in M'Bour, Senegal (Derimian et al., 2008). Other field campaigns such as POLCA ("POLlution des Capitales Africaines" on the Pollution of African Capitals) highlighted the presence of anthropogenic sources of aerosols linked to the strong demographic growth, limited traffic pollution regulations and traditional activities such as slash-and-burn cultivation that generates huge amounts of BB aerosols (Liousse et al., 2010). Its aim was rather on the chemical characterization of $PM_{2.5}$, especially Black Carbon (Doumbia et al., 2012), and the impact on health (Val et al., 2013). Nevertheless, to the best of our knowledge, only one other study has performed on-line and real-time chemical characterization of major PM_1 constituents on the African continent. It was conducted during one year in Welgegund, South Africa, at a site influenced by anthropogenic sources and devoid of mineral dust or marine contribution (Tiitta et al., 2014). Their results have shown that the submicron fraction was dominated by organic and sulfate species, with a chemical composition similar to those encountered in megacities like Beijing (Sun et al., 2012), Mexico (Salcedo et al., 2006) or Pittsburgh (Zhang et al., 2005). Such a pattern differs strongly from those recently measured in European urban cities, where the main submicron pollutants are organic and nitrate species (Petit et al., 2015; Schlag et al., 2015).

In this study we offer the first insight of a real-time, continuous and long-term chemical characterization of PM_1 in West Africa, performed in M'Bour, Senegal from March to June 2015 as part of the first intensive observation period (IOP-1) of the SHADOW (SaHAran Dust Over West Africa) field campaign. An Aerosol Chemical Speciation Monitor (ACSM) was chosen for the quantification and chemical characterization of non-refractory submicron particles, the instrument being better suited for unattended and long term monitoring. Parallel measurements of BC and total PM_1 allowed for mass closure. This paper reports the chemical composition of the submicron fraction and the temporal behaviour of particulate species. The sources and processes responsible for the concentrations encountered at the M'Bour site over the period have been assessed using source-receptor modeling as well as dynamic meteorological measurements parameters and back-trajectory analyses.

2 Instrumentation and methods

2.1 Site description and the SHADOW campaign

The sampling site is located within the '*Institut de Recherche et Développement*' (IRD) facility in M'Bour (14°23'38''N, 16°57'32''W), Senegal. This site, located near the seashore at 80 km south of Dakar (Figure 1), is known to be under the influence of Saharan dust, sea salt, and biomass burning during part of the dry season ~~(from~~

~~December to March)~~. The site may also be affected by regional anthropogenic emissions from surrounding cities including M'Bour and Dakar, and from traditional fish-smoking activities and open waste burning areas. These potential aerosol source locations are reported in Figure 1. The M'Bour station, as part of the international AERONET network (Holben et al., 1998) is routinely equipped with active and passive remote sensing instruments for cloud, aerosol and meteorological monitoring (CIMEL sun/sky photometer, CIMEL micro-Lidar, fluxmeters and a weather station). Since the AMMA campaigns in 2006, M'Bour is also one of the three ground-based stations of the "Sahelian Dust Transect" where PM_{10} mass concentrations are measured continuously (every 5 minutes) thanks to a Tapered Element Oscillating Microbalance (TEOM) (Marticorena et al., 2010; Kaly et al., 2015).

SHADOW main objectives are to better determine the physical and chemical properties of particles in this region largely influenced by high concentrations, and to establish a link between them, the atmospheric dynamics and the aerosol load and optical properties. A large panel of high-performance instruments has therefore been added to the AERONET station (Holben et al., 1998) implemented in M'Bour since 1996 (Derimian et al., 2008). Optical and microphysical aerosol measurements (results not presented) were also performed on site by active and passive remote-sensing instruments, like the LiLAS LIDAR (Bovchaliuk et al., 2014; Veselovskii et al., 2016) and a PLASMA airborne sun photometer (Karol et al., 2013). PM_{10} in situ optical measurements at the surface were carried out by a mono-wavelength aethalometer and a nephelometer. Fine and coarse particle size distributions were recorded by a GRIMM optical particle counter, while ground and airborne filter sampling were collected through a 4-stage DEKATI cascade impactor to be analyzed off-line by individual particle analysis. A Doppler Lidar was implemented to improve our understanding of the atmospheric dynamics between the surface and up to 2-3 km over the IRD station in order to provide more accurate micro-meteorological information.

The online chemical composition measurements presented here were acquired during IOP-1, which took place from March 20 to June 22, 2015. Results discussed in this paper focus on the chemical characterization of surface PM_1. The instruments presented hereafter were set up in an air-conditioned room located underneath the flat roof of the IRD main building. Co-located wind speed and direction were measured by an ultrasonic anemometer (model USA-1, METEK GmbH) deployed on the rooftop (about 12 m above ground).

2.2 Instrumentation

2.2.1 ACSM

The chemical characterization of non-refractory submicron particles (NR-PM_1), that is to say material vaporizing around 600°C under close-to-vacuum conditions, was performed on-line and in real time every 30 minutes by an ACSM (Aerodyne Research Inc.). This instrument is based on the same principle as the aerosol mass spectrometers (AMS), without providing size distribution information. A full description of the instrument is presented in Ng et al. (2011). Basically it is composed of an aerodynamic lens that focuses the particle beam (with vacuum aerodynamic diameters below 1 µm) and directs it through three vacuum chambers, the last one being a detection chamber in which particles are vaporized by impaction on a surface heated at 600°C. Non-refractory species, such as organic matter (OM), sulfate (SO_4), nitrate (NO_3), ammonium (NH_4) and non-refractory chloride (Chl), are vaporized at this temperature and then ionized by electron impact (70 eV). The above mentioned names of the different NR species

correspond to the sum of all m/z fragments related to one given species in the fragmentation table (Allan et al., 2004), that is to say $H_{0\leq x\leq 2}S_{0\leq y\leq 1}O_{0\leq z\leq 4}$ for sulfate, $NH_{0\leq x\leq 2}$ for ammonium, $NO_{0\leq x\leq 2}$ and HNO_3 for nitrate, and $H_{0\leq x\leq 1}Cl$ for chloride.~~Non refractory species, such as organic matter (OM), sulfate (SO_4^{2-}), nitrate (NO_3^-), ammonium (NH_4^+) and non refractory chloride (Chl), are vaporized at this temperature and then ionized by electron impact (70 eV)~~. Particles are then detected by mass spectrometry thanks to a residual gas analyser (RGA). Because of a simplest operating system and the use of a quadrupole mass spectrometer, the instrument has lower time-resolution and sensitivity but remains better suited for long-term monitoring. A $PM_{2.5}$ cut-off inlet (URG Cyclone 2000-30EH, Chapel Hill, NC, USA) was placed on the roof at the entrance of the sampling line with a primary flow of 3 LPM and vertically connected to the instrument. A Nafion dryer (PD-200T-12 MPS, Perma Pure) upstream of the inlet reduces the sample relative humidity (RH). Particle losses were evaluated using the Particle Loss calculator (Von der Weiden et al., 2009) and were inferior to 2% between 50 nm and 1 µm.

Several calibrations were performed with ammonium nitrate, ammonium sulfate and ammonium chloride individual solutions (at 0.005 mol L^{-1} in purified water) prior to IOP-1. An average of all previous calibrations with this instrument gives a mean NO_3 response factor (RF) of 3.63×10^{-11} and mean relative ionization efficiencies (RIE) of 5.72, 0.58 and 2.26 for ammonium, sulfate and chloride, respectively (see Supplementary Information S1 – Figure S1(a-~~d~~e) and Zhang et al., in prep., for more details). Organic and nitrate RIE default values of 1.4 and 1.1, respectively, were used (Canagaratna et al., 2007). Detection limits in µg m^{-3} were determined by Ng et al. (2011) to be 0.284 for ammonium, 0.148 for organic matter, 0.024 for sulfate, 0.012 for nitrate and 0.011 for chloride. It must be noted however that the uncertainties on mass concentrations with aerosol mass spectrometers are estimated at 20-35% (2σ) for the total mass (Bahreini et al., 2009). Furthermore, Crenn et al. (2015) reported reproducibility expanded uncertainties of Q-ACSM concentration measurements of 9, 15, 19, 28, and 36% for NR-PM_1, nitrate, organic matter, sulfate, and ammonium, respectively, during an intercomparison that involved 13 Q-ACSM in the Paris area during springtime.~~The ACSM intercomparison which took place in Paris during winter 2013 has also allowed to determine expanded reproducibility uncertainties of 15, 9, 28 and 36% for NO_3, OM, SO_4 and NH_4 mass concentrations, respectively (Crenn et al., 2015).~~ In addition to the relative ion transmission efficiency correction applied using a naphthalene internal standard, the Collection Efficiency (CE) due to particle losses induced by an incomplete vaporization and/or transmission through the aerodynamic lens was also determined for the whole dataset. Those parameters are mainly influenced by particle shape (size, sphericity) and acidity, ammonium nitrate fraction and RH in the sampling line. Middlebrook et al. (2012) have developed a correction algorithm based on AMS datasets which is applied on ACSM mass concentrations and which considers both RH and aerosol chemical composition to obtain a time-dependent correction of CE values ranging from 0.45 to 0.83 (Figure S1~~e~~f). Nonetheless due to the presence of the Nafion dryer at the entrance of the instrument no RH corrections were necessary as RH values were below 30%. A minor fraction (3.2%) of the data was excluded from the dataset due to unstable parameters, which were generally observed after restarting the instrument following power outages.

2.2.2 AE33 aethalometer

Real-time measurements of aerosol absorption were performed every minute by a seven-wavelength (370, 470, 520, 590, 660, 880 and 950 nm) aethalometer (AE33, Magee Scientific Inc.). The instrument was equipped with a PM_1 impactor inlet (BGI model SCC-0.732, Waltham, MA, USA) and sampled at 5 L min^{-1}. The aethalometer principle is based on the measurement of light transmission through a filter onto which aerosols deposit. The attenuation is then converted into an aerosol absorption coefficient σ_{aer} for each wavelength. BC concentrations are retrieved by applying a specific mass absorption cross section of 7.77 m^2 g^{-1} to the absorption coefficient at 880 nm. The AE33 instrument uses internal corrections based on the Weingartner et al. (2003) algorithm to account for multiple scattering by the filter and a dual spot technology (Drinovec et al., 2015) to compensate the loading effect. Even if DD absorption is limited at 880 nm, its occurrence in high concentrations on site might cause an overestimation of BC concentrations derived from absorption measurements. The method developed by Fialho et al. (2005, 2006, 2014) was used to correct BC concentration data from mineral dust interference. This method is further explained in section II.3.2.

2.2.3 Other instruments

To achieve mass closure in the submicron fraction and account for the expected refractory material (mineral dust and sea salt), ambient air was sampled at 16.7 L min^{-1} through a PM_{10}-inlet (Thermo Fisher Scientific Inc.) mounted on a PM_1 cyclone (SCC 2.229, BGI Inc., Waltham, MA). Gravimetric measurements of the total mass concentrations were performed every 6 minutes using a TEOM operating at a temperature of 30°C and equipped with a filtered dynamic measurement system (TEOM-FDMS 1405-F, Thermo Scientific) that can account for semi-volatile material by maintaining temperature under 30°C and relative humidity (RH) below 25 %, as described by Grover et al. (2005). Some data had to be discarded, mainly due to high temperatures encountered during dust events leading to FDMS failure to maintain proper operating conditions.

Micro-meteorological parameters (wind speed and direction) at the surface (~10 m high) were obtained from 15-minutes accumulation (at 20 Hz) with an ultrasonic anemometer (model USA-1 by METEK GmbH) with a resolution of 0.01 m s^{-1} and 1°, respectively. A weather station (Campbell Scientific) provided precipitation, RH and temperature data every 10 min.

2.3 Analysis strategy

2.3.1 Classification of air masses

The station of M'Bour is under the influence of a typical Sahelian climatic cycle composed of two contrasted dry and wet seasons observed around the Equator, which originate from the closeness of the Intertropical Convergence Zone (ITCZ), bringing moist air masses and heavy precipitations. Kaly et al. (2015), based on 5 years of observations (2006-2010) at M'Bour, defined the dry season as the period during which no precipitation occurs from November to April and the wet season from May to October, where significant precipitation is measured, with a transition during April/May. In Mortier et al. (2016), who analyzed data from 2006 to 2012 at M'Bour, the seasons are defined based on RH levels: from December to March/April (RH < 40%) for the dry season and from June to September (RH ~

80%) for the wet season. They also observed different wind patterns at the ground level, that is to say trade winds coming mostly from the North-East during the dry season, whereas the wet season was characterized by winds from the west. During the AMMA field campaign in the Sahelian belt, Haywood et al. (2008) defined the period from May to June as the monsoon onset. Finally, Slingo et al. (2008) also mentioned large inter-annual variability in the seasonal progression of moisture, with no clearly reproducible pattern from year-to-year in Niamey, Niger.

Therefore we based the definition of the dry and wet seasons in this work on the observed weather parameters during the field campaign. Since absolutely no precipitation was observed during the whole period, but differences in RH levels – though not as pronounced as reported by Mortier et al. (2016) – and wind patterns were clearly visible (Figure 2a), we considered March (RH = 49%) and April (68%) to belong to the dry season, and May (82%) and June (84%) to the transition period.~~The station of M'Bour is under the influence of a typical Sahelian climatic cycle composed of a dry and wet season. The dry season is generally defined from November to April and corresponds to a period for which no significant precipitation is recorded (Kaly et al., 2015). The period from May to October, defined as the wet season, corresponds to the period when precipitation is measured, although significant precipitation is generally limited to a few months, i.e. between July and September in M'Bour during which heavy rain and thunderstorms occur (Kaly et al., 2015). The site is influenced by two important wind flows: the Harmattan conditions, with winds coming from North to North East (N-NE, 0-45°) during the dry season, and the monsoon conditions during the wet season associated to winds from South-West to North-West (SW-NW, 225-315°). Our study taking place from March to June allowed for the observation of both the late part of the dry season (March-April) and the beginning of the wet season (May-June).~~

During IOP-1 two main prevailing directions were found (Fig. 2a). The first one corresponds to an oceanic influence characterized by surface winds coming from West-South-West to North-West (210-300°) with a total frequency of 56% and wind speeds between 2 and 4 m s^{-1}. The second predominant direction is observed for winds originating from NW to NE (300 to 60°) with a total frequency of around 42% and similar wind speeds (2-4 m s^{-1}). The remaining wind sector (60-210°) is a negligible fraction (2%) (Fig. 2a). The maximum wind speed, 6.8 m s^{-1}, was measured on June 21, 2015, with values above 6 m s^{-1} recorded between 2 and 6 a.m. and associated to SW direction. The period from end of March to April was dominated by winds coming from NW to NE (~62%) with some occurrences (~33%) of Western winds during the sea breezes, while from May to June winds were mainly originating from the West (72%).

Our measurements during IOP-1 are generally consistent with monthly average frequencies of M'Bour surface wind directions reported by Kaly et al. (2015) between 2006 and 2010. Indeed, their climatology has shown that spring months are generally influenced by winds coming predominantly from two main sectors, North to East (0-90°, prevailing in March-April) and North-West to South-West (315-225°, dominant in May-June).

Each sampling day of IOP-1 was classified according to the locally measured surface wind directions. Three categories of days were indeed identified: (i) days exclusively under northern (N) trade wind influences, i.e. within ± 45° of the North (0°) direction, associated with continental influence, have been defined as "continental" (Fig. 2b);(ii) days dominated by westerly winds corresponding to oceanic air masses have been classified as "marine" days (Fig. ~~2d~~2b); (iii) an intermediate category called "sea breeze" days has been observed during which measurements show winds coming from the NE before 2 pm, then shifting from the N to W directions between 2 and 7 pm, and

returning to the NW in the evening (Fig. 2~~c~~b). This phenomenon has been previously observed in M'Bour during the AMMA campaigns as reported by Derimian et al. (2008), Léon et al. (2009) and Deboudt et al. (2012). In summary, among the 91 days of IOP-1, 19% were classified as continental days, 32% as sea breeze days and 49% as marine days. The frequent occurrence of marine days can be explained by the transition from dry to wet season from April to June in the Sahelian region (Redelsperger et al., 2006; Slingo et al., 2008).

2.3.2 Interpretation of absorption measurements

M'Bour being largely under the influence of mineral dust, a possible overestimation of the amount of BC derived from absorption coefficients measured by the aethalometer (due to DD absorbing properties at shorter wavelengths) has to be considered (Bond and Bergstrom, 2006). These interferences may be enhanced during the dry season by internal mixture of BB and DD, as encountered and evidenced during AMMA by Deboudt et al. (2010) at the surface and by Hand et al. (2010) and Paris et al. (2010) at higher altitude. Consequently, BC absorption coefficients have been recalculated following the method developed by Fialho et al. (2005, 2006, 2014) in order to obtain BC concentrations unbiased by DD influence. It consists in a deconvolution of the wavelength-dependent aerosol absorption coefficient over time, $\sigma_{aer}(\lambda, t)$, into two terms that take into account DD and BC contributions, through the following equations:

$$\sigma_{aer}(\lambda, t) = \sigma_{BC}(\lambda, t) + \sigma_{DD}(\lambda, t) \quad (1)$$

where $\sigma_{BC}(\lambda, t)$ and $\sigma_{DD}(\lambda, t)$ are BC and DD absorption coefficients, respectively, which can be expressed as a function of the species concentrations $\langle C_i(t) \rangle$:

$$\sigma_{BC}(\lambda, t) = K_{BC}\lambda^{\alpha}\langle C_{BC}(t) \rangle \quad (2)$$

$$\sigma_{DD}(\lambda, t) = K_{DD}\lambda^{\beta}\langle C_{DD}(t) \rangle \quad (3)$$

K_{BC} and K_{DD} are empirical constants depending of instrument characteristics, and α and β are respectively BC and DD absorption exponents. α and β values of - 1 and - 4, respectively, have been determined in the visible range (from 470 to 660 nm) by Fialho et al. (2014) with a dataset acquired in the Cape Verde Islands located at approximately 500 km from our sampling site.

Fialho et al. (2006) have replaced dust by iron in order to calculate an iron concentration from dust absorption:

$$K_{Fe}\langle C_{Fe}(t) \rangle = K_{DD}\langle C_{DD}(t) \rangle \quad (4)$$

Indeed, DD absorption is known to be mainly influenced by the iron content (Lafon et al., 2006) even if this element presents rather low mass contribution to the mineral dust total mass. As mentioned by Fialho et al. (2014), this method allows to estimate elemental iron concentrations only in the absence of brown carbon since an absorption Angström exponent of 1 (which correspond to fossil fuel BC) is applied. Therefore, other methods, such as the one proposed by Sandradewi et al. (2008) to deconvolve BC from fossil fuel and biomass burning, cannot be used in our conditions.~~As mentioned by Fialho et al. (2014), this method allows to estimate elemental iron concentrations only in the absence of brown carbon.~~ The m/z 60 signal ($C_2H_4O_2^+$, fragment characteristic of levoglucosan from biomass burning) was mostly absent of the ACSM dataset during IOP-1, representing on average only 0.003 (0.007 and 0.012 for the 95th and 99th percentiles, respectively, see Figure ~~S5~~S7) of the total OM, which is identical to the threshold value of 0.3% suggested by Cubison et al. (2011) to assess the presence of BB aerosols. This point is discussed

further in the source apportionment results, in which we tend to attribute m/z 60 emissions to other sources. A few data points (less than 1% of the dataset), under the influence of other combustion processes from specific local activities that may cause a bias in the deconvolution algorithm, have been excluded to derive Fe concentrations (see further discussion in section III.2.2).

Combining Eq.(4) with Eq.(1, 2 and 3) leads to the following expression:

$$\frac{\sigma_{aer}(\lambda,t)}{\lambda^{\alpha}} = K_{BC}\langle C_{BC}(t)\rangle + K_{Fe}\langle C_{Fe}(t)\rangle\,\lambda^{(\beta-\alpha)} \quad (5)$$

Eq. (5) can be plotted as a linear equation at each time t to determine the intercept at the origin, a(t), and the slope, b(t). BC and Fe concentrations are then derived using K_{BC} = 14.625 µm m^2 g^{-1} in Eq. (6) and K_{Fe} = 0.234 µm^4 m^2 g^{-1} in Eq. (7), respectively:

$$\langle C_{BC}(t)\rangle = \frac{a(t)}{K_{BC}} \quad (6)$$

$$\langle C_{Fe}(t)\rangle = \frac{b(t)}{K_{Fe}} \quad (7)$$

In the rest of the paper, when BC and Fe concentrations are mentioned, it corresponds to the deconvolved values based on the above-mentioned method.

Applying the propagation for uncertainties approach on the values of K_{Fe} (10%) and the slope b (39%, calculated using a variability of 0.2 for α and β (Fialho et al., 2006)) gives an overall uncertainty of ~40% for iron concentrations. However the deconvolution algorithm is highly sensitive to the values of the Angström absorption exponents (α and β) and a more detailed discussion can be found in Appendix S2.

2.3.3 Positive Matrix Factorization (PMF)

The PMF model is a statistical source-receptor model developed by Paatero and Tapper (1994), largely employed in source apportionment of atmospheric pollutants when the source profiles and contributions are not known *a priori*. In this study, PMF was applied on the ACSM organic and chloride mass spectra by using the Multilinear Engine (Paatero and Tapper, 1999) and the version 5.3 of the Source Finder (SoFi) described in Canonaco et al. (2013) and operated with IgorPro 6.37 (Wavemetrics). PMF is based on a bilinear model described by the following equations:

$$X = GF + E \quad (8)$$

$$x_{ij} = \sum_{k=1}^{p}(g_{i,k}f_{k,j}) + e_{i,j} \quad (9)$$

where X, corresponding to model entries, represents the matrix of mass fragment spectra measured, and G and F are matrices of a *k*-factor concentration time series and m/z profile, respectively, where *i* denotes the time step and *j* the mass fragment. The number of factors *p* is formerly determined by the user. The residual matrix E, containing the unexplained fraction of the PMF solution, is minimized by iterations of the model using the Q function:

$$Q = \sum_i \sum_j \left(\frac{e_{ij}}{s_{ij}}\right)^2 \quad (10)$$

where s_{ij} represents the measurement uncertainties of fragment *j* at time *i*. The Q value is then normalized by Q_{exp}, representing the degrees of freedom of the model solution. This normalization is used as an indicator for the solution reliability. Thus a ratio Q/Q_{exp} equal to one means that both variability and uncertainties are totally explained by the model. In case of mixed (known) factors, the solution can be furthermore constrained by imposing reference factor

profiles (F, from the literature) as inputs. The user can apply those constraints with a certain degree of freedom defined by a scalar a-value ranging from 0 (no degree of freedom) up to 1 (totally unconstrained).

2.3.4 Geographical origins of air masses and chemical species

Air masses reaching the site were characterized through 48-hour back-trajectories (every 3 hours) retrieved from the computer version of the Hybrid Single-Particle Lagrangian Integrated Trajectory model (HYSPLIT; Draxler and Hess (1998)), for an altitude set at one half of the mixed layer depth and coupled with the GDAS (1 degree) meteorological database. Note that sea breeze phenomena, which occur at short time and spatial scales, cannot be satisfactorily reproduced by this type of model. However given the dynamics of sea breezes, only back-trajectories arriving on site at 3 pm and eventually at 6 pm during sea breeze days (< 8.2%) could not be representative of the ground dynamic observations. Therefore all the back-trajectories available for IOP-1 were kept and could be statistically grouped into clusters according to the variation of the total spatial variance, for the whole period and also by day type.

We also used pollution roses to identify local wind directions leading to high concentrations for each species or PMF factors, but also two additional tools provided by the ZeFir Igor-based package developed by Petit et al. (2017): (i) Non-parametric regression (NWR, Henry et al. (2009)) plots, which combine smoothed surface concentrations and local wind speed and direction, to discriminate between local and more distant/regional sources; (ii) Potential Source Contribution Function (PSCF, (Polissar et al., 2001)) maps for regional sources, which couple time series of one variable with air mass back-trajectories to redistribute the concentrations observed at the site into geographical emission parcels

3. Results and discussion

3.1 Chemical characterization and temporal behavior

3.1.1 NR-PM_1, PM_1 and PM_{10} mass concentrations

As previously mentioned, Senegal is widely influenced by DD events transported from arid and semi-arid regions of Sahara and Sahel. Moreover, M'Bour being a coastal site, the influence of sea salt (SS) particles on the measured aerosol mass concentrations may be significant. Thus, the contributions of these two aerosol types, in both the coarse and fine fractions of aerosol, have been investigated. PM_1 chemical mass closure was checked for all day types by subtracting from the TEOM-FDMS measurements the mass concentrations of species determined by ACSM (NR-PM_1) and aethalometer (BC + Fe); the fraction of unaccounted material therefore corresponded to DD and SS contributions.

Figure 3a shows the mass concentration time series of NR-PM_1 measured by ACSM, total PM_1 by TEOM-FDMS, and PM_{10} by TEOM during IOP-1. It must be noted that total PM_1 data acquired between March 28 and April 10 had

to be invalidated due to instrument overheating during a dust storm event when the outside temperature reached 42°C and PM_{10} concentrations exceeded 600 µg m^{-3}.

The temporal evolutions of the three aerosol fractions do not show any particular correlations (the highest correlation coefficient is obtained between the PM_1 and PM_{10} mass concentrations with r = 0.39 for n = 2666). The weak correlation (r = 0.26, n = 2946) between NR-PM_1 and PM_1 might be explained by the contribution of refractory material (DD and SS) to the total PM_1, while the absence of correlation (r = 0.08, n = 3424) between NR-PM_1 and PM_{10} was expected, as well as the low average contribution (8%) of NR-PM_1 to PM_{10}. Indeed, the coarse fraction of aerosol (PM_{10}) at this site is dominated by DD and SS (Flament et al., 2011). NR species represent on average 71% of the total PM_1, which underlines the significant influence of refractory material in the fine fraction of aerosol measured at M'Bour. During IOP-1, as shown in Figure 3b, despite an important variability (values ranging between 4 and 25%) submicron particles (both refractory and non-refractory fractions) represent on average 11% of the PM_{10} fraction whatever the day type. This pattern has already been observed at other sites influenced by Saharan emissions, and consequently under the influence of DD like Granada (Titos et al., 2015) or Cape Verde (Pio et al., 2014).

Despite similar orders of magnitude between the values of NR-PM_1 and total PM_1, their ratio exhibits different trends depending on day type (Figure 3c). When comparing PM_1 and NR-PM_1 concentrations for marine days, NR species appeared to account for most of the PM_1 fraction over IOP-1 (slope: 0.71, r = 0.82, n = 452), suggesting a minor influence of sea salt in the PM_1 fraction. This conclusion is consistent with the analysis of Flament et al. (2011) during the AMMA SOP-0 in M'Bour, with a reported PM_2 fraction composed of 18 to 77% of DD and less than 20% of soluble ions (dominated by NaCl). Additionally for continental and sea breeze scatter plots also reported in Figure 3c, the discrepancies between NR- and total PM_1 mass concentrations are higher (slopes of 0.49 and 0.56, respectively), underlying that continental air masses – predominant during those days – carried additional refractory material such as DD in the submicron fraction. The unaccounted fraction was determined as the difference between the gravimetrically measured PM_1 mass concentration and the sum of chemical species from ACSM (Org, NO_3, SO_4, NH_4, Chl) and aethalometer (BC, Fe) measurements. It corresponded to 27%, 26% and 16% of the PM_1 mass for continental, sea breeze and marine days, respectively (see Figure S3). ~~The unaccounted fraction (determined as the difference between the gravimetrically measured PM_1 mass concentration and the sum of chemical species from ACSM and aethalometer measurements) corresponds to 27%, 26% and 16% of the PM_1 mass for continental, sea breeze and marine days, respectively (see Figure S2).~~ A more significant difference could have been expected for continental compared to other days, but this might be explained by the absence of PM_1 mass measurements during the more intense dust events, as mentioned previously. Nevertheless, these results stress the need to apply Fialho et al. (2014) deconvolution in order to separate DD and BC absorption contribution.

3.1.2 Estimation of absorbing compound concentrations in PM_1

Fe and BC concentrations obtained after correction led to averaged values of (0.55 ± 0.85) and (0.36 ± 0.37) µg m^{-3}, respectively, over the whole IOP-1 dataset. The deconvolution led to an average decrease of 45% of BC concentrations (factor of 2.2), which is much higher than the 11% decrease observed by Doumbia et al. (2012) in

Dakar where local BC sources are predominant. In our study the decrease even reached 83% under the influence of Saharan dust events and therefore the influence of DD on absorption measurements could never be neglected. As depicted in Figure 4, BC concentrations hardly exceeded 3 µg m^{-3}, except throughout punctual and short-term episodes during which they reached higher values, with a half-hourly average maximum of 3.6 µg m^{-3} reached on April 2, 2015. The higher concentrations can be attributed to local anthropogenic combustion processes as BC concentrations present a significant correlation (r = 0.79) with the ACSM m/z 57 tracer of all types of combustion.~~The higher concentrations can be attributed to local anthropogenic combustion processes as BC concentrations present a significant correlation (r = 0.79) with the ACSM m/z 57 combustion tracer~~. BC concentrations measured in M'Bour are on average much lower than those measured in Dakar during POLCA (Doumbia et al., 2012), where BC yearly average was (10.5 ± 3.5) µg m^{-3}. The lower concentrations measured here can be explained by the differences in sampling site type and population with the IRD center being located at the outskirts of the city of M'Bour (180 000-200 000 inhabitants) area while the site in Dakar (about 3 million inhabitants within the metropolitan area) was located in an urban area. It can be noted that the range of BC concentrations (0.01-3.6 µg m^{-3}) obtained during IOP-1 in M'Bour is within the same order of magnitude than the one reported by Liousse et al. (2010) for the rural site of Djougou, Benin between Dec. 2005-Feb. 2006 (0.4-8.2 µg m^{-3}).

Fe concentrations estimated from PM_1 absorption measurements are considered as an indicator of DD in the fine fraction. The following comparisons were carried out only on coincident measurements, due to missing data in the PM_1 and PM_{10} datasets, corresponding to lower average concentrations of Fe (0.39 and 0.53 µg m^{-3} for the PM_1 and PM_{10} data comparison, respectively). Although weak correlations were found between Fe and total PM_1 concentrations (r = 0.55) and unaccounted PM_1 (r = 0.47), Fe concentrations showed higher correlations with PM_{10} (r = 0.70, see Figure 4). This could be explained by the lack of PM_1 mass concentration measurements during intense dust events, as well as DD domination in the coarse fraction, while the fine fraction is mainly driven by NR and BC species during most of the IOP-1 (Figure 3c).~~Although a weak correlation (r = 0.55) was found between Fe and total PM_1 concentrations, Fe concentrations showed higher correlations with PM_{10} (r = 0.70, see Figure 4). This could be explained by DD domination in the coarse fraction, while the fine fraction is mainly driven by NR and BC species during most of the IOP-1 (Figure 3c).~~ As depicted in Figure 4, most of the low iron concentrations were related to days under marine influence, while the highest Fe concentrations (> 8.0 µg m^{-3}) are generally associated with continental and sea breeze days. These maxima also coincide with PM_{10} highest concentrations (> 400 µg m^{-3}) and confirm iron as a constituent of mineral dust emitted by the Saharan and Sahel regions.

From the only study in the literature focusing on iron concentrations in the submicron fraction in West Africa (Val et al., 2013), we could infer an elemental iron contribution of 7.8% to PM_1 dust, in Dakar, in the absence of dust events. Other studies focused on dust gave the iron contribution for size fractions higher than PM_1, thus no straightforward comparisons can be made with our average ratios of Fe/DD_{PM1} (20, 23, 21 and 16% for respectively IOP-1, continental, sea breeze and marine days). It can nevertheless be interesting to have in mind values retrieved within the same region as it is known that iron oxides mainly belong to the finest fraction (Journet et al., 2014; Kandler et al., 2009) and therefore the elemental iron contribution should be lower for larger sizes, which is consistent with

values reported in Table S2.2.~~Fe contributions to PM_{10} estimated in M'Bour (average Fe/PM_{10} ratio of 0.51% over IOP 1 and 0.89% for continental days) are in excellent agreement with the ~1% of elemental iron in the PM_{100} fraction reported by Joshi et al. (2017) for a DD sample collected at the same location in 2015 after a dust storm. It is however significantly lower than the average content of 11-12% of elemental iron estimated by Formenti et al. (2008) in the PM_{40} dust fraction for samples collected at the ground level in Banizoumbou (Niger). Nonetheless they measured for the same samples an averaged iron concentration of 10 µg m^{-3}, in the same order of magnitude as our maximum concentration of 11.2 µg m^{-3} in PM_1. Besides, Lafon et al. (2006) measured a total iron content of 6 to 8% in PM_{10} bulk samples collected in Niger and Cape Verde, while Moreno et al. (2006) observed a 4% contribution of iron oxides in western Saharan soil samples. Concerning the finer fraction, a mean value of 4.7% was obtained for the Fe/PM_1 ratio over IOP 1 and 7.7% for continental days. The latter value is very close to the 8% of iron content (relative to all oxide mass) observed by Lafon et al. (2006) in the fine mode dust of Nigerian soil samples.~~

3.1.3 PM_1 average chemical composition

Table 1 reports ACSM measurements performed at M'Bour between March 20 and June 22, 2015, as well as other field campaigns carried out worldwide. This study shows an average value of 5.4 µg m^{-3} for NR-PM_1 with a maximum half-hourly average of 68.3 µg m^{-3}. The total PM_1 mean concentration (including BC and Fe) is 8.2 µg m^{-3} (maximum half-hourly average: 143 µg m^{-3}), a value which is about 10 times lower than the PM_{10} mean concentration of 103.5 µg m^{-3} over the same period. This PM_{10} average is consistent with the range of monthly averages reported by Kaly et al. (2015) at M'Bour for the March-June period of 2006-2010 (between 63 and 126 µg m^{-3}). When compared to similar studies conducted around the world, M'Bour clearly appears much less polluted than megacities like Beijing (Sun et al., 2012) or Paris area during winter (Petit et al., 2014). The mean NR-PM_1 measured at M'Bour is close to the only other value reported in Africa for Welgegund, South Africa (Tiitta et al., 2014), ~~regional~~ continental background sites such as MontSec, Spain (Ripoll et al., 2015) or during summer in Paris with an average of 4.5 µg m^{-3} (Petit et al., 2015).

The average NR-PM_1 chemical composition measured in M'Bour was composed of OM (39%), SO_4 (35%), NH_4 (15%) ~~and~~ NO_3 (9%) and Chl (~1%), which is again rather similar to what was observed in South Africa by (Tiitta et al., 2014). Indeed, the OM and SO_4 predominance has been also observed in the majority of cities where ACSM (see Table 1) and AMS (Zhang et al., 2007) campaigns were implemented. Nonetheless, during winter, some European sites like Paris (Petit et al., 2015), Cabauw (Schlag et al., 2015) or Zurich (Lanz et al., 2010) present a fine fraction mainly dominated by nitrate and organic species. In our case these differences could be explained both by the semi-volatile nature of NH_4NO_3 combined with the limited use of fertilizers that prevent NH_3 emissions and ammonium nitrate formation, and more sources of non sea salt(nss)-SO_4 such as marine DMS oxidation processes. The first point can be assessed by emission inventories that provide annual NH_3 emissions (in 2010) of 53 kT in Senegal against 870 kT in France and 204 kT in the Netherlands (source EC-JRC/PBL. EDGAR version 4.2. http://edgar.jrc.ec.europa.eu/, 2011). nss-SO_4 comes from secondary origin and has been investigated in PM_{10} at the Cape Verde Atmospheric Observatory (Fomba et al., 2014). This study showed increased concentrations of nss-SO_4

during dust events, linked to the oxidation of anthropogenic SO_2 transported by continental air masses. They also evidenced a seasonal variability of nss-SO_4 for marine air masses, increasing during summer, which was attributed to increased photochemistry and changes in the emission of dimethyl sulfide (DMS) due to higher biological activities in the ocean. This activity can be traced back using satellite data from AQUA/MODIS, in particular the algae concentrations along the Senegalese coast (Ocean biology processing group, 2003).~~In our case these differences could be explained both by the semi volatile nature of NH_4NO_3 combined with the limited use of fertilizers that prevent NH_3 emissions and ammonium nitrate formation, and more sources of SO_2 such as marine DMS oxidation processes.~~

Figure 5 represents the average contributions of NR-PM_1 species, BC and Fe in PM_1 over the entire IOP-1 and more specifically for continental, sea breeze and marine days. Total PM_1 pie charts, including unaccounted-for aerosol species obtained by chemical mass closure, have been reported in the supplementary material section (Figure S~~2~~3). Figure 5 shows that although an almost equal proportion of organic and sulfate species (31 and 32% respectively) was measured on average over the whole IOP-1, strong differences regarding day types can be highlighted: continental and sea breeze days present similar averaged compositions, with a major contribution of OM (36-40%) followed by SO_4 with 21-24%. Similarities between the two profiles are probably due to a longer influence of northern wind compared to western ones during sea breeze days. On the other hand, for marine days the dominant fraction is sulfate (40%) while OM averaged contribution decreased to 25%. These changes could be explained by (i) oceanic air masses known to carry higher amount of sulfate species from the oxidation of dimethylsulfide (DMS) and organosulfur gases (Charlson et al., 1987; Fitzgerald, 1991) and (ii) long-range transport of polluted air masses from the continent, carried back to M'Bour through oceanic air masses. BC and Fe from anthropogenic and continental origins, respectively, are also less abundant during marine days compared to continental/sea breeze days with fractions decreasing from 7 to 3% and 14-16% to 3%, respectively.

Comparable dynamics was already observed at M'Bour during AMMA SOP-0. For instance, Haywood et al. (2008) highlighted that BB aerosols carried in altitude (~3 km) from the African continent to the Atlantic Ocean were then driven back through south-westerly winds. Similar contributions have been observed in Welgegund (Tiitta et al., 2014) where PM_1 measured during the dry season were dominated by OM (57%), followed by SO_4 (16%) and BC (10%), and the wet season marked by high contributions of SO_4 (42%) and lower contributions of OM and BC (35 and 4%, respectively). In M'Bour, we obtained a significant correlation (r = 0.74, Figure S~~7~~9) between the OM and BC time series and an average BC/OM ratio of 0.15, whatever the day type, suggesting similar emission sources and therefore pointing to continental origins either directly linked to combustion processes, as both species displayed a more important contribution during continental and sea breeze days, or due to the mixing of anthropogenic emissions with biogenic precursors or secondary organic aerosols (SOA).

Aerosol acidity can be considered as an indicator of the age of particles as they will get neutralized during their stay in the atmosphere. In order to estimate the degree of neutralization of ACSM inorganic species, NH_4 measured concentrations (as NH_2^+, NH_3^+ and NH_4^+ ions) are compared to predicted ones, which are equal to the amount of NH_4 required to fully neutralize sulfate, nitrate and chloride anions according to the following equation (Zhang et al., 2007):

$$NH_{4,pred} = M(NH_4) \times \left(2 \times \frac{SO_4^{2-}}{M(SO_4^{2-})} + \frac{NO_3^-}{M(NO_3^-)} + \frac{Cl^-}{M(Cl^-)}\right) \quad (11\text{~~0~~})$$

with SO_4^{2-}, NO_3^- and Cl^- the mass concentrations of inorganic species in µg m^{-3} and M(X) their molecular weights (NH_4 18; SO_4 96; NO_3 62; and Cl 35.5 g mol^{-1}).

The slope obtained between NH_4 measured and predicted (1.02, r = 0.92; see Figure S3a) underlined that most of inorganic species are neutralized over IOP-1, and additionally that there is no strong bias in the calibration values used for ACSM measurements. Nonetheless, a few points digress from the 1:1 line indicating partially neutralized species (as mentioned above). On one hand, ~~P~~points significantly above the 1:1 ratio suggest the presence of NH_4 under other forms than $(NH_4)_2SO_4$, NH_4NO_3 and NH_4Cl. As these points also correspond to higher levels of OM, BC and chloride, circled in red (Figure S~~3~~4~~b~~c), they might be related to nitrogen-containing species associated with combustion processes at low RH (<50%; Figure S3a-b), where chlorine could come from the combustion of sea salt and/or chlorine-containing materials such as plastics. On the other hand, 23% of the data are associated to a $NH_{4,meas}/NH_{4,predict}$ ratio inferior to 0.75 and correspond to points under the 1:1 line in Figure S3a. For such points, the amount of NH_4 predicted is overestimated in comparison to the amount measured on site, and considering that NH_4 will preferentially react with SO_4, other anions like NO_3 and Chl are partially under chemical states other than ammonium nitrate and chloride. As mentioned previously and developed in section 3.2, this can be explained by chloride species emitted by local combustion processes but also by HNO_3 adsorption on dust as already reported in the literature (Fairlie et al., 2010; Savoie et al., 1989) and this is consistent with ratio values inferior to 0.75 which are mainly observed while the site is under dust influence (Figure S3b). Nevertheless these periods also correspond to low levels of inorganic species in PM_1.

3.1.4 Variations of PM_1 chemical species

Figure 6 displays the 30-minute temporal variability of NR-PM_1 species during IOP-1. At such a timestamp a total of 13 pollution events – characterized by NR-PM_1 concentrations exceeding a threshold value of 15 µg m^{-3}, corresponding to three times the average – were detected. In terms of chemical composition, the highest average - over the whole IOP-1- concentrations were obtained for OM and SO_4 with respective values of 2.12 and 1.85 µg m^{-3} (n = 3931). Moreover OM concentrations could present a high variability over short periods, like on May 12, 2015 when OM jumped from 0.9 to 61.7 µg m^{-3} over an interval of 30 minutes, while the sum of other NR-PM_1 species remained below 10 µg m^{-3}.

OM and SO_4 daily fractions exhibit opposite trends, with periods dominated by OM (> 30%) at the beginning of IOP-1 and from May 20 to June 8, 2015, corresponding to days under continental or sea breeze influences. OM concentrations encountered during these periods are generally related to punctual intense episodes, suggesting an influence linked to emissions by rather local anthropogenic activities rather than long-range transport sources. Periods from April 25 to May 21 and after June 9, 2015, associated with oceanic air masses, are dominated by SO_4 (> 30%), with generally more moderate concentrations and less intense peaks, except for May 13th 2015, with NR-PM_1 reaching its maximum at 68 µg m^3.

The daily profiles of all identified PM_1 species and meteorological parameters (wind speed, temperature and wind roses) are presented in Figure 7 according to day types. Strong similarities can be observed between the continental

and sea breeze daily profiles (Fig. 7a-b), both presenting a morning peak around 8 am marked by a distinct rise in OM (> 4 µg m^{-3}) and BC (~1 µg m^{-3}) concentrations and to a lesser extent in NH_4 and chloride concentrations. Continental and sea breeze daily profiles also show a common peak at 8 pm, less intense than the morning one, but characterized by an increase in OM and BC. It can be noticed that this evening peak is less pronounced for continental days (OM ~ 3.5 µg m^{-3} and BC ~ 0.7 µg m^{-3}) than for sea breeze days (OM ~ 4.5 µg m^{-3} and BC ~ 0.9 µg m^{-3}). As mentioned previously, the BC/OM ratio is on average of 0.13-0.14 for sea breeze and continental days (see Figure S9~~7~~) but during the morning and evening peaks these ratios can reach a maximum of ~0.25 meaning that BC emissions are enhanced during these hours. A specific pattern of continental days is a peak measured at noon for OM and BC concentrations (constant BC/OM ratio ~ 0.16), probably combining local emissions and reduced dispersion due to dynamic phenomena as suggested by the slight wind speed decrease. On the other hand, for sea breeze days a peak occurring at 3 pm, with an intense increase in OM, a moderate one in SO_4 and almost no variation of BC (ratio of 0.1), coincide with the sea breeze establishment (discernible through wind plots and the slight drop in temperature). BC for continental and sea breeze daily profiles show a maximum intensity of 1.1 µg m^{-3} for the continental morning peak (8 am), a value which is quite consistent with maximal hourly concentrations (up to 4 µg m^{-3}) measured at 8 am, 4 pm and 8 pm in M'Bour by Deboudt et al. (2010). These peaks are measured for air masses coming from the continent and correspond to traffic and/or cooking hours. Chloride peaks associated to intense OM and BC ones tend to confirm combustion sources for these species, as previously observed during winter in Beijing by Sun et al. (2013).

The marine averaged daily profiles show a very distinctive pattern, compared to continental/sea breeze days (Fig. 7a), and are characterized by a sharp decrease of OM, BC and Fe, with nitrate, ammonium and chloride presenting rather constant profiles, while sulfate exhibits a higher and almost constant concentration of 2.4 µg m^{-3}. This pattern as well as the sulfate peak associated with the sea breeze tends to confirm the regional transport of sulfate to M'Bour through oceanic air masses. It is noticeable that for marine days, OM and BC profiles reached maximum concentrations of 2.5 and 0.35 µg m^{-3} during the night (between 8 pm and 2 am), in coincidence with low wind speed (Fig. 7d). Thus, this night time increase of concentrations measured for marine days might be due to lower dilution of aerosols species from local emissions. The results obtained at M'Bour for marine days are in agreement with those reported by Topping et al. (2004) in Korea, with inorganic species such as SO_4, NO_3 and NH_4 increasing significantly during days under marine influence.

In Figure 7b, Fe and BC profiles showed distinctive behaviors depending on day types. As expected, both profiles for marine days are characterized by very low concentrations of both BC and Fe in comparison to those measured for sea breeze and continental days. In the latter cases, a major difference can be observed for Fe concentrations which are almost twice higher than BC ones. Fe exhibits an additional intense peak around 3 pm and concentrations above 1.5 µg m^{-3} from noon to 8 pm during continental days, which can be attributed to the intense dust events occurring around the end of March and on April 10th when comparing average and median profiles. These patterns suggest a transport of BC and DD (through Fe) by continental air masses – from the areas north and north-east of M'Bour. Most probably air masses loaded in DD coming from the Saharan region (Fe continental profile) are then enriched in BC during their transport above cities. Nonetheless local traffic activities may also be a non-negligible source of dust

through resuspension processes, which would also explain the synchronized peaks of BC and Fe observed for continental profiles even when excluding desert dust events.

3.2 Origins and sources of aerosols

3.2.1 Geographical origins of chemical species

As observed previously, most of the winds reaching M'Bour during IOP-1 were associated with the north and west sectors, carrying respectively air masses from the continent and the ocean, with an averaged wind speed of 2.6 m s^{-1}. These results are consistent with the five-year measurements of wind direction reported by Kaly et al. (2015) in M'Bour for the dry season. From back-trajectory analysis (Figure S5a) three different clusters were encountered during the whole period. The prevailing one (77% for the whole IOP-1; 91, 80 and 43% for continental, sea breeze and marine days, respectively) evidences air masses transported along the Western African coast and over Dakar. A second cluster corresponds to air masses purely originating from the ocean (19% of the total back-trajectories) and appeared as two clusters during marine days. A last cluster coming from the Saharan desert contributes only 4% of the IOP-1 air masses but reaches 9 and 10% for the continental and sea breeze days, respectively. Figure 8 presents pollution roses obtained combining the time series of the different PM_1 components and co-located surface wind direction/speed measurements, thus offering a first insight into the geographical origins of chemical species. NWR plots and PSCF maps can be found in Figure S5b and S5c, respectively. Similar spatial origins can be observed for several species; in particular, OM, BC and Chl maximum concentrations are rather associated with north-east (NE) winds during morning peaks and north-west (NW) winds at the end of the day (Fig. 7), pointing out to a common origin of the higher concentrations observed for these species, that would be linked to combustion processes due to the presence of BC. BC and NO_3 both exhibit local and regional influences, as suggested by their NWR plots (Figure S5b). The corresponding PSCF maps (Figure S5c) indicate regional background concentrations could come from anthropogenic emissions from Dakar (~1 million inhab. within city limits and ~3 in the metropolitan area) and possibly from maritime traffic along the Western African coast.

Figure 8 also highlights an oceanic origin for some OM (with moderate intensity), SO_4 (as already observed in Fig. 5), NO_3 and NH_4. There is no clear trend linked to the wind speed (slower along the coast and higher when perpendicular to it), meaning particulate chemical species are rather transported or formed above the ocean than directly emitted by sea spray (Ovadnevaite et al., 2012). Emissions of DMS and organosulfur gases by microorganisms (as mentioned previously) could explain part of the SO_4 and OM concentrations observed when the site is under western influence. These species may also be released by anthropogenic activities in distant cities like Dakar, whose emissions may be carried toward the ocean and brought back to M'Bour by western winds. This hypothesis is also supported by back-trajectory analysis (Figure S5a). ~~These species may also be released by anthropogenic activities in distant cities like Dakar, whose emissions may be carried toward the ocean and brought back to M'Bour by western winds.~~ A long-term PM_{10} chemical characterization conducted in Cape Verde by Fomba et al. (2014) has also shown that marine air masses were mostly composed of sulfate (10% on average) rather than organic matter (3.5%) but the proportion in PM_1 is more balanced.

Regarding the iron pollution rose and NWR plots reported in Figure 8 and Figure S5b, maxima are measured when the site is under the influence of NE winds. The NWR plot evidences both local emissions possibly linked to traffic resuspension of DD and a regional component, that the Fe PSCF map clearly attributes to the Saharan region. ~~Regarding the iron pollution rose plot reported in Figure 8, maxima are measured when the site is under the influence of NE winds.~~ For such directions we also observe maximum values of the total PM_1 concentrations (> 60 µg m^{-3}), which correspond to the April 10, 2015, most probably a resuspension event following previous dust storms, as observed on PM_1 and Fe concentrations time series (reported respectively on Figure 3 and 4).

3.2.2 Source apportionment of OM

PMF was first applied without constraints on the whole IOP-1 organic database and then separately on continental, sea breeze and marine extracted datasets (see also Supplementary Information Appendix S4). Three to ten factors were tested and for each run, only solutions with a normalized Q/Q_{exp} ratio close or inferior to 1 were taken into account. Mass spectra were compared to reference profiles for identification and the consistency with daily profiles was checked. Without any constraints applied to the model, one or two factors identified as oxygenated organic aerosols (OOA, dominated by the CO_2^+ fragment at m/z 44) were easily retrieved for all datasets. An unknown factor with peaks at m/z 58, 60, 83 and 91 appears for the whole IOP-1 when the number of factors increases (and is mixed with one of the OOA in the reduced datasets). This factor appeared constantly above 4 factors in the unconstrained runs from 3 to 10 factors (Appendix S6, Figure S6.1) and was associated with one of the OOA for the continental, sea breeze and marine 4-factor unconstrained solutions (Figure S6.2)~~This factor was associated with one of the OOA for the continental, sea breeze and marine 4-factor unconstrained solutions (Appendix S4, Figure S4.1)~~. Besides, the model encountered difficulties to separate hydrocarbon-like (HOA) from cooking-like (COA) organic aerosol for the entire IOP-1 dataset and the continental and marine days. Both COA and HOA share similar m/z peaks at 27, 41, 55 ($C_nH_{2n-1}^+$) and 29, 43, 57 ($C_nH_{2n+1}^+$) that correspond to hydrocarbon fragmentation. Nonetheless, they can be differentiated based on 41/43 and 55/57 ratios, more important for COA (Fröhlich et al., 2015a; Mohr et al., 2012), while HOA presents more specific and intense peaks at 69-71. Moreover under continental influence, they tend to be emitted from the same wind directions corresponding to the urbanized area from NW to NE. A good separation with characteristic factor profiles was nonetheless obtained for sea breeze days which present a more variable dynamics, with 4 factors identified, namely HOA, COA, as well as more oxidized and less-oxidized OOA (mixed with the unknown factor) (Appendix ~~S4~~S6, Figure ~~S4~~S6.~~1c~~2c). The unknown factor presents a rose plot and a daily profile consistent with local emissions from the open waste burning areas of Gandigal (NW) and Saly Douté (NE) and a fish-smoking area also located in the NE of M'Bour (Figure 1 and Appendix S6, Figure S6.3~~Appendix S4, Figure S4.2~~), hence it has been designated as LCOA (Local Combustion Organic Aerosol). Since the behavior of Chl had also been suspected to come from the same sources, PMF solutions adding the m/z 36 signal in the input matrix were investigated, and a solution is presented in Appendix S8, where regional OOA accounts for ~3/4 of the OOA and local OOA ~1/4.~~Since the behavior of Chl had also been suspected to come from the same sources, PMF solutions adding the m/z 36 signal in the input matrix were investigated, and a solution is presented in supplementary (Appendix 6).~~ No biomass burning OA (BBOA) profile appeared neither in our unconstrained (up to 10 factors) runs,

nor when HOA and COA were themselves constrained. Furthermore, local practices tend to use dry leaves and branches to feed livestock rather than as combustion fuel, and cooking in the urban area is mainly done on gas stoves. IOP-1 occurring at the transition between dry to wet seasons, the possibility of long-range emissions of BB from Savannah fire, like the one observed for example in South Africa (Tiitta et al., 2014) and northern Australia (Milic et al., 2016), or even other BB regional sources, was not discarded at first. Therefore, an average BBOA profile (Ng et al., 2011b) was used to constrain the PMF solution with different a-values. Using a rather strong constraint of a = 0.3 led to a satisfactory BBOA profile but either stable solutions presenting a mixture between LCOA and part of the OOA factor but no COA, or when LCOA, OOA and COA were well separated, the BBOA profile presented missing fragments and a high run-to-run instability. Moreover, solutions for more moderate constraints ($a \geq 0.5$) led to a BBOA profile with unusually low or missing important fragments (such as m/z 60) and an increasing correlation with COA (Crippa et al, 2013). Besides, the important photochemistry observed on site coupled with levoglucosan (m/z 60, 73) fast reactivity under photo-oxidative conditions (Hennigan et al., 2010) might lead to a fast transformation of BBOA into SOA (which would appear as an OOA factor in our PMF solution). Finally, additional in situ or remote sensing optical instruments specifically implemented for the SHADOW campaign, such as ground-based and airborne sunphotometers or the LILAS multiwavelength Mie-Raman lidar (Veselovskii et al., 2016), did not detect the presence of BB aerosol influence. For all these reasons, we decided not to constrain BBOA in our final solutions. In order to refine the solution, and due to the possible specificity of local emissions, the PMF model was run with mild constraints on the primary factor profiles observed in the different unconstrained runs (see Fig. S~~.4.1~~6.2) that is to say COA (Crippa et al., 2013) and HOA (Ng et al., 2011b) using the a-value approach with 30 to 90% of freedom ($0.3 < a < 0.9$) as explained in Canonaco et al. (2013). Indeed HOA are generally emitted by diesel or fuel exhaust, although in rural cities they have also been related to cooking activities (Sun et al., 2012). It has also been reported that African fuels supplied directly by Western company-owned petrol stations present higher levels or sulfur and polyaromatics, and that others are generally a mixture of refinery intermediate products and other (mostly unknown) chemicals, which could hamper the finding of a satisfactory solution. The robustness of the optimal solution was checked by 50 random seed iterations.

A final constrained solution of 4 factors is presented in Figure 9 through their respective mass spectra with associated pollution rose plots and daily profiles for continental, sea breeze and marine days.

The three primary (POA) factors linked to anthropogenic activities, that is to say HOA, COA, and LCOA corresponded to 18, 30 and 3% of the organic fraction, respectively. HOA and COA contributions to the OA fraction tend to be more important for continental and sea breeze days with respectively 21-24% and 24-31% than for marine days (11-20%), while LCOA slightly increases from 2 to 7%. The HOA profile is well correlated with BC (r = 0.79) and m/z 57 (r = 0.98). No specific external tracers have been identified nonetheless COA temporal variability appeared to correlate well with BC (r = 0.73). The HOA rose plot shows marked peaks in the directions of the two open waste burning areas and of the fish-smoking area located northeast of the site in the outskirts of M'Bour. HOA and Chl NWR plots are very similar, which suggests either common sources or a mixture of both compounds in the air masses which resulted into a correlation of 0.64 between these two variables. ~~The HOA rose plot shows marked peaks in the directions of the two open waste burning areas and of the fish-smoking area located northeast of the site~~

~~in the outskirts of M'Bour.~~ COA main origin in the northwest corresponds to the touristic area of Saly where a number of restaurants are located. BC concentrations previously linked to OM species present close correlations with both HOA and COA but this might be explained by the correlation of 0.82 between both time series suggesting concomitant emissions between traffic and cooking sources. The variability depicted by their continental and sea breeze daily profiles (Fig. 9b) highlights anthropogenic emissions of COA and HOA with pronounced peaks during morning and evening (0.46 to 0.55 µg m^{-3}) corresponding to human activities. The COA and HOA profiles present an additional peak after 11 am, reaching a maximum around noon then decreasing after 2 pm for continental days. The COA, OOA – and to a much lower extent, the HOA – sea breeze profiles differed from the continental ones by a delay in the midday peak which rises only after 2 pm. This difference could be explained by anthropogenic aerosols emitted in the morning, then transported toward the ocean, and carried back on site through sea breeze phenomena. A similar pattern could have been expected from HOA, but the low concentrations observed suggest faster oxidation processes occurring over the ocean which would contribute to the higher OOA peak. Both COA and HOA factors present low background concentrations during marine days.

As for LCOA which is a very small fraction of the total OA, the fact that it nonetheless consistently appears in the PMF analysis under both unconstrained and constrained conditions, suggests a specific behavior uncorrelated with other sources. Its robustness has been tested under various starting conditions (50 seed iterations) and through rotational ambiguity exploration (F-peak tested between -5 and +5 with a step of 0.5). Despite the fact that Chl species were presenting similar wind sectors origins, its correlation with LCOA remains low (r = 0.44) while LCOA presents higher correlation with m/z 36 and 58 (r = 0.55 and 0.84, respectively). This is mainly due to the influence of refractory chloride (NaCl) in our Chl measurements; which has been observed through m/z 35 negative values likely resulting from a slow vaporization both during filter and non-filter measurements (Nuaaman et al., 2015). Nonetheless m/z 36 (HCl^+) was mostly positive (0.03 ± 0.03, see Figure S~~5~~7) confirming that non-sea salt chloride was also detected. Indeed, if sea salt was predominant in LCOA, NaCl could explain the m/z 58 and 60 signals, but one would have expected a maximum on marine days, whereas LCOA pollution rose and NWR plots clearly point out toward the local combustion areas already mentioned previously~~whereas LCOA rose plot clearly points out toward the local combustion areas already mentioned previously~~, and also identified in the chloride rose plot (Figure 8). Although coal combustion used for cooking has been identified as a potential source of chloride emissions (Ianniello et al., 2011; McCulloch et al., 1999), this practice has not been observed in the area. However, chloride species may be emitted from household waste burning/smoldering, for which particle-bound polychlorinated dibenzo-p-dioxins and dibenzofurans (PCDD/Fs) and polychlorinated biphenyls (PCBs) have been measured in previous studies (Gullett et al., 2001; Lemieux et al., 2004; Tue et al., 2016; Zhang et al., 2009); or from sea salt particles subject to high-temperature combustion processes (since this factor is also observed to a lesser extent in the direction of the fish-smoking area). Besides the NWR plots of Chl (local influence) and LCOA (both local and regional) rather suggest the presence of chlorinated organics. The PSCF maps identify two possible origins, one clearly from the ocean that could be related to chlorine-driven photo-oxidation processes (Hossaini et al., 2016) and the other linked to air masses carried over Dakar where similar massive anthropogenic emissions from waste burning could be expected from Mbeubeuss, the largest dumpsite in Senegal located 25 km north-east of Dakar along the coast, which receives 250,000 tons of garbage per year from the Dakar region (Cissé, 2012).

Additionally, the measured NH_4 was higher than the predicted one in the directions of the waste burning areas - especially from the North-East (Figure ~~S3b~~S4b), also suggesting the formation of nitrogen-containing compounds that could lead to $R\text{-}N^+$ or $R\text{-}NO^+$ fragments at these same masses although high-resolution measurements would be needed to confirm this hypothesis. LCOA also present its most intense peaks in the morning (0.04 µg m^{-3}) and some more moderate in the evening (< 0.03 µg m^{-3}) for continental and sea breeze daily profiles, characteristics of point sources and/or local emissions. These may be linked to the start of the fires in the morning for the open waste burning areas and an evening increase of the OM due to temperature drop that would shift the partitioning of semi-volatile species toward the particulate phase. On the contrary its marine profile shows constant but higher concentrations all day long (~0.03 µg m^{-3}) with an increase after 8 am, which explains the slightly higher contribution to the OA fraction for the latter.

OOA are often considered as secondary organic aerosols (SOA) formed through gas-conversion processes of Volatile Organic Compounds (VOCs) or photochemical oxidation of primary OA emitted by biogenic (such as plants or algae) and/or anthropogenic sources. The hot temperatures and intense solar irradiation encountered in the region enhance these processes and can explain the major contribution (45%) observed for the OOA factor during IOP-1, and the predominance (~3/4) of the more-oxidized fraction in the solution presented in Appendix S8.~~The hot temperatures and intense solar irradiation encountered in the region enhance these processes and can explain the major contribution (45%) observed for the OOA factor during IOP-1.~~ Its profile showed intense peaks at m/z 18 and 44 (f_{44} = 0.36) and low 43/44 ratios (0.04), which underlined the high level of oxidation characteristic of aged particles, and presented a correlation of 0.88 with the OOA averaged profile reported by Ng et al. (2011). In our study, the temporal variability of OOA shows a higher correlation with NO_3 than SO_4 (r = 0.56 against r = 0.24). As NO_3 species are generally semi-volatile and associated with less aged air masses (Mohr et al., 2012), OOA might not be only emitted by long distant sources, as also suggested by its NWR plot (Figure S5b)~~OOA might not be only emitted by long distant sources~~. This is highlighted by daily continental and sea breeze profiles rising around 8 am, noon and 8 pm which emphasize direct emission of oxidized organic aerosols from anthropogenic activities. Also, it has been mentioned previously that NO_3 might not be locally emitted (Figure 8 and S5b) and OOA highest concentrations being associated with wind speeds above 3 m s^{-1}, we attribute also a regional origin to this factor. Both the OOA correlation with NO_3 and the fact that its daily cycles progressively increase/decrease with sunrise/sunset suggest an important and fast photochemistry (Robinson et al., 2007). The OOA rose plot shows rather similar concentrations regardless of wind sectors, even if some concentrations superior to 1.5 µg m^{-3} are connected to western wind influences (Figure 9). This oceanic origin is also highlighted by OOA sea breeze profile, which shows a maximum of 0.7 µg m^{-3} reached around 3 pm (Figure 9). It indicates that this SOA formation is enhanced during OA transport over the ocean which under specific atmospheric conditions can be initiated by chlorine atoms (Hallquist et al., 2009). The OOA PSCF map (Figure S5c) seems to trace back its origin along the entire Western African coast, where shipping emissions could be a major source of organic aerosols. OOA increasing during daytime regardless of day type, their high oxidation level and important contribution to OA, especially during marine days (62%), support emissions by regional sources. As shown by the PSCF map (Figure S5c), higher OOA concentrations are associated to air masses that moved along the coast and could transport oxidized anthropogenic species to the receptor site.

Previous observations of OM from daily filter measurements in the PM_2 fraction during AMMA SOP-0 were associated maximum values with winds coming from the coast (NW) and the ocean (W) (Flament et al., 2011) and attributed to emissions by local sources and cities along the Senegalese coast, suggesting they could originate from wood burning, cooking and dry leaf/grass burning. Only considering biomass burning and fossil fuel combustion as contributing to the absorption measurements during their field campaign in Dakar, Doumbia et al. (2012) also reported 12% of biomass burning emitted by regional sources against 88% by fossil fuel. Our measurements over a ~~large~~ period of ~~four~~ three months at high-time resolution suggest, as mentioned before, that biomass burning from local sources is rather negligible in the M'Bour area during the transition period from dry to wet seasons. Cooking, traffic and other local combustion sources such as traditional fish smoking and household waste burning have been identified as the primary local anthropogenic sources of OM.

4 Conclusions

The deployment of high time resolution instruments at the West African coastal site of M'Bour (Senegal) during three months encompassing the end of the dry season and the transition period toward the wet season of 2015 ~~during four months of the 2015 dry season~~ allowed to investigate the temporal variability and chemical composition of the poorly characterized PM_1 aerosols in this region. The average NR-PM_1 concentration (5.4 µg m^{-3}) was relatively low, comparable to levels generally reported in rural environments and also close to the one observed at a South African site. Although marine influence was dominant, various dynamic conditions were encountered during the campaign, with intense dust events, sea breeze phenomena and several anthropogenic episodes (NR-PM_1 reaching up to 68 µg m^{-3} over a 30-min period). PM_1 concentrations were on average 8.2 µg m^{-3} representing 11% of PM_{10}, and were dominated by NR species (71%) with minor contributions of absorbing species (9%). The remaining unaccounted fraction (20% on average, up to 75% during identified dust events) was mainly attributed to mineral dust, strongly suggesting a minor contribution of sea salt in the submicron fraction. Fe concentrations (5%) obtained from the deconvolution of absorption measurements were consistent with the dust events observed on site. Among the species identified in the PM_1 fraction, sulfate and organics represented 32 and 31%, respectively, followed by ammonium 14%, nitrate 9%, BC 5%, Fe 9% and Chl <1%. OM dominated the NR-PM_1 fraction when the sampling site was under continental air mass influences (north-eastern winds), whereas marine air masses (from western winds) preferentially brought higher concentrations of sulfate species on site.

Source apportionment of the organic fraction allowed to identify four types of OA. The organic fraction is composed of a highly-oxidized OOA (45%), whose regional origin is underlined by its important contribution to the organic fraction during marine days (62%) but also by its increasing concentration during daytime with a maximum under sea breeze influence. Nonetheless, its higher correlation with NO_3 as well as morning and evening peaks observed for continental and sea breeze daily profiles tend to associate it partially to direct emissions or fast oxidation processes of anthropogenic compounds. Three primary OA linked to anthropogenic activities from nearby sources were also identified: HOA (22%), COA (28%) and a new factor LCOA (3%) related to local combustion sources (emissions from open-waste burning and fish smoking areas), for which a good correlation with particulate chloride (m/z 36) was consistently found. Non-refractory chloride fragments from waste burning or fish smoking areas were

suggested to originate from local plastic smoldering/flaming processes (for the former) and/or sea salt (for both) submitted to high temperatures under continental influence. This factor, although minor on average, could represent as high as 7% on a 30-minute time period when the air masses were blowing from the local waste burning areas, and very likely resulted in the concomitant emissions of highly-toxic compounds such as dioxins that would require further investigation. Back-trajectories also suggest possible distant sources of combustion, with part of LCOA, OOA and BC associated to processed oceanic air masses which could be influenced by Dakar traffic emissions and waste burning activities, as well as shipping emissions along the West African coast. ~~. Three primary OA linked to anthropogenic activities from nearby sources were also identified: HOA (22%), COA (28%) and a new factor LCOA (3%) related to local combustion sources (emissions from open waste burning and fish smoking areas), for which a good correlation with particulate chloride (m/z 36) was consistently found. Non-refractory chloride fragments from waste burning or fish smoking areas were suggested to originate from plastic smoldering (for the former) and/or sea salt (for both) submitted to high temperatures. This factor, although minor on average, could represent as high as 7% on a 30-minute time period when the air masses were blowing from the waste burning areas, and very likely resulted in the concomitant emissions of highly-toxic compounds such as dioxins that would require further investigation.~~

Overall, our study suggests that natural sources strongly influence PM_1 levels in M'Bour, mainly due to the large influence of marine conditions associated with high sulfate levels, and additional significant influence of desert dust. Our measurements carried out at a suburban site away from megacities allowed to provide new insight into the complex mixture between local anthropogenic sources and regional background aerosols in the PM_1 fraction in West Africa at the end of the dry season.

As shown during this field campaign, at least half of the organic aerosols measured in the submicron fraction are from anthropogenic origins (HOA + COA + LCOA) and we were able to attribute them to specific sources. On the contrary, little is known about the oxygenated fraction – often associated to secondary organic aerosols, which constitutes the other half of OA and therefore efforts should be directed toward better characterizing SOA precursors (anthropogenic and biogenic) and their concentration levels in West Africa. Moreover, the specific LCOA source puts an emphasis on open waste burning, which is highly problematic in terms of health issues, and should be addressed through the implementation of waste disposal facilities and an effective waste collection infrastructure.

Data availability

Data from ACSM and aethalometer instruments are available upon request to the corresponding author, V. Riffault. PM_{10} data can be accessed by request to A. Féron (LISA).

Acknowledgements

LHR's PhD grant and the SHADOW campaign are financially supported by the CaPPA project (Chemical and Physical Properties of the Atmosphere), which is funded by the French National Research Agency (ANR) through

the PIA (*Programme d'Investissement d'Avenir*) under contract "ANR-11-LABX-0005-01", by the Regional Council "*Hauts-de-France*" and the European Regional Development Fund (ERDF).

References

Bond, T. C. and Bergstrom, R. W.: Light Absorption by Carbonaceous Particles: An Investigative Review, Aerosol Sci. Technol., 40(1), 27–67, doi:10.1080/02786820500421521, 2006.

Bovchaliuk, V., Podvin, T., Mortier, A., Goloub, P., Dubovik, O., Tanré, D., Veselovskii, I. and Victori, S.: Aerosol optical and microphysical properties retrieved from combination LIDAR with sun/sky photometer: preliminary results over Lille, Data Process., 4, 02, 2014.

Brauer, M., Amann, M., Burnett, R. T., Cohen, A., Dentener, F., Ezzati, M., Henderson, S. B., Krzyzanowski, M., Martin, R. V., Van Dingenen, R., van Donkelaar, A. and Thurston, G. D.: Exposure Assessment for Estimation of the Global Burden of Disease Attributable to Outdoor Air Pollution, Environ. Sci. Technol., 46(2), 652–660, doi:10.1021/es2025752, 2012.

Bressi, M., Cavalli, F., Belis, C. A., Putaud, J.-P., Fröhlich, R., Martins dos Santos, S., Petralia, E., Prévôt, A. S. H., Berico, M., Malaguti, A. and Canonaco, F.: Variations in the chemical composition of the submicron aerosol and in the sources of the organic fraction at a regional background site of the Po Valley (Italy), Atmos Chem Phys, 16(20), 12875–12896, doi:10.5194/acp-16-12875-2016, 2016.

Brook, R. D., Franklin, B., Cascio, W., Hong, Y., Howard, G., Lipsett, M., Luepker, R., Mittleman, M., Samet, J. and Smith, S. C.: Air pollution and cardiovascular disease A statement for healthcare professionals from the expert panel on population and prevention science of the American Heart Association, Circulation, 109(21), 2655–2671, 2004.

Budisulistiorini, S. H., Canagaratna, M. R., Croteau, P. L., Baumann, K., Edgerton, E. S., Kollman, M. S., Ng, N. L., Verma, V., Shaw, S. L., Knipping, E. M., Worsnop, D. R., Jayne, J. T., Weber, R. J. and Surratt, J. D.: Intercomparison of an Aerosol Chemical Speciation Monitor (ACSM) with ambient fine aerosol measurements in downtown Atlanta, Georgia, Atmos Meas Tech, 7(7), 1929–1941, doi:10.5194/amt-7-1929-2014, 2014.

Canagaratna, M. R., Jayne, J. T., Jimenez, J. L., Allan, J. D., Alfarra, M. R., Zhang, Q., Onasch, T. B., Drewnick, F., Coe, H., Middlebrook, A., Delia, A., Williams, L. R., Trimborn, A. M., Northway, M. J., DeCarlo, P. F., Kolb, C. E., Davidovits, P. and Worsnop, D. R.: Chemical and microphysical characterization of ambient aerosols with the aerodyne aerosol mass spectrometer, Mass Spectrom. Rev., 26(2), 185–222, doi:10.1002/mas.20115, 2007.

Canonaco, F., Crippa, M., Slowik, J. G., Baltensperger, U. and Prévôt, A. S. H.: SoFi, an IGOR-based interface for the efficient use of the generalized multilinear engine (ME-2) for the source apportionment: ME-2 application to aerosol mass spectrometer data, Atmos Meas Tech, 6(12), 3649–3661, doi:10.5194/amt-6-3649-2013, 2013.

Charlson, R. J., Lovelock, J. E., Andreae, M. O. and Warren, S. G.: Oceanic phytoplankton, atmospheric sulphur, cloud albedo and climate, Nature, 326(6114), 655–661, 1987.

Chiapello, I., Bergametti, G., Gomes, L., Chatenet, B., Dulac, F., Pimenta, J. and Suares, E. S.: An additional low layer transport of Sahelian and Saharan dust over the north-eastern Tropical Atlantic, Geophys. Res. Lett., 22(23), 3191–3194, doi:10.1029/95GL03313, 1995.

Chou, C., Formenti, P., Maille, M., Ausset, P., Helas, G., Harrison, M. and Osborne, S.: Size distribution, shape, and composition of mineral dust aerosols collected during the African Monsoon Multidisciplinary Analysis Special Observation Period 0: Dust and Biomass-Burning Experiment field campaign in Niger, January 2006, J. Geophys. Res. Atmospheres, 113(D23), D00C10, doi:10.1029/2008JD009897, 2008.

Crenn, V., Sciare, J., Croteau, P. L., Verlhac, S., Fröhlich, R., Belis, C. A., Aas, W., Äijälä, M., Alastuey, A., Artiñano, B., Baisnée, D., Bonnaire, N., Bressi, M., Canagaratna, M., Canonaco, F., Carbone, C., Cavalli, F., Coz, E., Cubison, M. J., Esser-Gietl, J. K., Green, D. C., Gros, V., Heikkinen, L., Herrmann, H., Lunder, C., Minguillón, M. C., Močnik, G., O'Dowd, C. D., Ovadnevaite, J., Petit, J.-E., Petralia, E., Poulain, L., Priestman, M., Riffault, V., Ripoll, A., Sarda-Estève, R., Slowik, J. G., Setyan, A., Wiedensohler, A., Baltensperger, U., Prévôt, A. S. H., Jayne, J. T. and Favez, O.: ACTRIS ACSM intercomparison – Part 1: Reproducibility of concentration and fragment results from 13 individual Quadrupole Aerosol Chemical Speciation Monitors (Q-ACSM) and consistency with co-located instruments, Atmos Meas Tech, 8(12), 5063–5087, doi:10.5194/amt-8-5063-2015, 2015.

Crippa, M., El Haddad, I., Slowik, J. G., DeCarlo, P. F., Mohr, C., Heringa, M. F., Chirico, R., Marchand, N., Sciare, J. and Baltensperger, U.: Identification of marine and continental aerosol sources in Paris using high resolution aerosol mass spectrometry, J. Geophys. Res. Atmospheres, 118(4), 1950–1963, 2013.

Cubison, M. J., Ortega, A. M., Hayes, P. L., Farmer, D. K., Day, D., Lechner, M. J., Brune, W. H., Apel, E., Diskin, G. S., Fisher, J. A., Fuelberg, H. E., Hecobian, A., Knapp, D. J., Mikoviny, T., Riemer, D., Sachse, G. W., Sessions, W., Weber, R. J., Weinheimer, A. J., Wisthaler, A. and Jimenez, J. L.: Effects of aging on organic aerosol from open biomass burning smoke in aircraft and laboratory studies, Atmos Chem Phys, 11(23), 12049–12064, doi:10.5194/acp-11-12049-2011, 2011.

Deboudt, K., Flament, P., Choël, M., Gloter, A., Sobanska, S. and Colliex, C.: Mixing state of aerosols and direct observation of carbonaceous and marine coatings on African dust by individual particle analysis, J. Geophys. Res. Atmospheres, 115(D24), D24207, doi:10.1029/2010jd013921, 2010.

Derimian, Y., Léon, J.-F., Dubovik, O., Chiapello, I., Tanré, D., Sinyuk, A., Auriol, F., Podvin, T., Brogniez, G. and Holben, B. N.: Radiative properties of aerosol mixture observed during the dry season 2006 over M'Bour, Senegal (African Monsoon Multidisciplinary Analysis campaign), J. Geophys. Res. Atmospheres, 113(D23), D00C09, doi:10.1029/2008JD009904, 2008.

Doumbia, E. H. T., Liousse, C., Galy-Lacaux, C., Ndiaye, S. A., Diop, B., Ouafo, M., Assamoi, E. M., Gardrat, E., Castera, P., Rosset, R., Akpo, A. and Sigha, L.: Real time black carbon measurements in West and Central Africa urban sites, Atmos. Environ., 54, 529–537, doi:10.1016/j.atmosenv.2012.02.005, 2012.

Drinovec, L., Močnik, G., Zotter, P., Prévôt, A. S. H., Ruckstuhl, C., Coz, E., Rupakheti, M., Sciare, J., Müller, T., Wiedensohler, A. and Hansen, A. D. A.: The "dual-spot" Aethalometer: an improved measurement of aerosol black carbon with real-time loading compensation, Atmos Meas Tech, 8(5), 1965–1979, doi:10.5194/amt-8-1965-2015, 2015.

Du, W., Sun, Y. L., Xu, Y. S., Jiang, Q., Wang, Q. Q., Yang, W., Wang, F., Bai, Z. P., Zhao, X. D. and Yang, Y. C.: Chemical characterization of submicron aerosol and particle growth events at a national background site (3295 m a.s.l.) in the Tibetan Plateau, Atmos Chem Phys Discuss, 15(9), 13515–13550, doi:10.5194/acpd-15-13515-2015, 2015.

Fialho, P., Hansen, A. D. A. and Honrath, R. E.: Absorption coefficients by aerosols in remote areas: a new approach to decouple dust and black carbon absorption coefficients using seven-wavelength Aethalometer data, J. Aerosol Sci., 36(2), 267–282, doi:10.1016/j.jaerosci.2004.09.004, 2005.

Fialho, P., Freitas, M. C., Barata, F., Vieira, B., Hansen, A. D. A. and Honrath, R. E.: The Aethalometer calibration and determination of iron concentration in dust aerosols, J. Aerosol Sci., 37(11), 1497–1506, doi:10.1016/j.jaerosci.2006.03.002, 2006.

Fialho, P., Cerqueira, M., Pio, C., Cardoso, J., Nunes, T., Custódio, D., Alves, C., Almeida, S. M., Almeida-Silva, M., Reis, M. and Rocha, F.: The application of a multi-wavelength Aethalometer to estimate iron dust and black carbon concentrations in the marine boundary layer of Cape Verde, Atmos. Environ., 97, 136–143, doi:10.1016/j.atmosenv.2014.08.008, 2014.

Fitzgerald, J. W.: Marine aerosols: A review, Atmospheric Environ. Part Gen. Top., 25(3–4), 533–545, doi:10.1016/0960-1686(91)90050-H, 1991.

Flament, P., Deboudt, K., Cachier, H., Châtenet, B. and Mériaux, X.: Mineral dust and carbonaceous aerosols in West Africa: Source assessment and characterization, Atmos. Environ., 45(22), 3742–3749, doi:10.1016/j.atmosenv.2011.04.013, 2011.

Fomba, K. W., Müller, K., van Pinxteren, D., Poulain, L., van Pinxteren, M. and Herrmann, H.: Long-term chemical characterization of tropical and marine aerosols at the Cape Verde Atmospheric Observatory (CVAO) from 2007 to 2011, Atmospheric Chem. Phys., 14(17), 8883–8904, doi:10.5194/acp-14-8883-2014, 2014.

Formenti, P., Rajot, J. L., Desboeufs, K., Caquineau, S., Chevaillier, S., Nava, S., Gaudichet, A., Journet, E., Triquet, S., Alfaro, S., Chiari, M., Haywood, J., Coe, H. and Highwood, E.: Regional variability of the composition of mineral dust from western Africa: Results from the AMMA SOP0/DABEX and DODO field campaigns, J. Geophys. Res. Atmospheres, 113(D23), D00C13, doi:10.1029/2008jd009903, 2008a.

Formenti, P., Rajot, J. L., Desboeufs, K., Caquineau, S., Chevaillier, S., Nava, S., Gaudichet, A., Journet, E., Triquet, S., Alfaro, S., Chiari, M., Haywood, J., Coe, H. and Highwood, E.: Regional variability of the composition of mineral dust from western Africa: Results from the AMMA SOP0/DABEX and DODO field campaigns, J. Geophys. Res. Atmospheres, 113(D23), D00C13, doi:10.1029/2008JD009903, 2008b.

Fröhlich, R., Cubison, M. J., Slowik, J. G., Bukowiecki, N., Canonaco, F., Croteau, P. L., Gysel, M., Henne, S., Herrmann, E., Jayne, J. T., Steinbacher, M., Worsnop, D. R., Baltensperger, U. and Prévôt, A. S. H.: Fourteen months of on-line measurements of the non-refractory submicron aerosol at the Jungfraujoch (3580 m a.s.l.) – chemical composition, origins and organic aerosol sources, Atmos Chem Phys, 15(19), 11373–11398, doi:10.5194/acp-15-11373-2015, 2015.

Grover, B. D., Kleinman, M., Eatough, N. L., Eatough, D. J., Hopke, P. K., Long, R. W., Wilson, W. E., Meyer, M. B. and Ambs, J. L.: Measurement of total PM2.5 mass (nonvolatile plus semivolatile) with the Filter Dynamic Measurement System tapered element oscillating microbalance monitor, J. Geophys. Res. Atmospheres, 110(D7), D07S03, doi:10.1029/2004JD004995, 2005.

Gullett, B. K., Lemieux, P. M., Lutes, C. C., Winterrowd, C. K. and Winters, D. L.: Emissions of PCDD/F from uncontrolled, domestic waste burning, Chemosphere, 43(4–7), 721–725, doi:10.1016/S0045-6535(00)00425-2, 2001.

Hallquist, M., Wenger, J. C., Baltensperger, U., Rudich, Y., Simpson, D., Claeys, M., Dommen, J., Donahue, N. M., George, C., Goldstein, A. H., Hamilton, J. F., Herrmann, H., Hoffmann, T., Iinuma, Y., Jang, M., Jenkin, M. E., Jimenez, J. L., Kiendler-Scharr, A., Maenhaut, W., McFiggans, G., Mentel, T. F., Monod, A., Prévôt, A. S. H., Seinfeld, J. H., Surratt, J. D., Szmigielski, R. and Wildt, J.: The formation, properties and impact of secondary organic aerosol: current and emerging issues, Atmospheric Chem. Phys., 9(14), 5155–5236, doi:10.5194/acp-9-5155-2009, 2009.

Hand, V. L., Capes, G., Vaughan, D. J., Formenti, P., Haywood, J. M. and Coe, H. C. D.: Evidence of internal mixing of African dust and biomass burning particles by individual particle analysis using electron beam techniques, J. Geophys. Res. Atmospheres, 115(D13), n/a-n/a, doi:10.1029/2009jd012938, 2010.

Haywood, J. M., Pelon, J., Formenti, P., Bharmal, N., Brooks, M., Capes, G., Chazette, P., Chou, C., Christopher, S., Coe, H., Cuesta, J., Derimian, Y., Desboeufs, K., Greed, G., Harrison, M., Heese, B., Highwood, E. J., Johnson, B., Mallet, M., Marticorena, B., Marsham, J., Milton, S., Myhre, G., Osborne, S. R., Parker, D. J., Rajot, J. L., Schulz, M., Slingo, A., Tanré, D. and Tulet, P.: Overview of the Dust and Biomass-burning Experiment and African Monsoon Multidisciplinary Analysis Special Observing Period-0, J. Geophys. Res. Atmospheres, 113(D23), D00C17, doi:10.1029/2008jd010077, 2008.

Hennigan, C. J., Sullivan, A. P., Collett, J. L. and Robinson, A. L.: Levoglucosan stability in biomass burning particles exposed to hydroxyl radicals, Geophys. Res. Lett., 37(9), L09806, doi:10.1029/2010GL043088, 2010.

Holben, B. N., Eck, T. F., Slutsker, I., Tanré, D., Buis, J. P., Setzer, A., Vermote, E., Reagan, J. A., Kaufman, Y. J., Nakajima, T., Lavenu, F., Jankowiak, I. and Smirnov, A.: AERONET—A Federated Instrument Network and Data Archive for Aerosol Characterization, Remote Sens. Environ., 66(1), 1–16, doi:10.1016/S0034-4257(98)00031-5, 1998.

Ianniello, A., Spataro, F., Esposito, G., Allegrini, I., Hu, M. and Zhu, T.: Chemical characteristics of inorganic ammonium salts in $PM_{2.5}$ in the atmosphere of Beijing (China), Atmospheric Chem. Phys., 11(21), 10803–10822, doi:10.5194/acp-11-10803-2011, 2011.

IPCC: Climate change 2007-the physical science basis: Working group I contribution to the fourth assessment report of the IPCC, Cambridge University Press., 2007.

IPCC: Climate Change 2013: The Physical Science Basis: Working Group I Contribution to the Fifth Assessment Report of the Intergovernmental Panel on Climate Change, Cambridge University Press., 2013.

Joshi, N., Romanias, M., Riffault, V. and Thévenet, F.: Investigating water adsorption on natural mineral dust particles: A DRIFT and BET theory study, submitted to Aeolian Research, 2017.

Kaly, F., Marticorena, B., Chatenet, B., Rajot, J. L., Janicot, S., Niang, A., Yahi, H., Thiria, S., Maman, A., Zakou, A., Coulibaly, B. S., Coulibaly, M., Koné, I., Traoré, S., Diallo, A. and Ndiaye, T.: Variability of mineral dust concentrations over West Africa monitored by the Sahelian Dust Transect, Atmospheric Res., 164–165, 226–241, doi:10.1016/j.atmosres.2015.05.011, 2015.

Karol, Y., Tanré, D., Goloub, P., Vervaerde, C., Balois, J. Y., Blarel, L., Podvin, T., Mortier, A. and Chaikovsky, A.: Airborne sun photometer PLASMA: concept, measurements, comparison of aerosol extinction vertical profile with lidar, Atmos Meas Tech, 6(9), 2383–2389, doi:10.5194/amt-6-2383-2013, 2013.

Kelly, F. J. and Fussell, J. C.: Size, source and chemical composition as determinants of toxicity attributable to ambient particulate matter, Atmos. Environ., 60, 504–526, 2012.

Lafon, S., Sokolik, I. N., Rajot, J. L., Caquineau, S. and Gaudichet, A.: Characterization of iron oxides in mineral dust aerosols: Implications for light absorption, J. Geophys. Res. Atmospheres, 111(D21), D21207, doi:10.1029/2005JD007016, 2006.

Lanz, V. A., Prévôt, A. S. H., Alfarra, M. R., Weimer, S., Mohr, C., DeCarlo, P. F., Gianini, M. F. D., Hueglin, C., Schneider, J., Favez, O., D'Anna, B., George, C. and Baltensperger, U.: Characterization of aerosol chemical composition with aerosol mass spectrometry in Central Europe: an overview, Atmos Chem Phys, 10(21), 10453–10471, doi:10.5194/acp-10-10453-2010, 2010.

Lemieux, P. M., Lutes, C. C. and Santoianni, D. A.: Emissions of organic air toxics from open burning: a comprehensive review, Prog. Energy Combust. Sci., 30(1), 1–32, doi:10.1016/j.pecs.2003.08.001, 2004.

Léon, J.-F., Derimian, Y., Chiapello, I., Tanré, D., Podvin, T., Chatenet, B., Diallo, A. and Deroo, C.: Aerosol vertical distribution and optical properties over M'Bour (16.96° W; 14.39° N), Senegal from 2006 to 2008, Atmos Chem Phys, 9(23), 9249–9261, doi:10.5194/acp-9-9249-2009, 2009.

Liousse, C., Guillaume, B., Grégoire, J. M., Mallet, M., Galy, C., Pont, V., Akpo, A., Bedou, M., Castéra, P., Dungall, L., Gardrat, E., Granier, C., KonarÃ©, A., Malavelle, F., Mariscal, A., Mieville, A., Rosset, R., Serça, D., Solmon, F., Tummon, F., Assamoi, E., Yoboué, V. and Van Velthoven, P.: Updated African biomass burning emission inventories in the framework of the AMMA-IDAF program, with an evaluation of combustion aerosols, Atmos Chem Phys, 10(19), 9631–9646, doi:10.5194/acp-10-9631-2010, 2010.

Marticorena, B., Chatenet, B., Rajot, J. L., Traoré, S., Coulibaly, M., Diallo, A., Koné, I., Maman, A., Ndiaye, T. and Zakou, A.: Temporal variability of mineral dust concentrations over West Africa: analyses of a pluriannual

monitoring from the AMMA Sahelian Dust Transect, Atmos Chem Phys, 10(18), 8899–8915, doi:10.5194/acp-10-8899-2010, 2010.

Martiny, N. and Chiapello, I.: Assessments for the impact of mineral dust on the meningitis incidence in West Africa, Atmos. Environ., 70(0), 245–253, doi:10.1016/j.atmosenv.2013.01.016, 2013.

McCulloch, A., Aucott, M. L., Benkovitz, C. M., Graedel, T. E., Kleiman, G., Midgley, P. M. and Li, Y.-F.: Global emissions of hydrogen chloride and chloromethane from coal combustion, incineration and industrial activities: Reactive Chlorine Emissions Inventory, J. Geophys. Res. Atmospheres, 104(D7), 8391–8403, doi:10.1029/1999JD900025, 1999.

Middlebrook, A. M., Bahreini, R., Jimenez, J. L. and Canagaratna, M. R.: Evaluation of Composition-Dependent Collection Efficiencies for the Aerodyne Aerosol Mass Spectrometer using Field Data, Aerosol Sci. Technol., 46(3), 258–271, doi:10.1080/02786826.2011.620041, 2012.

Milic, A., Mallet, M. D., Cravigan, L. T., Alroe, J., Ristovski, Z. D., Selleck, P., Lawson, S. J., Ward, J., Desservettaz, M. J., Paton-Walsh, C., Williams, L. R., Keywood, M. D. and Miljevic, B.: Aging of aerosols emitted from biomass burning in northern Australia, Atmos Chem Phys Discuss, 2016, 1–24, doi:10.5194/acp-2016-730, 2016.

Minguillón, M., Ripoll, A., Pérez, N., Prévôt, A., Canonaco, F., Querol, X. and Alastuey, A.: Chemical characterization of submicron regional background aerosols in the Western Mediterranean using an Aerosol Chemical Speciation Monitor, Atmospheric Chem. Phys. Discuss., 15(1), 965–1000, 2015.

Mohr, C., DeCarlo, P. F., Heringa, M. F., Chirico, R., Slowik, J. G., Richter, R., Reche, C., Alastuey, A., Querol, X., Seco, R., Peñuelas, J., Jiménez, J. L., Crippa, M., Zimmermann, R., Baltensperger, U. and Prévôt, A. S. H.: Identification and quantification of organic aerosol from cooking and other sources in Barcelona using aerosol mass spectrometer data, Atmos Chem Phys, 12(4), 1649–1665, doi:10.5194/acp-12-1649-2012, 2012.

Moreno, T., Querol, X., Castillo, S., Alastuey, A., Cuevas, E., Herrmann, L., Mounkaila, M., Elvira, J. and Gibbons, W.: Geochemical variations in aeolian mineral particles from the Sahara–Sahel Dust Corridor, Chemosphere, 65(2), 261–270, doi:10.1016/j.chemosphere.2006.02.052, 2006.

Ng, N. L., Herndon, S. C., Trimborn, A., Canagaratna, M. R., Croteau, P. L., Onasch, T. B., Sueper, D., Worsnop, D. R., Zhang, Q., Sun, Y. L. and Jayne, J. T.: An Aerosol Chemical Speciation Monitor (ACSM) for Routine Monitoring of the Composition and Mass Concentrations of Ambient Aerosol, Aerosol Sci. Technol., 45(7), 780–794, doi:10.1080/02786826.2011.560211, 2011a.

Ng, N. L., Canagaratna, M. R., Jimenez, J. L., Zhang, Q., Ulbrich, I. M. and Worsnop, D. R.: Real-Time Methods for Estimating Organic Component Mass Concentrations from Aerosol Mass Spectrometer Data, Environ. Sci. Technol., 45(3), 910–916, doi:10.1021/es102951k, 2011b.

Nuaaman, I., Li, S.-M., Hayden, K. L., Onasch, T. B., Massoli, P., Sueper, D., Worsnop, D. R., Bates, T. S., Quinn, P. K. and McLaren, R.: Separating refractory and non-refractory particulate chloride and estimating chloride depletion by aerosol mass spectrometry in a marine environment, Atmos Chem Phys Discuss, 15(2), 2085–2118, doi:10.5194/acpd-15-2085-2015, 2015.

Osborne, S. R., Johnson, B. T., Haywood, J. M., Baran, A. J., Harrison, M. A. J. and McConnell, C. L.: Physical and optical properties of mineral dust aerosol during the Dust and Biomass-burning Experiment, J. Geophys. Res. Atmospheres, 113(D23), D00C03, doi:10.1029/2007jd009551, 2008.

Ovadnevaite, J., Ceburnis, D., Canagaratna, M., Berresheim, H., Bialek, J., Martucci, G., Worsnop, D. R. and O'Dowd, C.: On the effect of wind speed on submicron sea salt mass concentrations and source fluxes, J. Geophys. Res. Atmospheres, 117(D16), D16201, doi:10.1029/2011JD017379, 2012.

Paatero, P. and Tapper, U.: Positive matrix factorization: A non-negative factor model with optimal utilization of error estimates of data values, Environmetrics, 5(2), 111–126, doi:10.1002/env.3170050203, 1994.

Paris, R., Desboeufs, K. V., Formenti, P., Nava, S. and Chou, C.: Chemical characterisation of iron in dust and biomass burning aerosols during AMMA-SOP0/DABEX: implication for iron solubility, Atmospheric Chem. Phys., 10(9), 4273–4282, doi:10.5194/acp-10-4273-2010, 2010.

Parworth, C., Fast, J., Mei, F., Shippert, T., Sivaraman, C., Tilp, A., Watson, T. and Zhang, Q.: Long-term measurements of submicrometer aerosol chemistry at the Southern Great Plains (SGP) using an Aerosol Chemical Speciation Monitor (ACSM), Atmos. Environ., 106, 43–55, doi:10.1016/j.atmosenv.2015.01.060, 2015.

Petit, J.-E., Favez, O., Sciare, J., Canonaco, F., Croteau, P., Močnik, G., Jayne, J., Worsnop, D. and Leoz-Garziandia, E.: Submicron aerosol source apportionment of wintertime pollution in Paris, France by double positive matrix factorization (PMF2) using an aerosol chemical speciation monitor (ACSM) and a multi-wavelength Aethalometer, Atmos Chem Phys, 14(24), 13773–13787, doi:10.5194/acp-14-13773-2014, 2014.

Petit, J.-E., Favez, O., Sciare, J., Crenn, V., Sarda-Estève, R., Bonnaire, N., Močnik, G., Dupont, J.-C., Haeffelin, M. and Leoz-Garziandia, E.: Two years of near real-time chemical composition of submicron aerosols in the region of Paris using an Aerosol Chemical Speciation Monitor (ACSM) and a multi-wavelength Aethalometer, Atmos Chem Phys, 15(6), 2985–3005, doi:10.5194/acp-15-2985-2015, 2015.

Pio, C. A., Cardoso, J., Cerqueira, M. A., Calvo, A., Nunes, T. V., Alves, C. A., Custodio, D., Almeida, S. M. and Silva, M. A.: Seasonal variability of aerosol concentration and size distribution in Cape Verde using a continuous aerosol optical spectrometer, Front. Environ. Sci., 2, doi:10.3389/fenvs.2014.00015, 2014.

Prenni, A. J., Day, D. E., Evanoski-Cole, A. R., Sive, B. C., Hecobian, A., Zhou, Y., Gebhart, K. A., Hand, J. L., Sullivan, A. P., Li, Y., Schurman, M. I., Desyaterik, Y., Malm, W. C., Collett Jr., J. L. and Schichtel, B. A.: Oil and gas impacts on air quality in federal lands in the Bakken region: an overview of the Bakken Air Quality Study and first results, Atmos Chem Phys, 16(3), 1401–1416, doi:10.5194/acp-16-1401-2016, 2016.

Redelsperger, J.-L., Thorncroft, C. D., Diedhiou, A., Lebel, T., Parker, D. J. and Polcher, J.: African Monsoon Multidisciplinary Analysis: An International Research Project and Field Campaign, Bull. Am. Meteorol. Soc., 87(12), 1739–1746, doi:10.1175/BAMS-87-12-1739, 2006.

Ripoll, A., Minguillón, M. C., Pey, J., Jimenez, J. L., Day, D. A., Sosedova, Y., Canonaco, F., Prévôt, A. S. H., Querol, X. and Alastuey, A.: Long-term real-time chemical characterization of submicron aerosols at Montsec (southern Pyrenees, 1570 m a.s.l.), Atmos Chem Phys, 15(6), 2935–2951, doi:10.5194/acp-15-2935-2015, 2015.

Robinson, A. L., Donahue, N. M., Shrivastava, M. K., Weitkamp, E. A., Sage, A. M., Grieshop, A. P., Lane, T. E., Pierce, J. R. and Pandis, S. N.: Rethinking Organic Aerosols: Semivolatile Emissions and Photochemical Aging, Science, 315(5816), 1259–1262, doi:10.1126/science.1133061, 2007.

Salcedo, D., Onasch, T. B., Dzepina, K., Canagaratna, M. R., Zhang, Q., Huffman, J. A., DeCarlo, P. F., Jayne, J. T., Mortimer, P., Worsnop, D. R., Kolb, C. E., Johnson, K. S., Zuberi, B., Marr, L. C., Volkamer, R., Molina, L. T., Molina, M. J., Cardenas, B., Bernabé, R. M., Márquez, C., Gaffney, J. S., Marley, N. A., Laskin, A., Shutthanandan, V., Xie, Y., Brune, W., Lesher, R., Shirley, T. and Jimenez, J. L.: Characterization of ambient aerosols in Mexico City during the MCMA-2003 campaign with Aerosol Mass Spectrometry: results from the CENICA Supersite, Atmos Chem Phys, 6(4), 925–946, doi:10.5194/acp-6-925-2006, 2006.

Schlag, P., Kiendler-Scharr, A., Blom, M. J., Canonaco, F., Henzing, J. S., Moerman, M. M., Prévôt, A. S. H. and Holzinger, R.: Aerosol source apportionment from 1 year measurements at the CESAR tower at Cabauw, NL, Atmos Chem Phys Discuss, 15(23), 35117–35155, doi:10.5194/acpd-15-35117-2015, 2015.

Schurman, M. I., Lee, T., Desyaterik, Y., Schichtel, B. A., Kreidenweis, S. M. and Collett Jr., J. L.: Transport, biomass burning, and in-situ formation contribute to fine particle concentrations at a remote site near Grand Teton National Park, Atmos. Environ., 112, 257–268, doi:10.1016/j.atmosenv.2015.04.043, 2015.

Slingo, A., Bharmal, N. A., Robinson, G. J., Settle, J. J., Allan, R. P., White, H. E., Lamb, P. J., Lélé, M. I., Turner, D. D., McFarlane, S., Kassianov, E., Barnard, J., Flynn, C. and Miller, M.: Overview of observations from the RADAGAST experiment in Niamey, Niger: Meteorology and thermodynamic variables, J. Geophys. Res. Atmospheres, 113(D13), D00E01, doi:10.1029/2008JD009909, 2008.

Sun, C., Lee, B. P., Huang, D., Jie Li, Y., Schurman, M. I., Louie, P. K. K., Luk, C. and Chan, C. K.: Continuous measurements at the urban roadside in an Asian megacity by Aerosol Chemical Speciation Monitor (ACSM): particulate matter characteristics during fall and winter seasons in Hong Kong, Atmos Chem Phys, 16(3), 1713–1728, doi:10.5194/acp-16-1713-2016, 2016.

Sun, Y., Wang, Z., Dong, H., Yang, T., Li, J., Pan, X., Chen, P. and Jayne, J. T.: Characterization of summer organic and inorganic aerosols in Beijing, China with an Aerosol Chemical Speciation Monitor, Atmos. Environ., 51(0), 250–259, doi:10.1016/j.atmosenv.2012.01.013, 2012.

Sun, Y. L., Wang, Z. F., Fu, P. Q., Yang, T., Jiang, Q., Dong, H. B., Li, J. and Jia, J. J.: Aerosol composition, sources and processes during wintertime in Beijing, China, Atmospheric Chem. Phys., 13(9), 4577–4592, doi:10.5194/acp-13-4577-2013, 2013.

Tiitta, P., Vakkari, V., Croteau, P., Beukes, J. P., van Zyl, P. G., Josipovic, M., Venter, A. D., Jaars, K., Pienaar, J. J., Ng, N. L., Canagaratna, M. R., Jayne, J. T., Kerminen, V. M., Kokkola, H., Kulmala, M., Laaksonen, A., Worsnop, D. R. and Laakso, L.: Chemical composition, main sources and temporal variability of PM1 aerosols in southern African grassland, Atmos Chem Phys, 14(4), 1909–1927, doi:10.5194/acp-14-1909-2014, 2014.

Titos, G., Lyamani, H., Pandolfi, M., Alastuey, A. and Alados-Arboledas, L.: Identification of fine (PM1) and coarse (PM10-1) sources of particulate matter in an urban environment, Atmos. Environ., 89(0), 593–602, doi:10.1016/j.atmosenv.2014.03.001, 2015.

Topping, D., Coe, H., McFiggans, G., Burgess, R., Allan, J., Alfarra, M. R., Bower, K., Choularton, T. W., Decesari, S. and Facchini, M. C.: Aerosol chemical characteristics from sampling conducted on the Island of Jeju, Korea during ACE Asia, Atmos. Environ., 38(14), 2111–2123, doi:10.1016/j.atmosenv.2004.01.022, 2004.

Tue, N. M., Goto, A., Takahashi, S., Itai, T., Asante, K. A., Kunisue, T. and Tanabe, S.: Release of chlorinated, brominated and mixed halogenated dioxin-related compounds to soils from open burning of e-waste in Agbogbloshie (Accra, Ghana), J. Hazard. Mater., 302, 151–157, doi:10.1016/j.jhazmat.2015.09.062, 2016.

Val, S., Liousse, C., Doumbia, E. H. T., Galy-Lacaux, C., Cachier, H., Marchand, N., Badel, A., Gardrat, E., Sylvestre, A. and Baeza-Squiban, A.: Physico-chemical characterization of African urban aerosols (Bamako in Mali and Dakar in Senegal) and their toxic effects in human bronchial epithelial cells: description of a worrying situation, Part Fibre Toxicol, 10(10), 2013.

Veselovskii, I., Goloub, P., Podvin, T., Bovchaliuk, V., Derimian, Y., Augustin, P., Fourmentin, M., Tanre, D., Korenskiy, M., Whiteman, D. N., Diallo, A., Ndiaye, T., Kolgotin, A. and Dubovik, O.: Study of African Dust with multi-wavelength Raman Lidar during the “SHADOW” campaign in Senegal, Atmospheric Chem. Phys. Discuss., 1–40, doi:10.5194/acp-2016-109, 2016.

Von der Weiden, S.-L., Drewnick, F. and Borrmann, S.: Particle Loss Calculator – a new software tool for the assessment of the performance of aerosol inlet systems, Atmos Meas Tech, 2(2), 479–494, doi:10.5194/amt-2-479-2009, 2009.

Weingartner, E., Saathoff, H., Schnaiter, M., Streit, N., Bitnar, B. and Baltensperger, U.: Absorption of light by soot particles: determination of the absorption coefficient by means of aethalometers, J. Aerosol Sci., 34(10), 1445–1463, doi:10.1016/S0021-8502(03)00359-8, 2003.

Zhang, Q., Worsnop, D. R., Canagaratna, M. R. and Jimenez, J. L.: Hydrocarbon-like and oxygenated organic aerosols in Pittsburgh: insights into sources and processes of organic aerosols, Atmospheric Chem. Phys., 5(12), 3289–3311, doi:10.5194/acp-5-3289-2005, 2005.

Zhang, Q., Jimenez, J. L., Canagaratna, M. R., Allan, J. D., Coe, H., Ulbrich, I., Alfarra, M. R., Takami, A., Middlebrook, A. M., Sun, Y. L., Dzepina, K., Dunlea, E., Docherty, K., DeCarlo, P. F., Salcedo, D., Onasch, T., Jayne, J. T., Miyoshi, T., Shimono, A., Hatakeyama, S., Takegawa, N., Kondo, Y., Schneider, J., Drewnick, F., Borrmann, S., Weimer, S., Demerjian, K., Williams, P., Bower, K., Bahreini, R., Cottrell, L., Griffin, R. J., Rautiainen, J., Sun, J. Y., Zhang, Y. M. and Worsnop, D. R.: Ubiquity and dominance of oxygenated species in organic aerosols in anthropogenically-influenced Northern Hemisphere midlatitudes, Geophys. Res. Lett., 34(13), L13801, doi:10.1029/2007GL029979, 2007.

Zhang, S., Riffault, V., Dusanter, S., Augustin, P., Fourmentin, M. and Delbarre, H.: One year of real-time chemical speciation measurements of submicron particulate matter (PM1) at a French coastal site: assessment of industrial and shipping emissions, in prep, n.d.

Zhang, Y., Wang, X., Chen, H., Yang, X., Chen, J. and Allen, J. O.: Source apportionment of lead-containing aerosol particles in Shanghai using single particle mass spectrometry, Chemosphere, 74(4), 501–507, doi:10.1016/j.chemosphere.2008.10.004, 2009.

Table 1. Averaged NR-PM1 concentrations (in µg m-3) - with maximum in parentheses when available - and respective contributions of NR compounds for this study compared to other ACSM campaigns from different locations.

$NR\text{-}PM_1$	Relative contributions (%)					Period	Location	Type of site	Reference
avg ($\mu g\ m^{-3}$)	OM	SO_4	NO_3	NH_4	Chl				
50.0	40	18	25	16	<1	Jun. - Aug. 2011	Beijing (China)	Urban	Sun et al. (2012)
25.9	58	23	7	11	<1	Sept.-Dec. 2015	Hong Kong (China)	Urban	Sun et al. (2016)
15.7 (80)	~44	~6	~38	~11	~1	Jan. - Mar. 2012	Paris (France)	Suburban	Petit et al. (2014)
15.3	72	15	6	8	< 1	Summer - Fall 2011	Atlanta (USA)	Urban	Budisulistiorini et al. (2014)
14.2	58	12	21	8	1	Mar. 2013 – Mar 2014	Ispra (Italy)	Rural background	Bressi et al. (2016)
10.8 (~75)	45	30	11	13	1	Sept. - Oct. 2013	Menyuan, Tibetan Plateau (China)	Rural	Du et al. (2015)
9	31	12	41	14	2	Jul. 2012 -Jun. 2013	Cabauw (The Netherlands)	Rural	Schlag et al. (2015)
7.5 (89)	48	32	7	13	<1	Sept. 2010 - Aug. 2011	Welgegund (South Africa)	Rural	Tiitta et al. (2014)
7.2	52	29	7	12	< 1	Jul. - Sept 2010	New-York (USA)	Urban	Ng et al. (2011)
7.0	57	12	21	9	< 1	Nov. 2010 - Jun. 2012	Southern Great plains (USA)	Rural	Parworth et al. (2015)
~7.0	54	19	11	11	< 5	Jun. 2012 - Jul. 2013	Montseny (Spain)	Rural	Minguillón et al. (2015)
5.4 (68.3)	39	35	9	15	<1	Mar. - Jun. 2015	M'Bour (Senegal)	Suburban	This study
4.9	53	25	7	12	< 1	Jul. 2011 - Apr. 2012	Montsec (Spain)	Rural	Ripoll et al. (2015)
0.3 (9.6)	43	30	7	17	/	Oct. 2012 - Oct. 2013	Jungfraujoch (Switzerland)	Rural	Fröhlich et al. (2015)

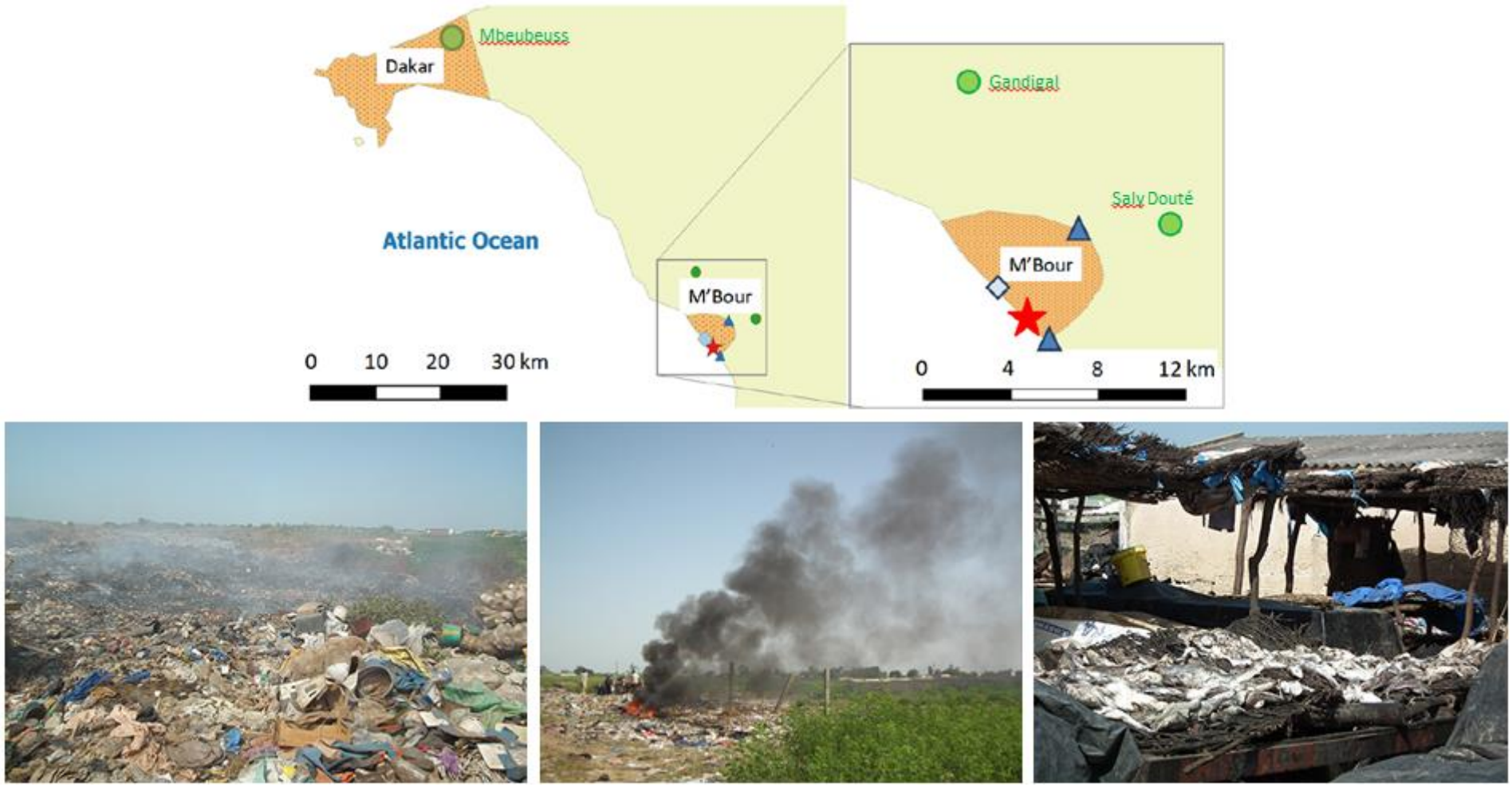

Figure1. (top left) Dakar and M'Bour locations with city delimitations in orange and (top right) local sources located around the IRD sampling site (red star), with open waste burning areas (green circles), fish-smoking sites (blue triangles) and the M'Bour port (light blue diamond). (bottom) Photographs of (from left to right) smoldering fire in the Gandigal open waste burning area; flaming fire in the Saly Douté open waste burning area; fish-smoking location (drying stage) in the suburb of M'Bour.

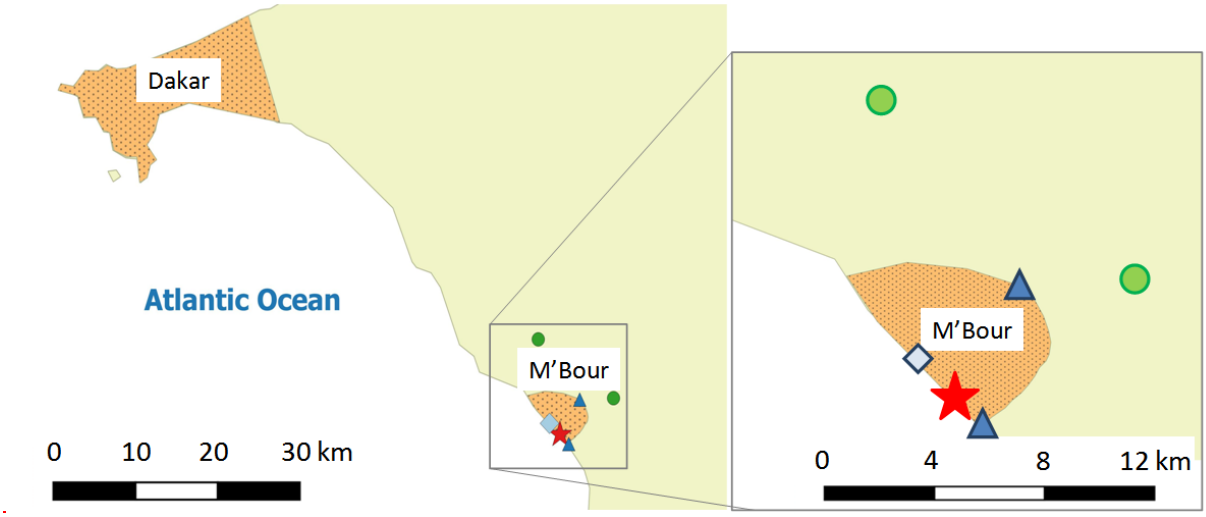

~~Fig. 1. (left) Dakar and M'Bour locations with city delimitations in orange and (right) local sources located around the IRD sampling site (red star), with open waste burning areas (green circles), fish-smoking sites (blue triangles) and the M'Bour port (light blue diamond).~~

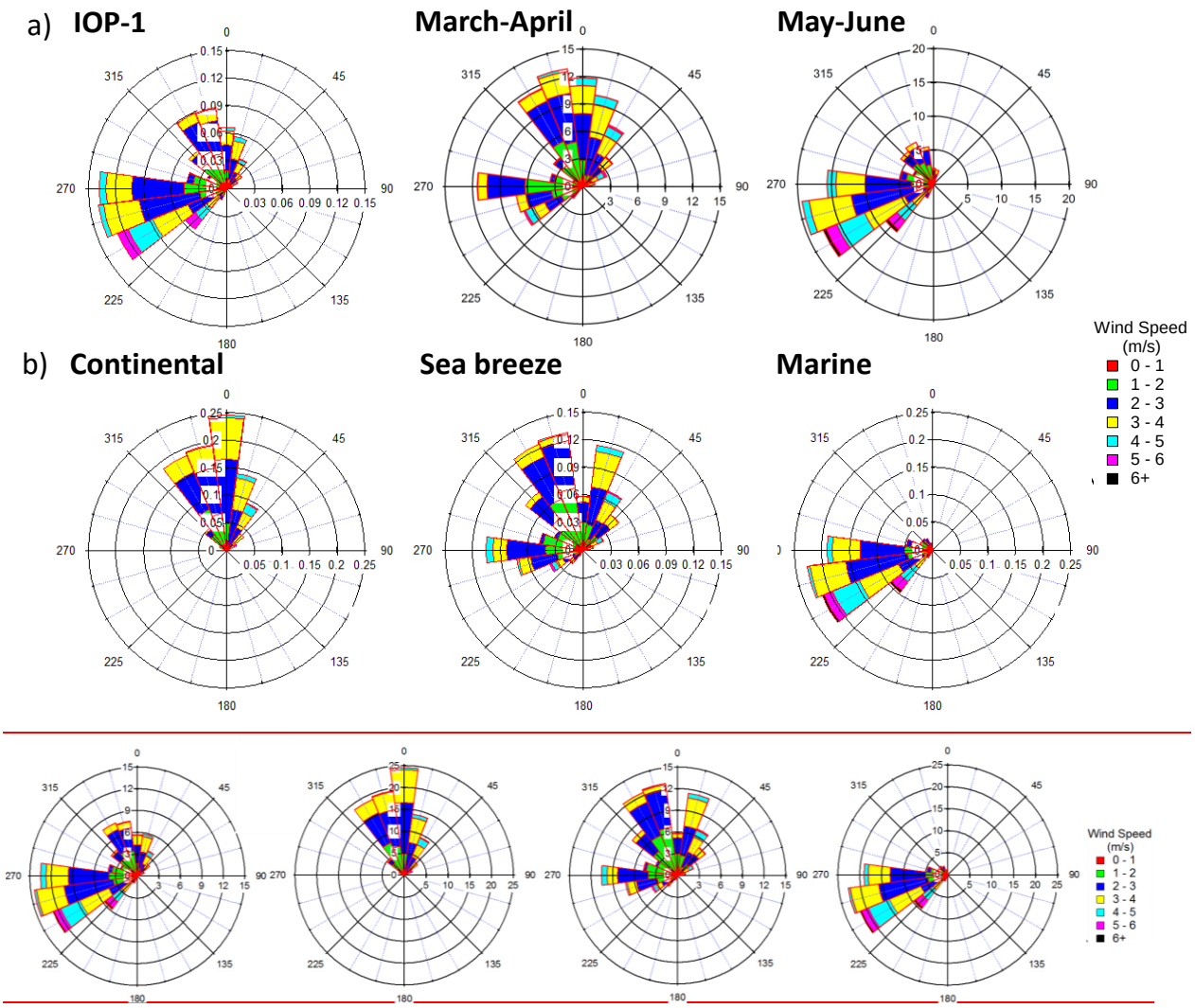

Fig. 2. Rose plots of wind direction divided into 15° sectors and averaged on 30 minutes (ACSM time step) with wind frequencies as radius (in %) and colored by wind speed intervals measured in M'Bour for (a) the whole dataset and dry and wet months, (b) days classified as continental (n = 17), ~~(c)~~ sea breeze (n = 29) and ~~(d)~~ marine (n = 45).

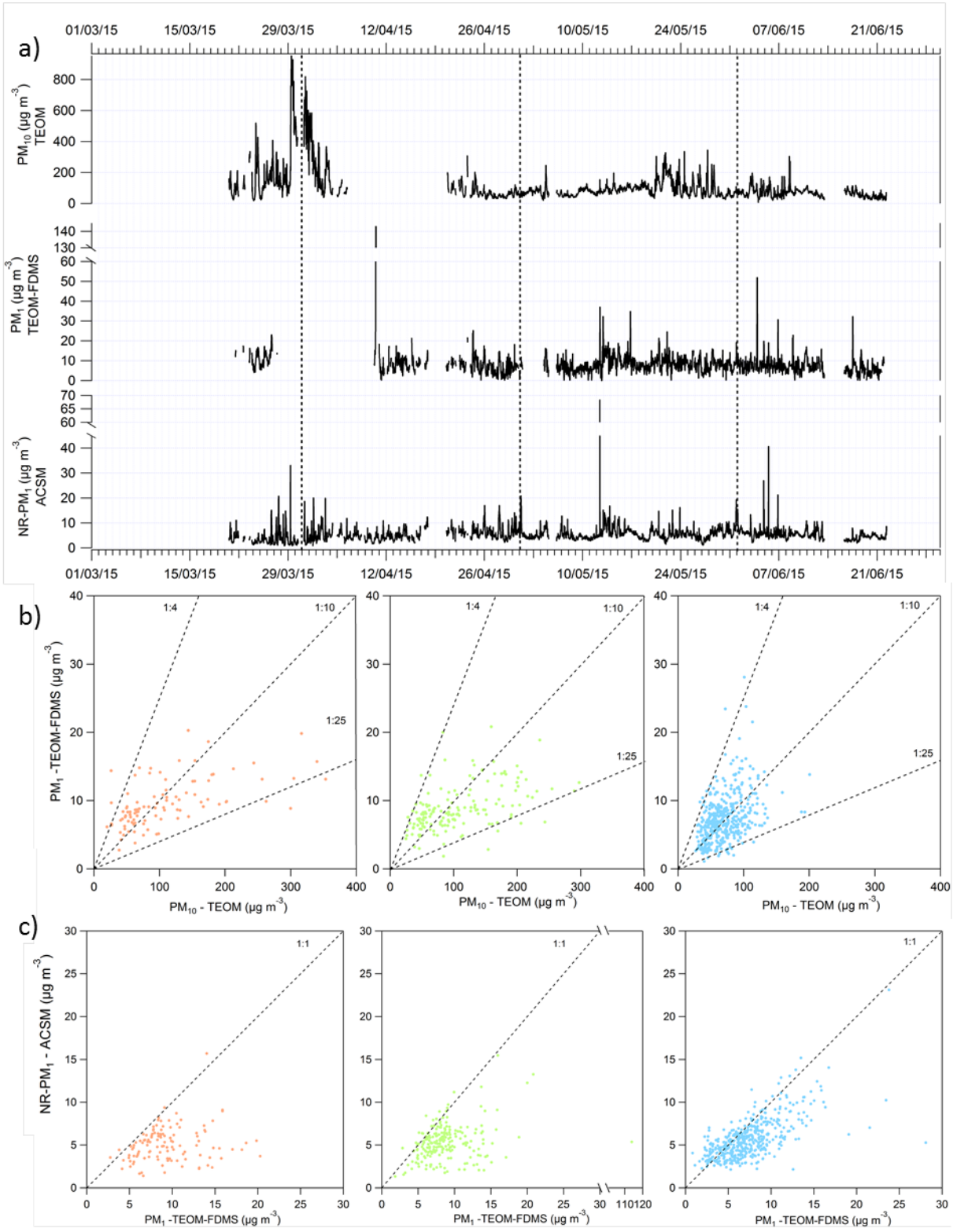

Fig. 3. (a) NR-PM_1, total PM_1 and PM_{10} time series (30-minute averages) measured over IOP-1, (b) 2h averaged scatter plots of total PM_1 vs PM_{10} and (c) NR-PM_1 vs PM_1 for (left) continental, (middle) sea breeze and (right) marine days (dotted lines are visual markers representing ratios between the different variables).

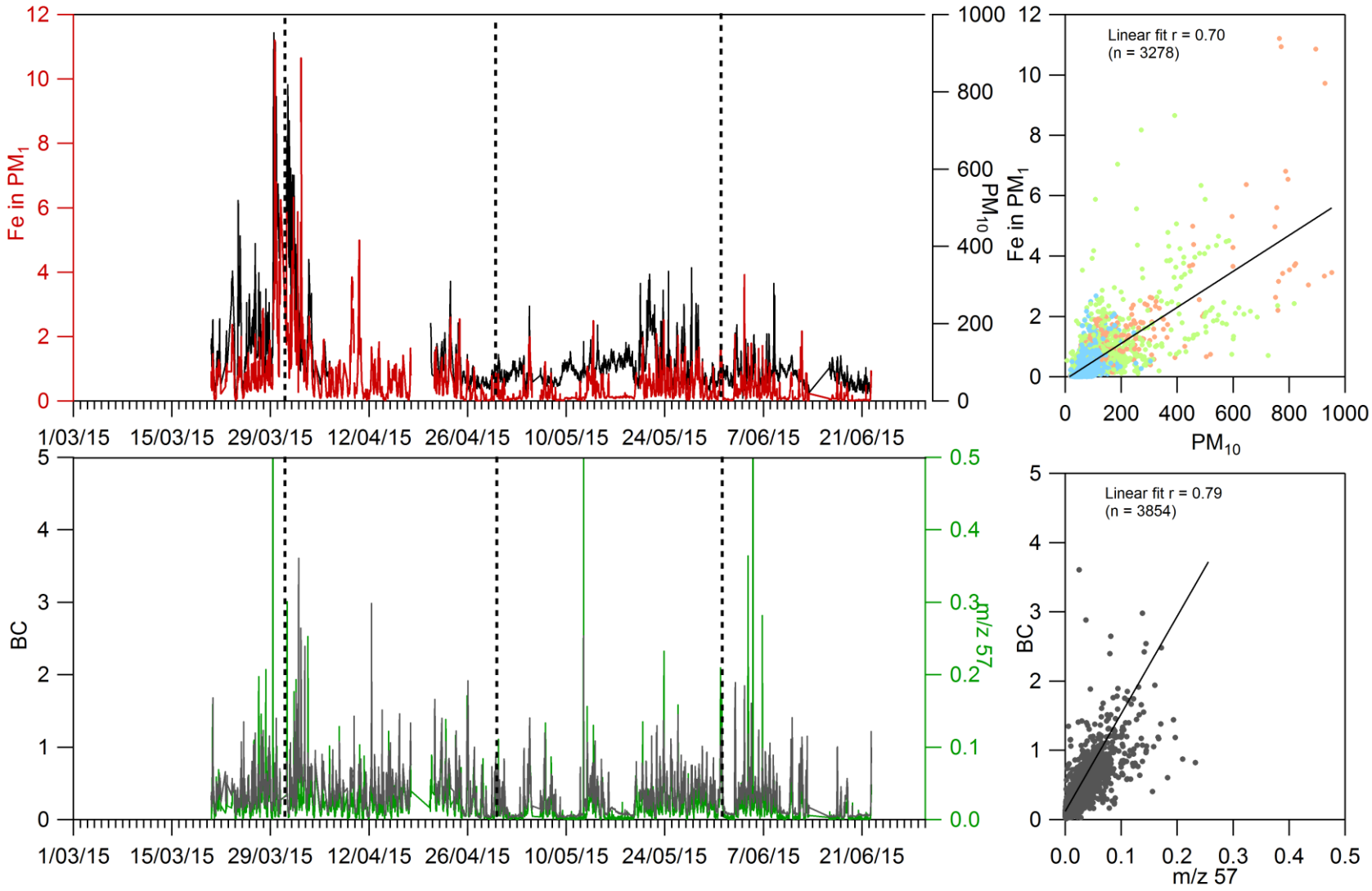

Fig. 4. (Left) Time series of (top) Fe and PM_{10} concentrations (in µg m^{-3}) and (bottom) BC concentration (in µg m^{-3}) and m/z 57 (ng m^{-3}) 30 min average. (Right) Corresponding scatter plots and their respective linear fits with Fe and PM_{10} data colored in red for continental, green for sea breeze and blue for marine days and BC and m/z 57 in grey dots.

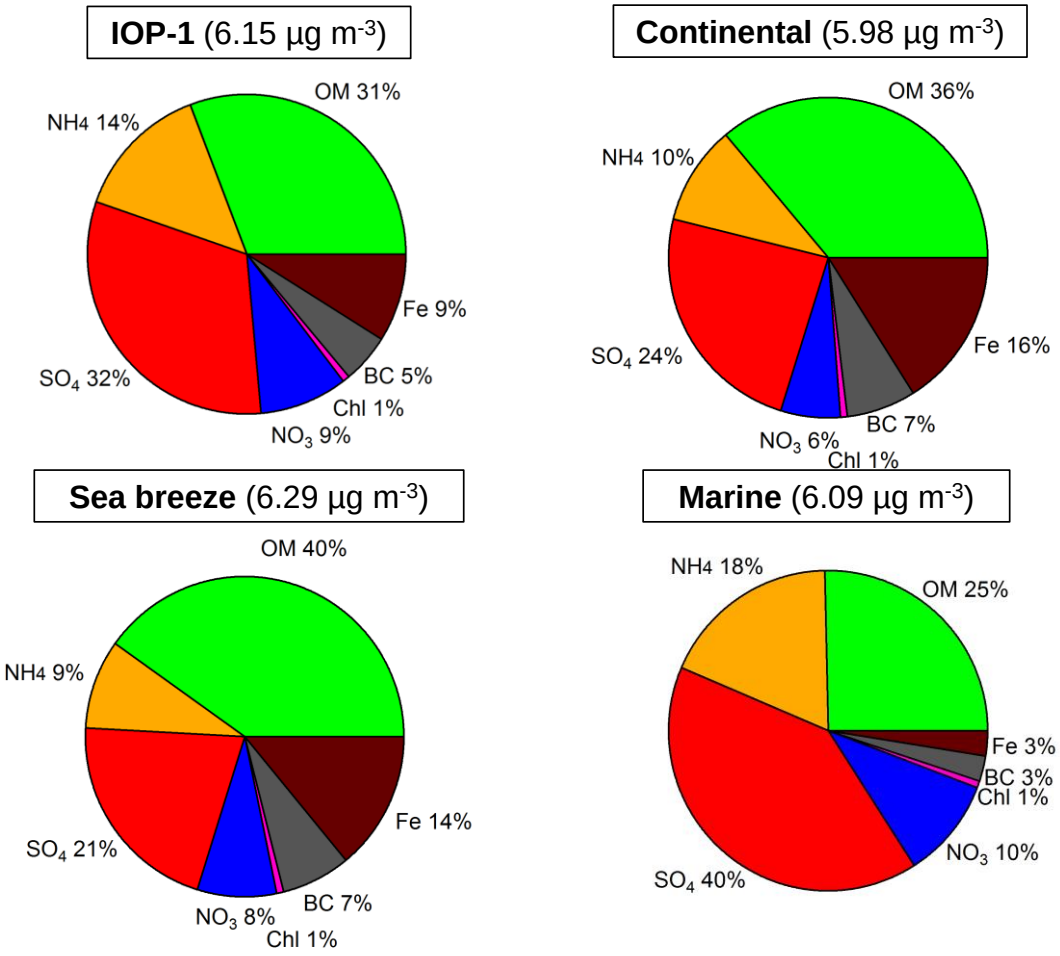
IOP-1 (6.15 µg m-3)
OM 31%
NH4 14%
Fe 9%
SO4 32%
BC 5%
Chl 1%
NO3 9%
Continental (5.98 µg m-3)
OM 36%
NH4 10%
SO4 24%
Fe 16%
NO3 6%
BC 7%
Chl 1%
Sea breeze (6.29 µg m-3)
OM 40%
NH4 9%
SO4 21%
Fe 14%
NO3 8%
BC 7%
Chl 1%
Marine (6.09 µg m-3)
NH4 18%
OM 25%
Fe 3%
BC 3%
Chl 1%
NO3 10%
SO4 40%

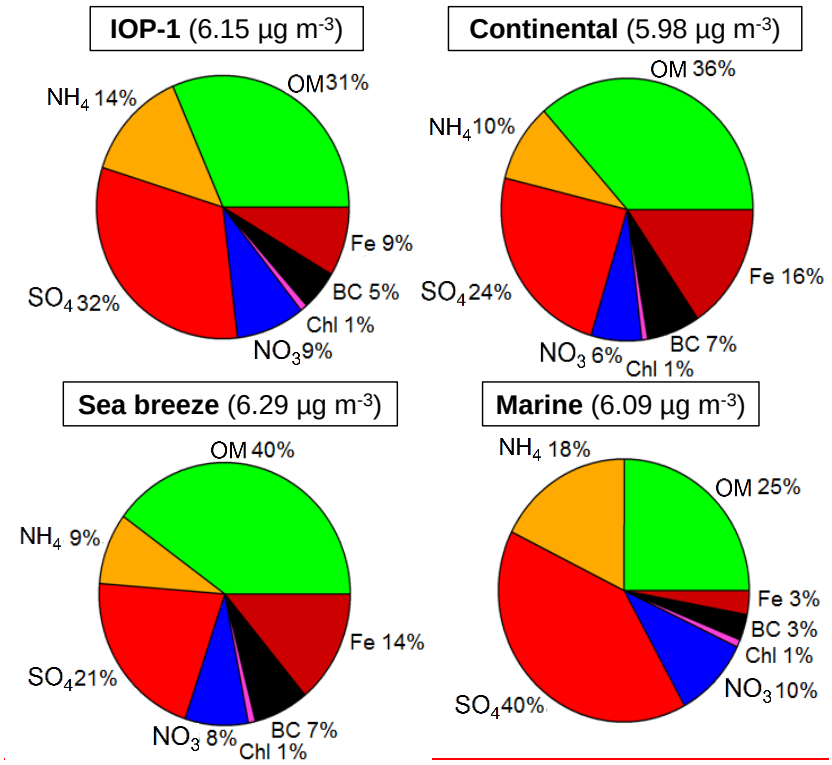

Fig. 5. Averaged contributions of NR-PM_1, BC and Fe for IOP-1 (n = 3771), continental (n = 307), sea breeze (n= 799) and marine days (n = 1843) (with average total concentration in µg m^{-3} in parenthesis).

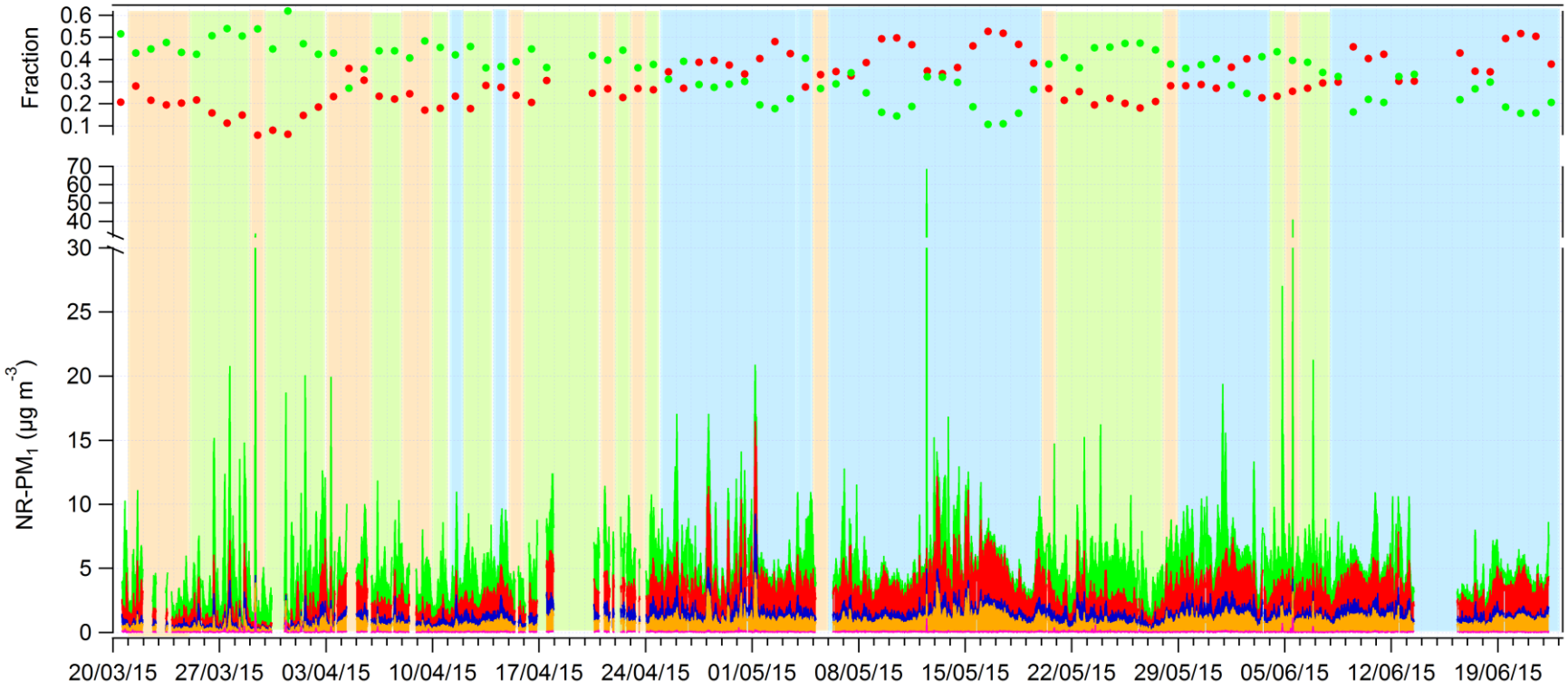

Fig. 6. (Bottom) IOP-1 stacked time series of OM (green), SO_4 (red), NO_3 (blue), NH_4 (orange) and Chl (pink) on ACSM time step (30 min) and (top) daily averaged fraction of OM and SO_4. Tinted areas correspond to continental days in light pink, sea breeze days in light green and marine days in light blue.

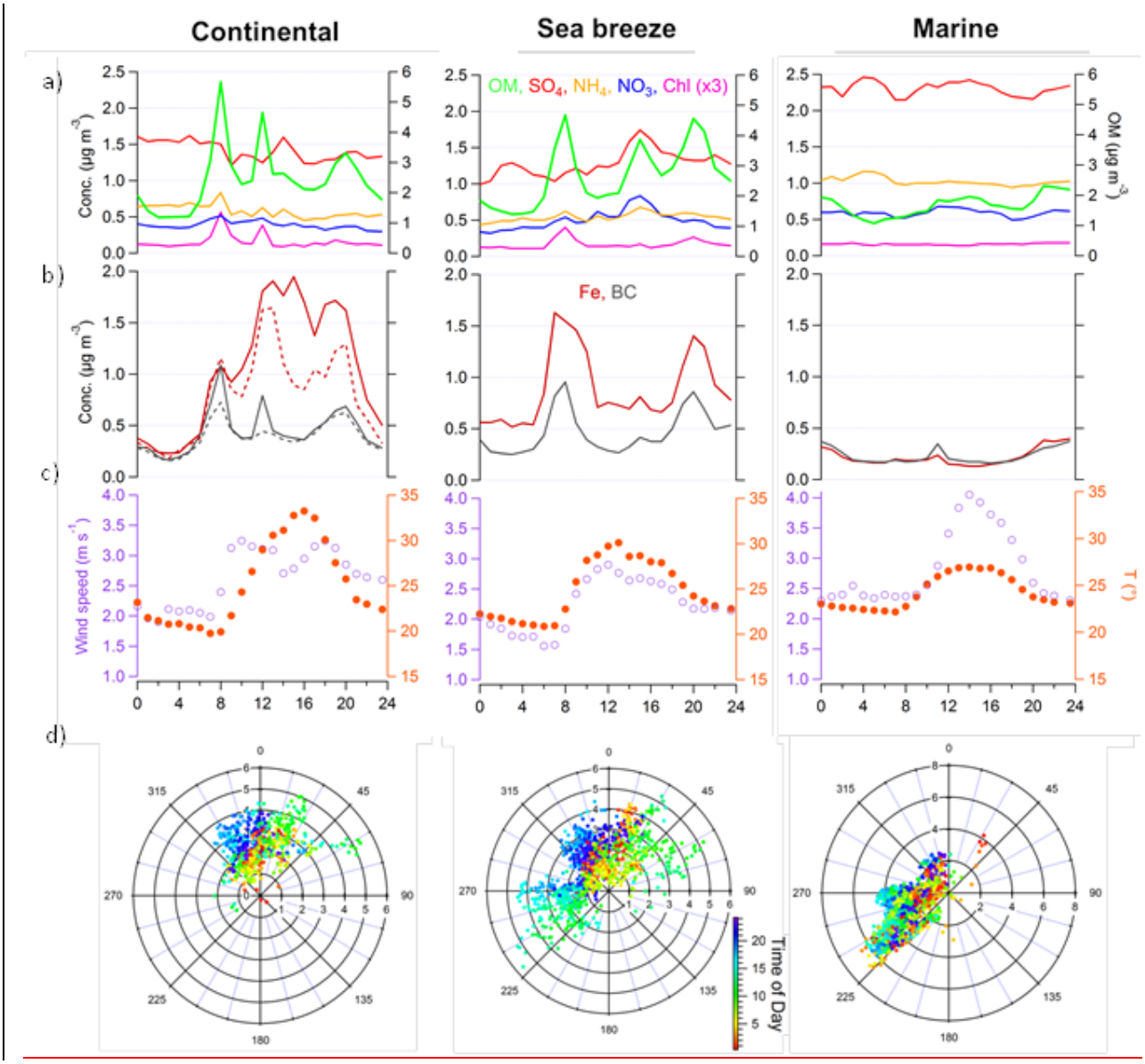
Continental
Sea breeze
Marine
a)
b)
c)
d)
Conc. (μg m-3)
OM, SO4, NH4, NO3, Chl (x3)
OM (μg m-3)
Fe, BC
Wind speed (m s-1)
T (°)
Time of Day

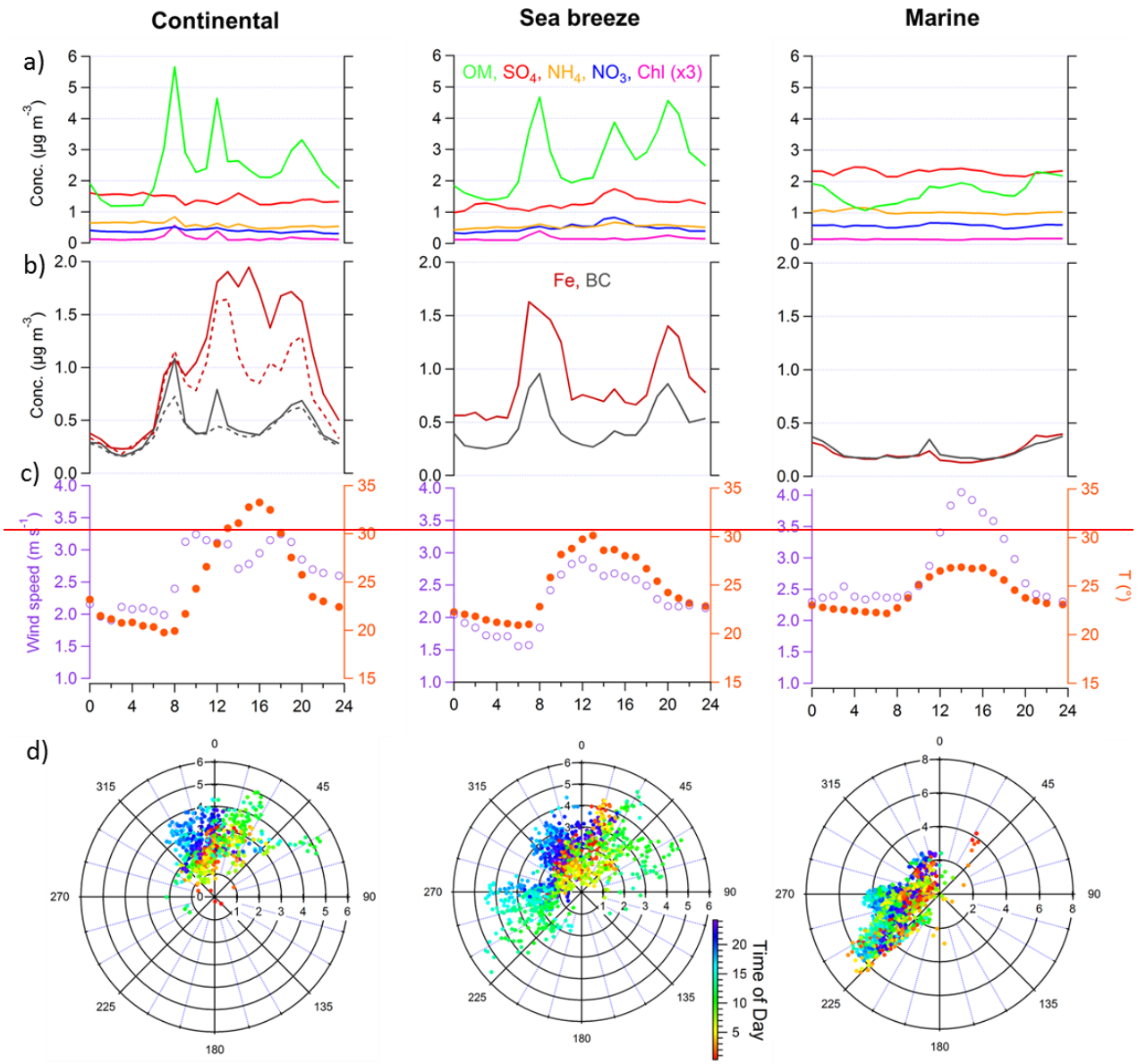

Fig.7. Average daily profiles of (a) NR-PM_1, (b) BC and Fe concentrations, (c) wind speed and temperature for (from left to right) continental (dotted lines: medians), sea breeze and marine days. (d) Associated wind roses (radius, wind speed in m s-1) colored by time of day in UTC.

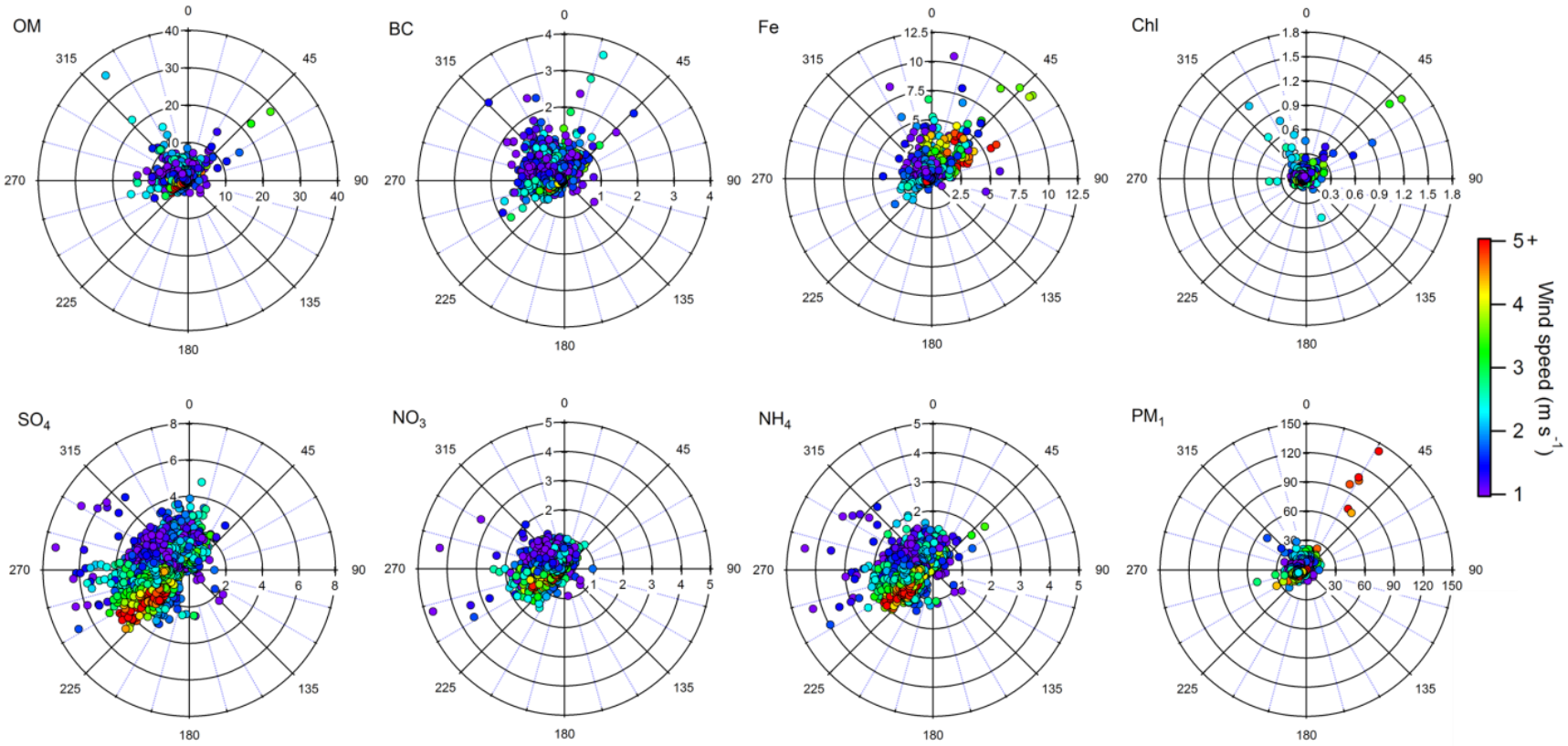

Fig. 8. Pollution rose plots of OM, BC, Chl, Fe, SO_4, NO_3, NH_4 and total PM_1 for the whole IOP-1, with concentrations (µg m^{-3}) as radius and colored by wind speed (measurements inferior to 1 m s^{-1} in grey).

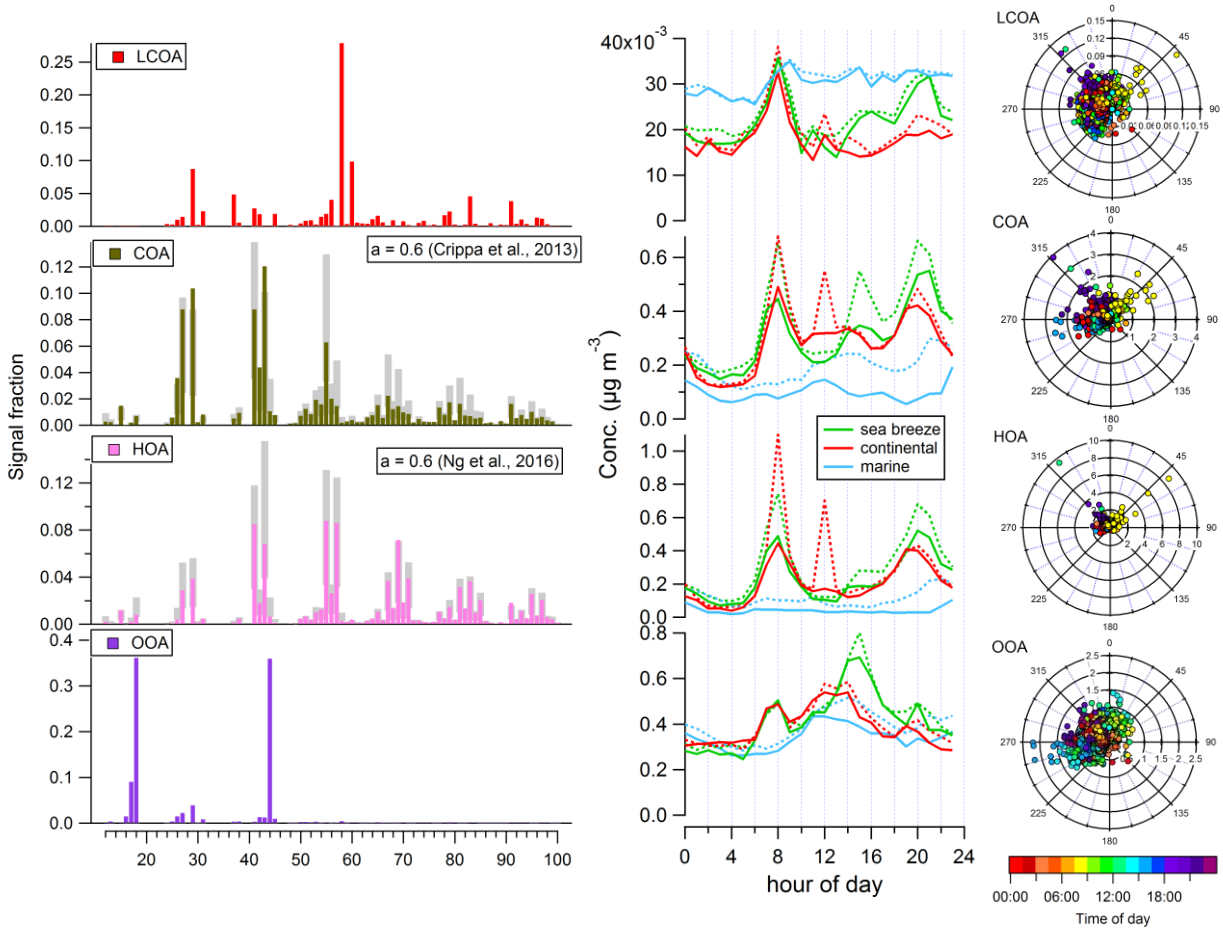
LCOA
COA
HOA
OOA
a = 0.6 (Crippa et al., 2013)
a = 0.6 (Ng et al., 2016)
Signal fraction
Conc. (µg m-3)
40x10-3
sea breeze
continental
marine
hour of day
Time of day
00:00
06:00
12:00
18:00

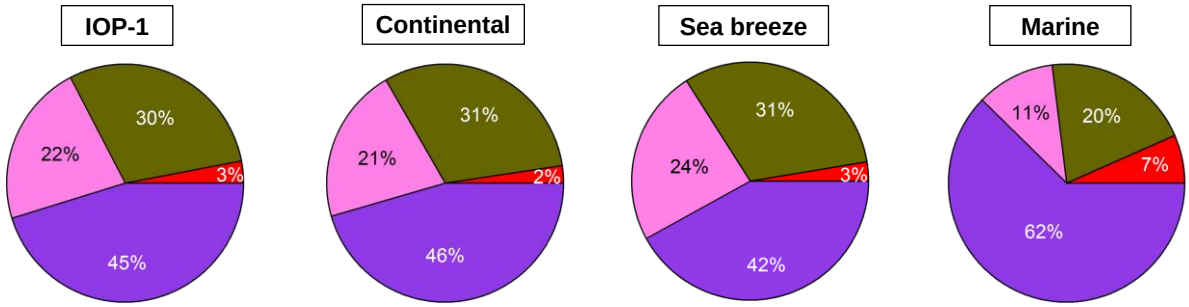
IOP-1
30%
22%
3%
45%
Continental
31%
21%
2%
46%
Sea breeze
31%
24%
3%
42%
Marine
11%
20%
7%
62%

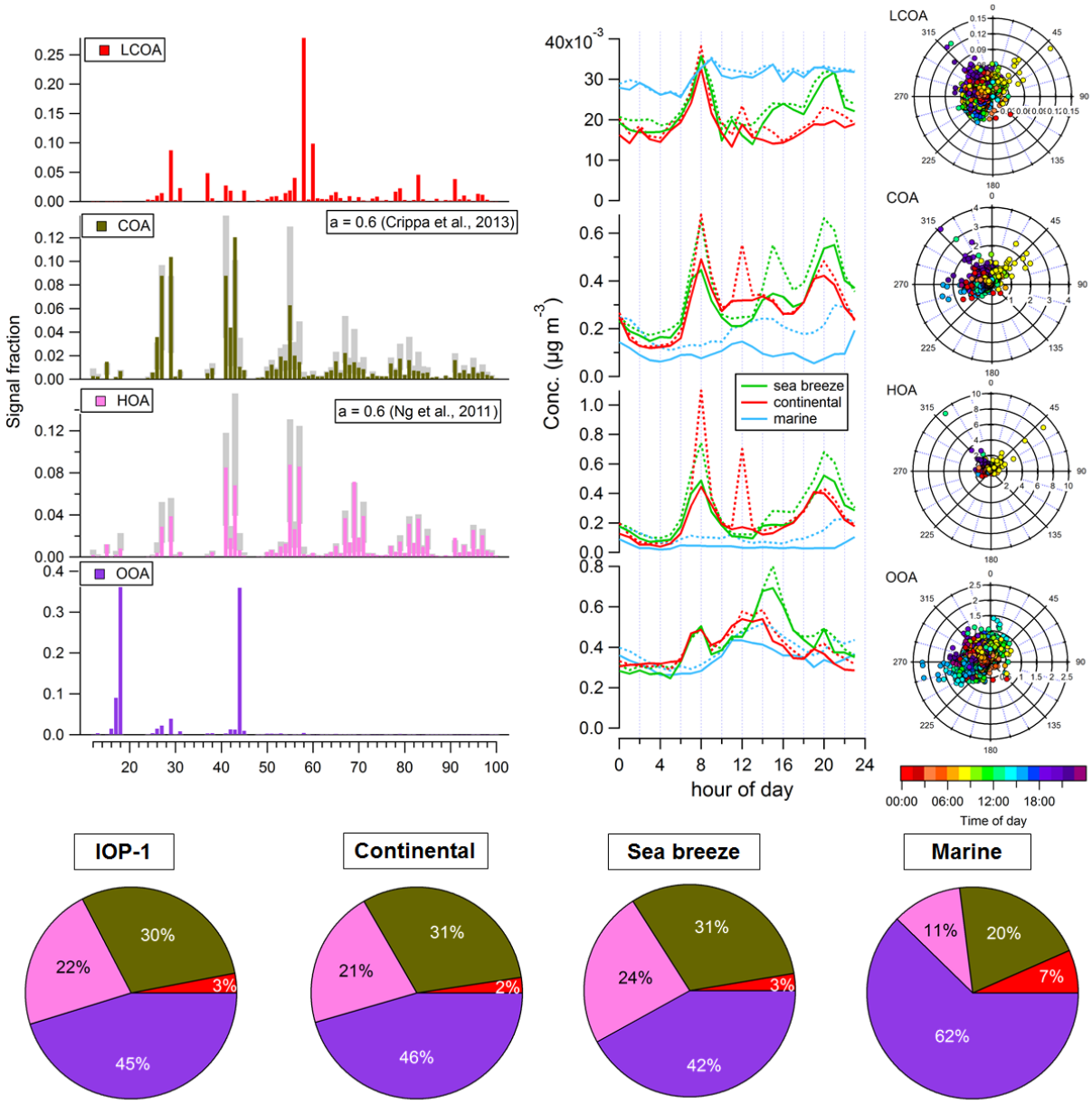

Fig. 9. PMF constrained 4-factor solution: (left) factor profiles of LCOA, COA, HOA (the two latter constrained), OOA; (middle) corresponding daily cycles according to day types (solid lines: median; dotted lines: average); and (right) pollution rose plots colored by time of day. (bottom) Average pie charts of the contributions to the total organic fraction for IOP-1, continental, sea breeze and marine days.

Supplementary material for manuscript:

Chemical characterization and source apportionment of submicron aerosols measured in Senegal during the 2015 SHADOW campaign

L.-H. Rivellini[1,2,*], I. Chiapello[2], E. Tison[1], M. Fourmentin[3], A. Féron[4], A. Diallo[5], T. N'Diaye[5], P. Goloub[2], F. Canonaco[6], A. S. H. Prévôt[6], and V. Riffault[1,*]

[1] IMT Lille Douai, Univ. Lille, SAGE - Département Sciences de l'Atmosphère et Génie de l'Environnement, F-59000 Lille, France
~~[1]Département Sciences de l'Atmosphère et Génie de l'Environnement, IMT Lille Douai, Douai, 59508, France~~
[2]Univ. Lille, CNRS, UMR8518 – LOA – Laboratoire d'Optique Atmosphérique, F-59000 Lille, France
~~[2]Laboratoire d'Optique Atmosphérique, Université de Lille - CNRS, Villeneuve d'Ascq, 59655, France~~
[3]Laboratoire de Physico-Chimie de l'Atmosphère, Université du Littoral Côte d'Opale, Dunkerque, F-59140, France
[4]Laboratoire Interuniversitaire des Systèmes Atmosphériques, CNRS - Université Paris Est Créteil - Université Paris Diderot, Créteil, F-94010, France
[5]Institut de Recherche pour le Développement, M'Bour, Senegal
[6]Laboratory of Atmospheric Chemistry, Paul Scherrer Institute, CH-5232 Villigen, Switzerland

[*] Corresponding authors:

Véronique Riffault

Tel.: +33 327 712 604, Fax: +33 327 712 914, e-mail: veronique.riffault@imt-lille~~mines~~imt-~~lille~~-douai.fr

Laura-Hélèna Rivellini

e-mail: laura.rivellini@imt-lille~~mines~~-douai.fr

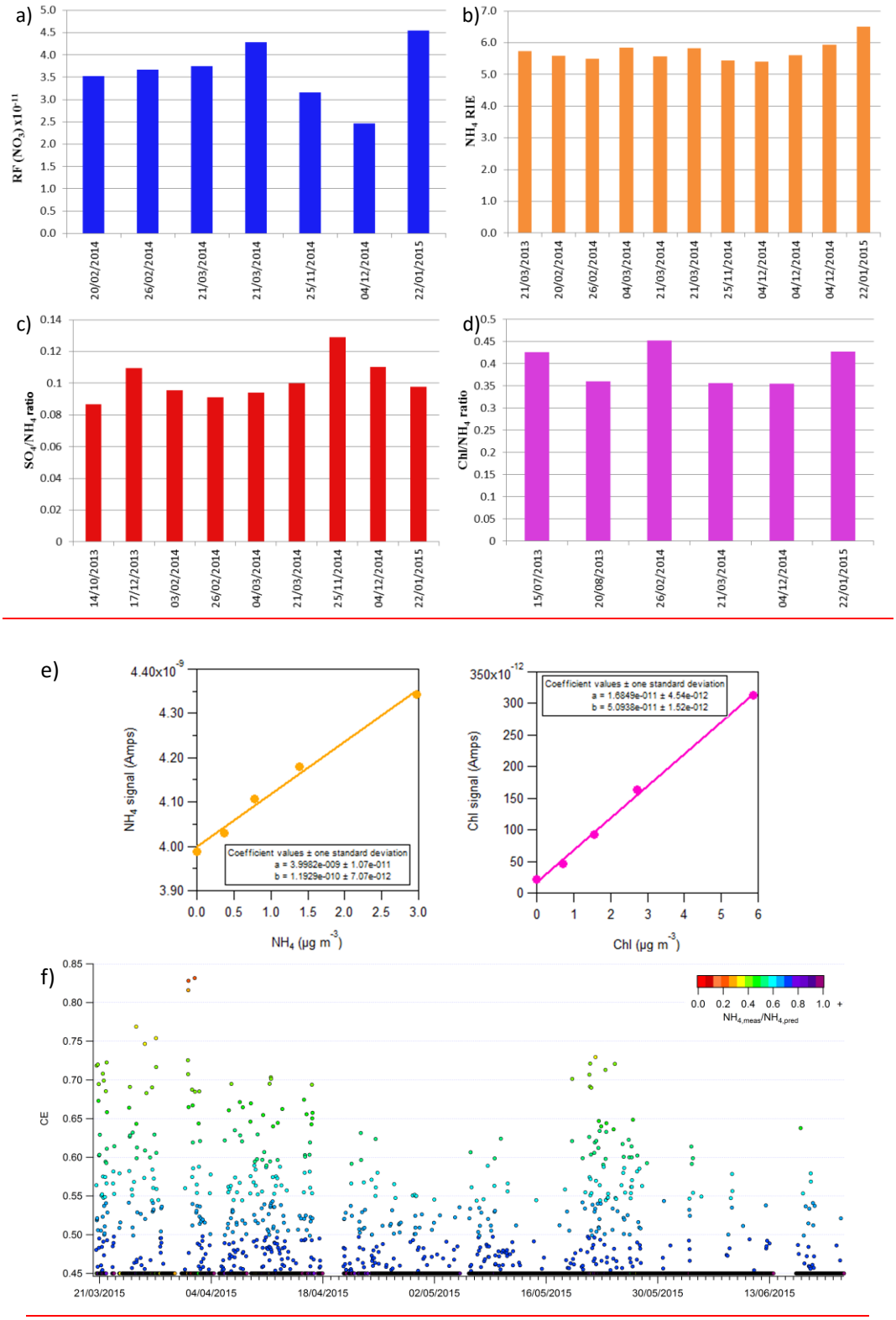

Figure S1. Values of (a) RF(NO_3), (b) RIE of ammonium, and ratios to ammonium for (c) sulfate and (d) chloride obtained from calibrations performed during a previous campaign (before Nov. 25th 2014; Zhang et al., in prep.) ~~(before Nov. 25th 2014)~~ and this study (~~after and including~~ Nov. 25th 2014 and beyond). (e) Chl and NH_4 calibration curves performed on January 22nd, 2015. (~~e~~f) T~~t~~ime series of CE values corrected following Middlebrook et al. (2012) algorithm colored by the $NH_{4,meas}/NH_{4,pred}$ ratio ~~of $NH_{4,meas}/NH_{4,pred}$~~.

Appendix S2. Deconvolution method uncertainties and comparison with literature data

The uncertainties on estimated Fe concentrations can be calculated by applying the propagation for uncertainties on the values of K_{Fe} (10%) and the slope b (39%, calculated using a variability of 0.2 for the two Angström absorption exponents (AAE), β and α (Fialho et al., 2006)), which gives an overall uncertainty of ~40%. However this method is highly sensitive to even small variations of α (BC) and β (DD), with values quite well known for BC from fossil fuel ranging from 0.8 to 1.1 (Hansen, 2005; Zotter et al., 2017 and references therein) but not so much for dust. In the manuscript, we chose to use β = - 4, according to Fialho et al. (2006) values determined at the Azores Islands for samples influenced by Saharan dust events. But other values can be found in the literature (Table S2.1), ranging from -1.6 to -6.5 and largely influenced by the wavelength range as well as dust origins and size fractions since the iron content differ depending on emission sources and particle size (Journet et al., 2014). Even during the SAMUM campaign (May to June 2006 in Morocco), a wide range of AAE values have been reported from -1.6 up to -5.1 for ground-based measurements in the same size fraction, as shown in Table S2.1.

Table S2.1. Mineral dust AAE values reported from field campaigns around the Saharan region.

Reference	Location / Period	Wavelengths (nm)	Fraction	β
Fialho et al. (2006) [a]	Azores Islands Jul. 2001 – Jun. 2005	370-950	-	-4
Müller et al. (2009) [a]	Tinfou, Morocco (SAMUM) Summer 2006	467/660	PM_{10}	-2.25 to -5.13
Petzold et al. (2009) [b]	South-East Morocco (SAMUM) Summer 2006	467/660	$PM_{2.5}$	-2 to -6.5
Schladitz et al. (2009) [a]	Tinfou, Morocco (SAMUM) Summer 2006	537/637	PM_{10}	-1.6 to -4.73
(Linke et al., 2006) [c]	Morocco Egypt	266/532	~PM_4	-4.2 -5.3
(Caponi et al., 2017) [c]	Morocco Lybia Algeria Mali	375-850 375-532 375-850 375-532	$PM_{2.5}$ ($PM_{10.6}$)	-2.6 -4.1 (-3.2) -2.8 (-2.5) -3.4

[a] In situ ground-based measurements; [b] Airborne measurements through dust plumes; [c] Laboratory experiments with resuspended soil samples

Applying a relatively small increase (resp. decrease) of 10% on the value of β for our dataset led to a 33% decrease (resp. 50% increase) of iron concentrations, as shown in Figure S2.1, but no change in the temporal behavior.

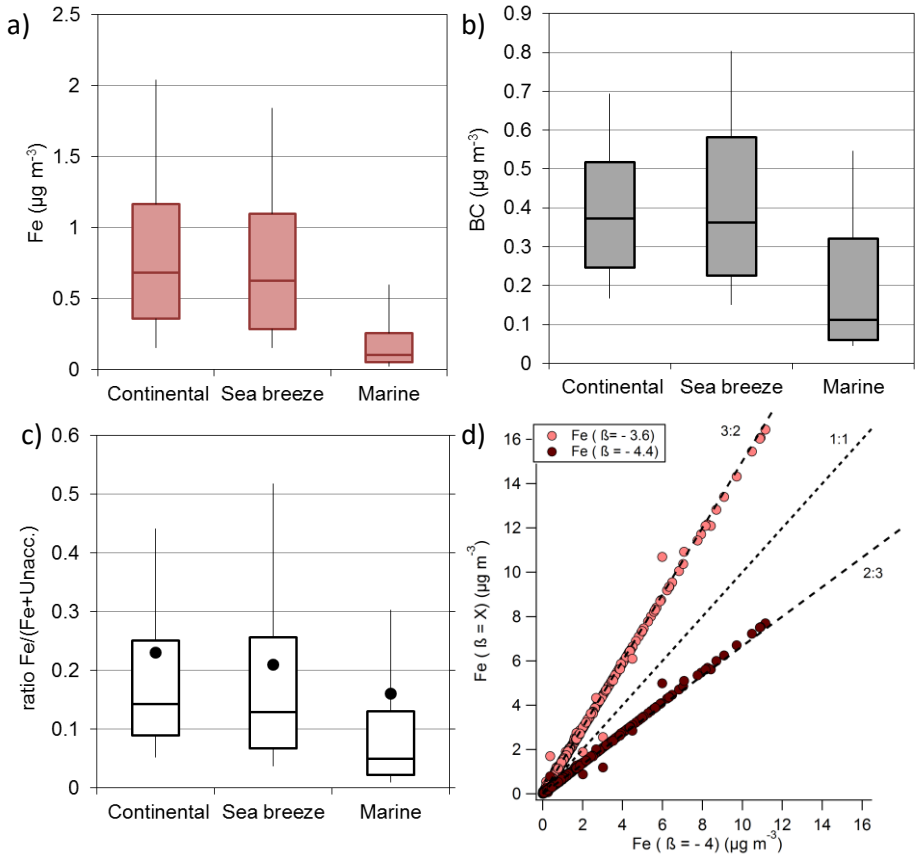

Figure S2.1. Box plots of (a) Fe, (b) BC concentrations and (c) Fe/(Fe+Unacc.) ratio for continental, sea breeze and marine days. (d) Scatter plot of iron concentrations (in µg m-3) obtained from Fialho's deconvolution method using an AAE value of ± 10% compared to the one from the literature and used in the manuscript.

Table S2.2 summarizes the iron content determined in Saharan samples, which shows that the relative contribution of iron determined in this work is in the same order of magnitude but still significantly higher. However iron oxides can be found mostly (for ~2/3) in the clay fraction (~$PM_{2.5}$) and ~1/3 in the silt (coarse) fraction (Journet et al., 2014; Kandler et al., 2009), which is consistent with increased ratios in the submicron fraction compared to larger ones. It is also worth noting that Val et al. (2013) measured the iron content in the ultrafine and fine fractions (corresponding to PM_1) of particles collected in Dakar, and measured a ratio in the upper range of those already reported in the literature, even in the absence of dust event.

The approach used here leads to an estimate of the absolute concentrations of iron, although with high uncertainties given all the necessary assumptions and the empirical algorithm used to deconvolve BC and Fe from absorption measurements. However the temporal profiles, non-parametric wind regression (NWR) plots and potential source contribution function (PSCF) maps (now provided in Figures S5b and S5c, respectively) are all consistent with the expected behavior of such a desert dust tracer and show that it can be useful in determining the contribution of dust to absorption measurements. There is nonetheless quite some room for improvement, in particular for a better estimation of the AAE value for dust similar to the efforts carried out to determine the AAE values for BC from fossil fuel and wood burning (Zotter et al., 2017). We strongly believe the lack of information for submicron particles in terms of chemical composition of refractory species and optical properties should be better addressed, but is beyond the scope of this work.

Table S2.2: Comparison of iron content (in %) determined in Saharan dust and soil samples

Reference	Location	Method [a]	Size fraction	%Fe [b]
Dust samples				
(Lafon et al., 2004)	Banizoumbou (Niger)	XRF; CBD	TSP	6.3; 7.8
(Lafon et al., 2006)	Banizoumbou,	XRF; CBD	TSP	4.3 – 6.1
(Lafon et al., 2006)	Cape Verde	XRF; CBD	TSP	5.3 – 6.0
(Formenti et al., 2008)	Banizoumbou	CBD	40 µm	5.8
(Val et al., 2013)	Dakar (Senegal)	ICP-MS	1 µm	7.8
This work	M'Bour	cf. text	1 µm	23 (continental) 21 (sea breeze) 16 (marine)
Soil samples				
(Moreno et al., 2006)	Saharan region (9 samples)	ICP-AES/ ICP-MS	TSP	2.0 – 4.7
(Lafon et al., 2006)	Banizoumbou,	XRF; CBD	10.2 µm [*] 2.5 µm [*]	5.3 5.8
(Joshi et al., 2017)	M'Bour, Bordj (Algeria), Nefta (Tunisia)	XRD	100 µm	< 0.5

[a] XRF: X-ray Fluorescence (XRF) Spectrometry for elemental analysis; CBD: chemical method based on citrate-bicarbonate-dithionite (CBD) reagent for quantification of iron oxides adapted from soil analysis (Mehra and Jackson, 1960)

[b] Percentages of iron relative to the mass of all oxides, classically taking into account Na_2O, MgO, Al_2O_3, SiO_2, K_2O, CaO, TiO_2 and Fe_2O_3.

[*] Soil samples resuspended using wind tunnel and collected with a 13-stage impactor

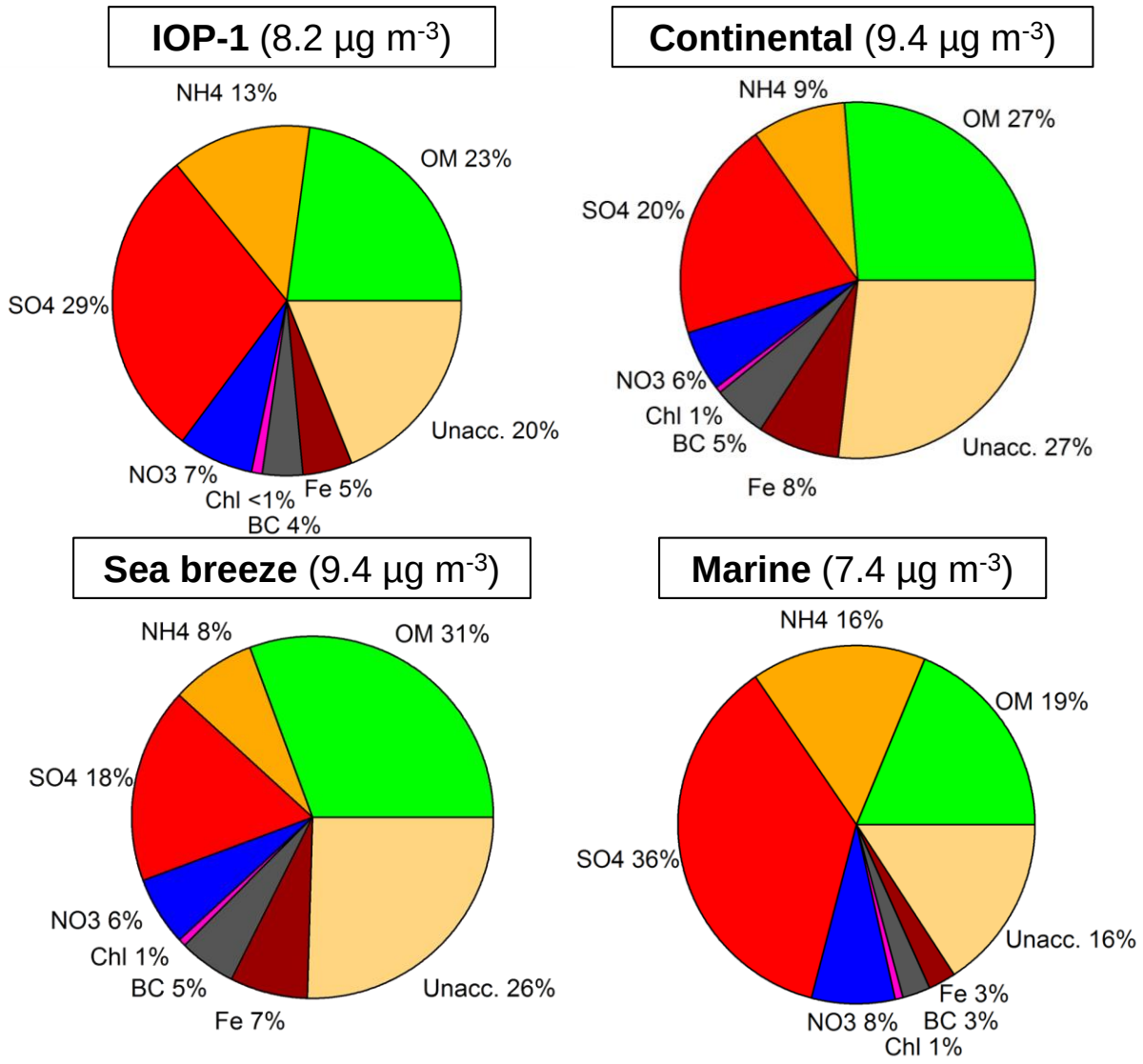

Figure S~~2~~3. Averaged PM_1 chemical composition for (a) IOP-1 (n = 2952), (b) continental (n = 307), (c) sea breeze (n = 799) and (d) marine days (n = 1846). Only days with at least 50% of the total PM_1 mass concentration measurements by TEOM-FDMS were taken into account for averaging, corresponding to 11 days for continental, 21 days for sea breeze and 42 days for marine days. Unacc.: unaccounted fraction determined as the difference between the gravimetrically measured PM_1 mass concentration and the sum of chemical species from ACSM and aethalometer measurements

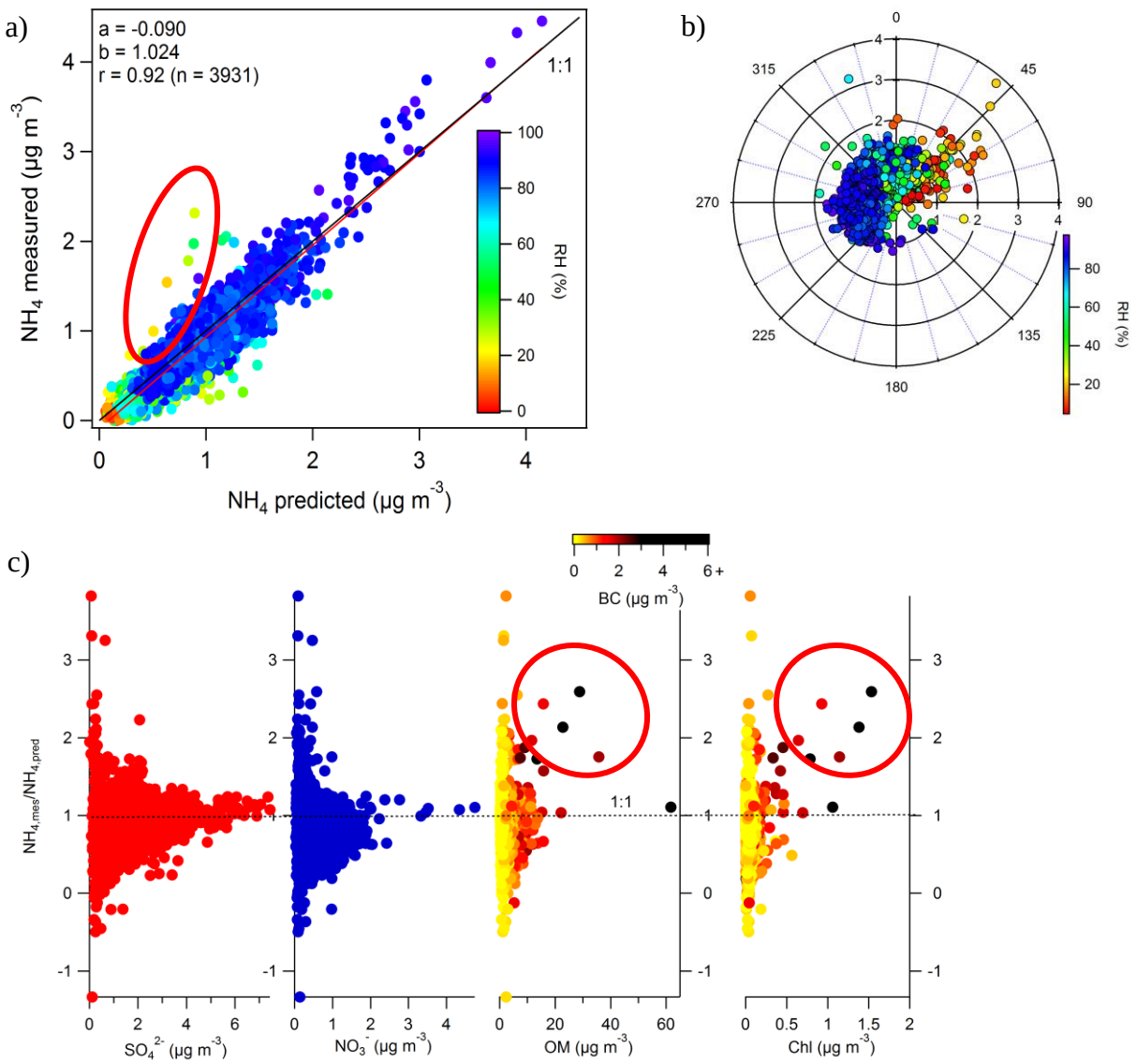

Figure S34. (a) Scatter plot between measured and predicted NH_4 colored by relative humidity and (b) associated rose plot, (c) $NH_{4,meas}/NH_{4,pred}$ ratios as a function of SO_4, NO_3, OM and Chl species, where OM and Chl data are colored by BC concentrations. The red ellipses highlight the data points deriving from the 1:1 ratio corresponding to aerosol neutralization.

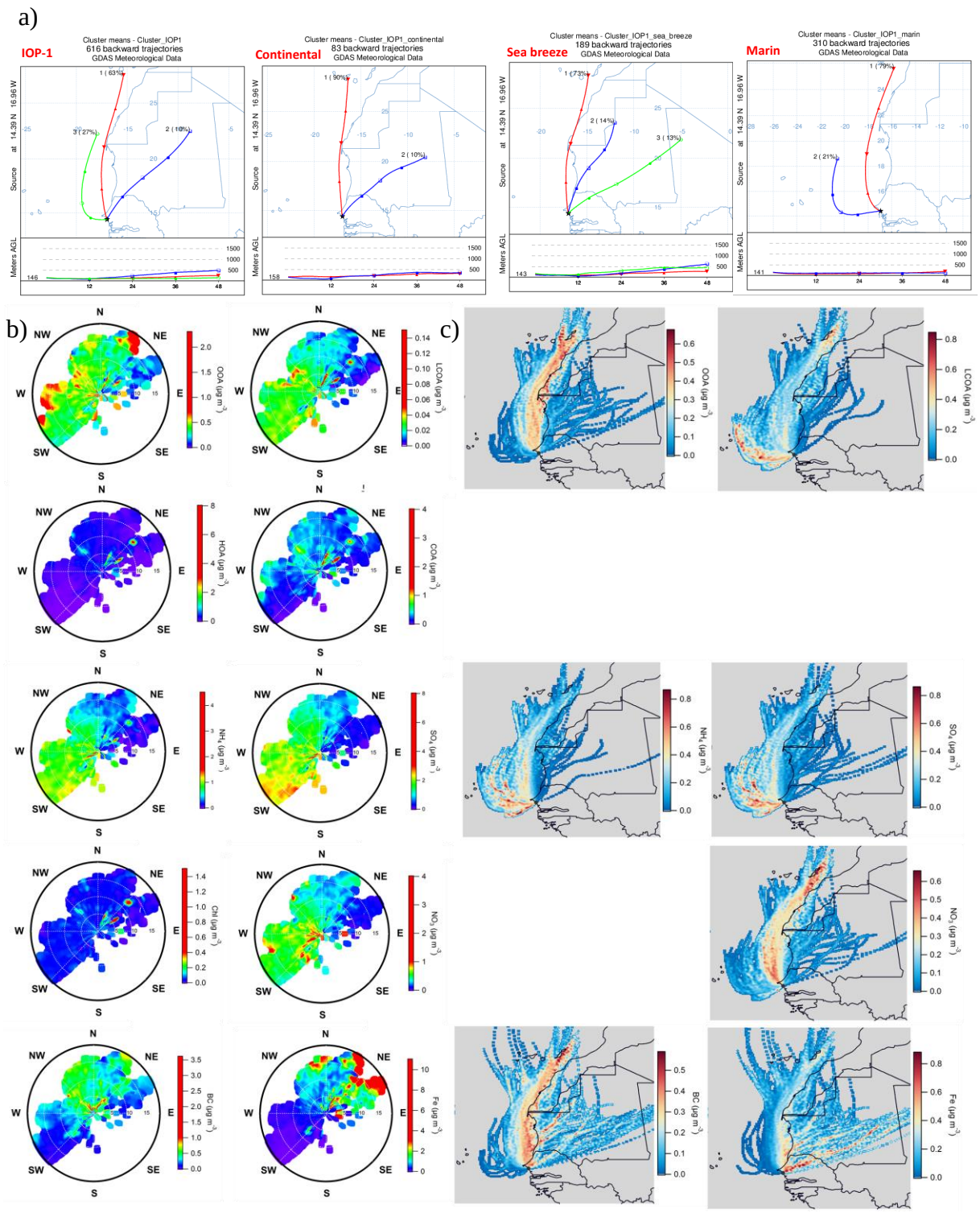

Figure S5. (a) 48-hour back trajectory clusters for (from left to right) IOP-1, continental, sea breeze and marine days. (b) NWR plots (input parameters: angular and radial resolution of 0.1, angle smoothing of 2 and radial smoothing of 1; upper limit of the color scale: 75th percentile) for PMF factors and NR-PM$_1$, BC and Fe species and corresponding (c) PSCF maps for species showing regional influence (threshold: 75th percentile) during IOP-1.

Appendix S46. Unconstrained PMF analysis

(a) 3-factor solution

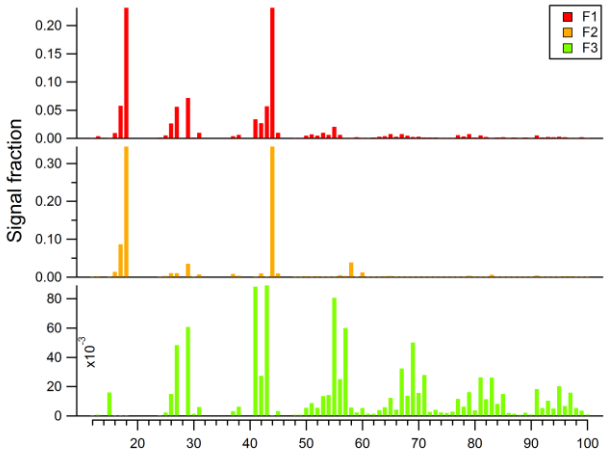

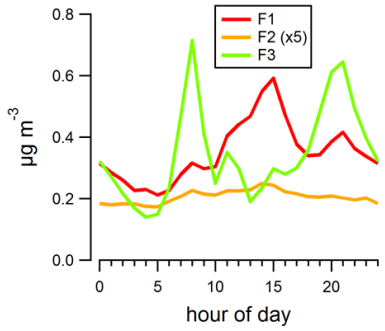

(b) 4-factor solution

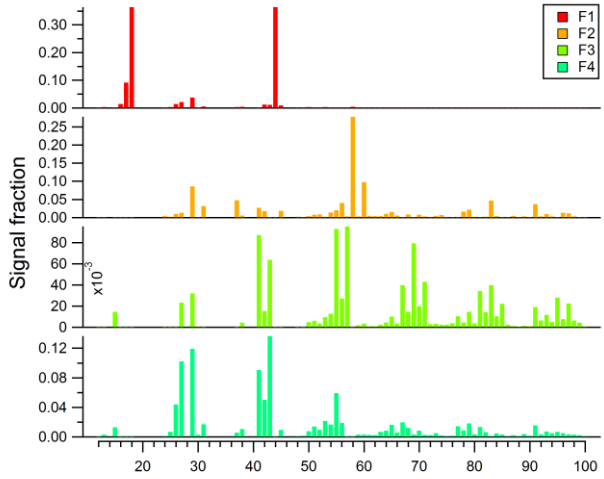

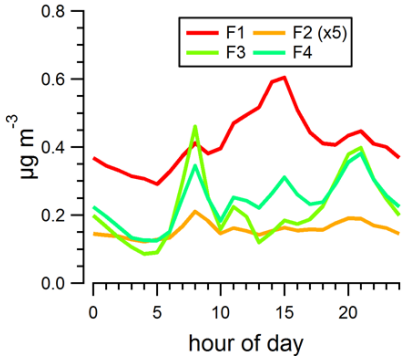

(c) 5-factor solution

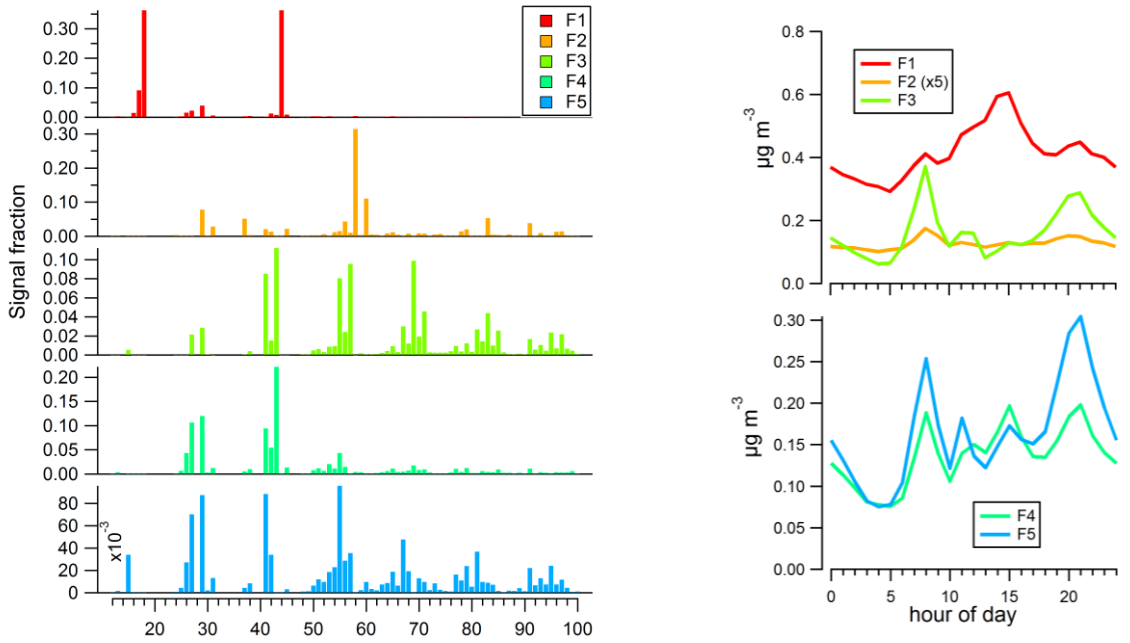

(d) 6-factor solution

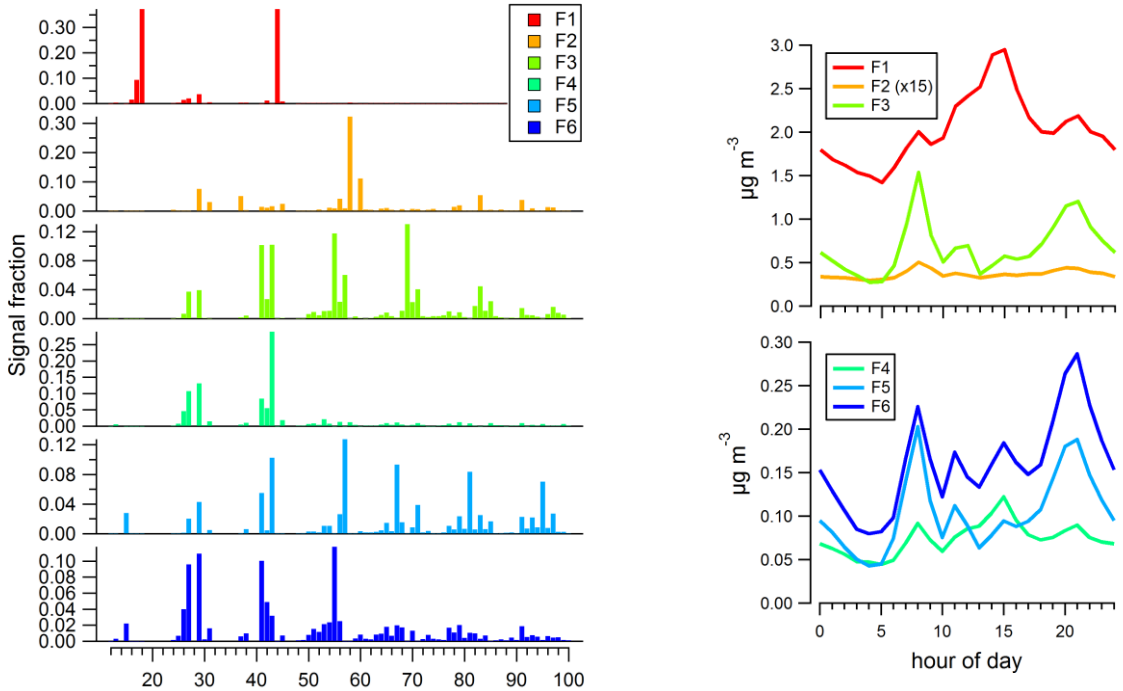

(e) 7-factor solution

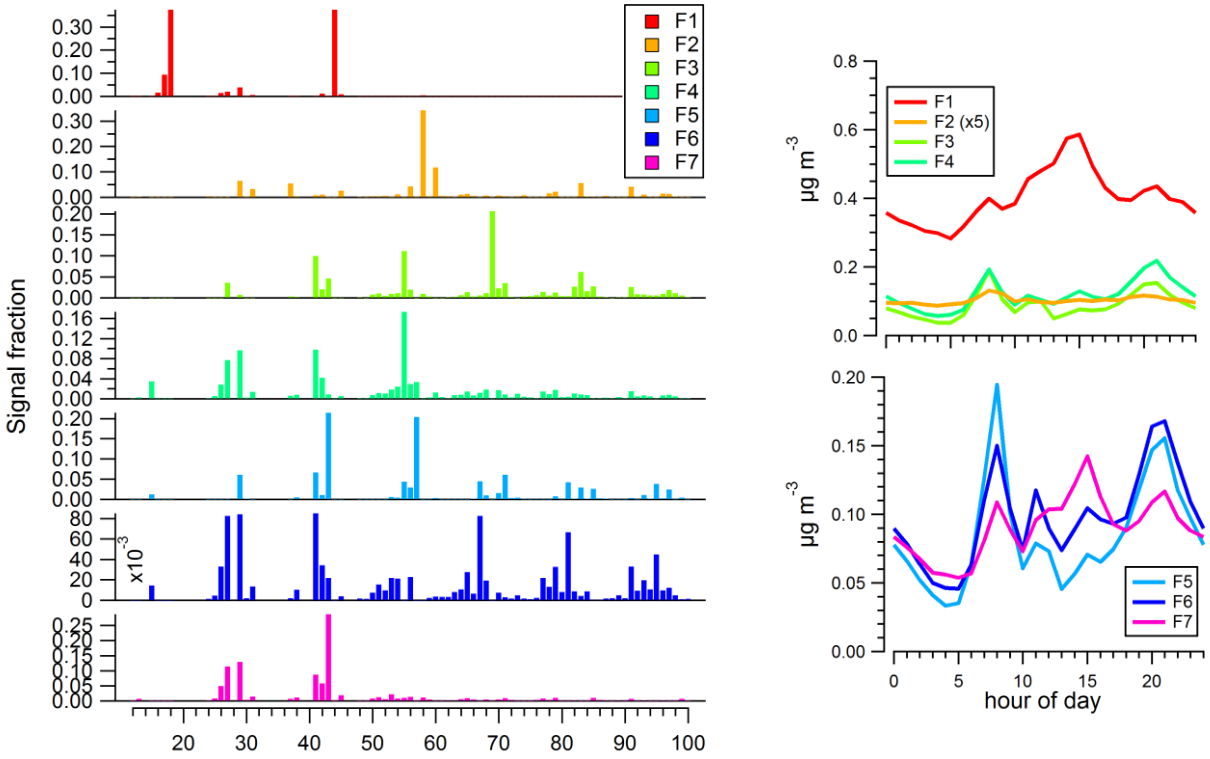

(f) 8-factor solution

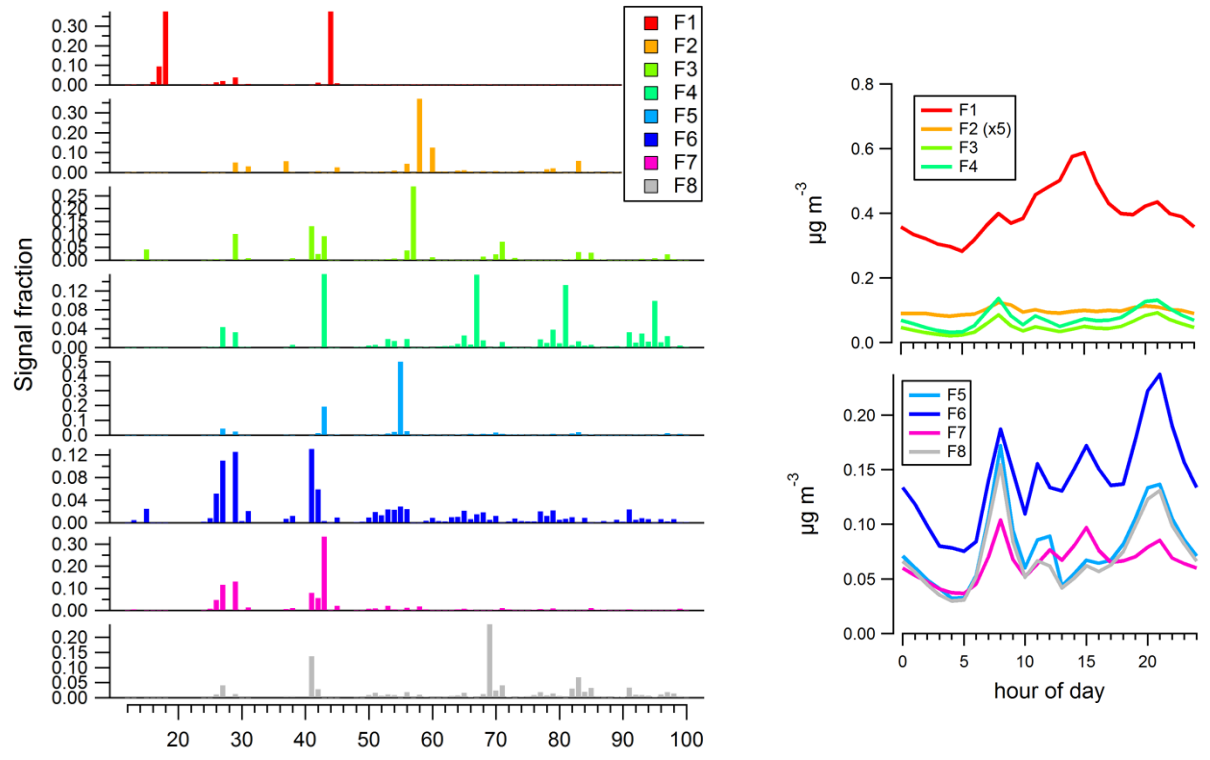

(g) 9-factor solution

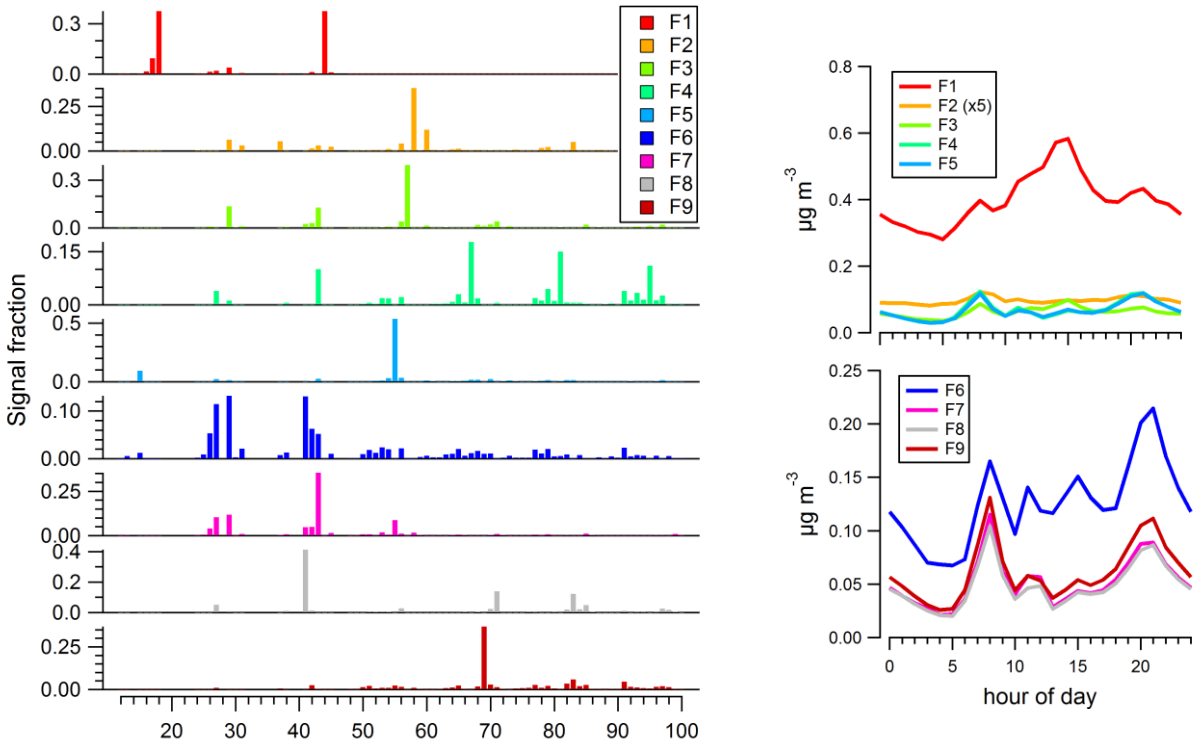

(h) 10-factor solution

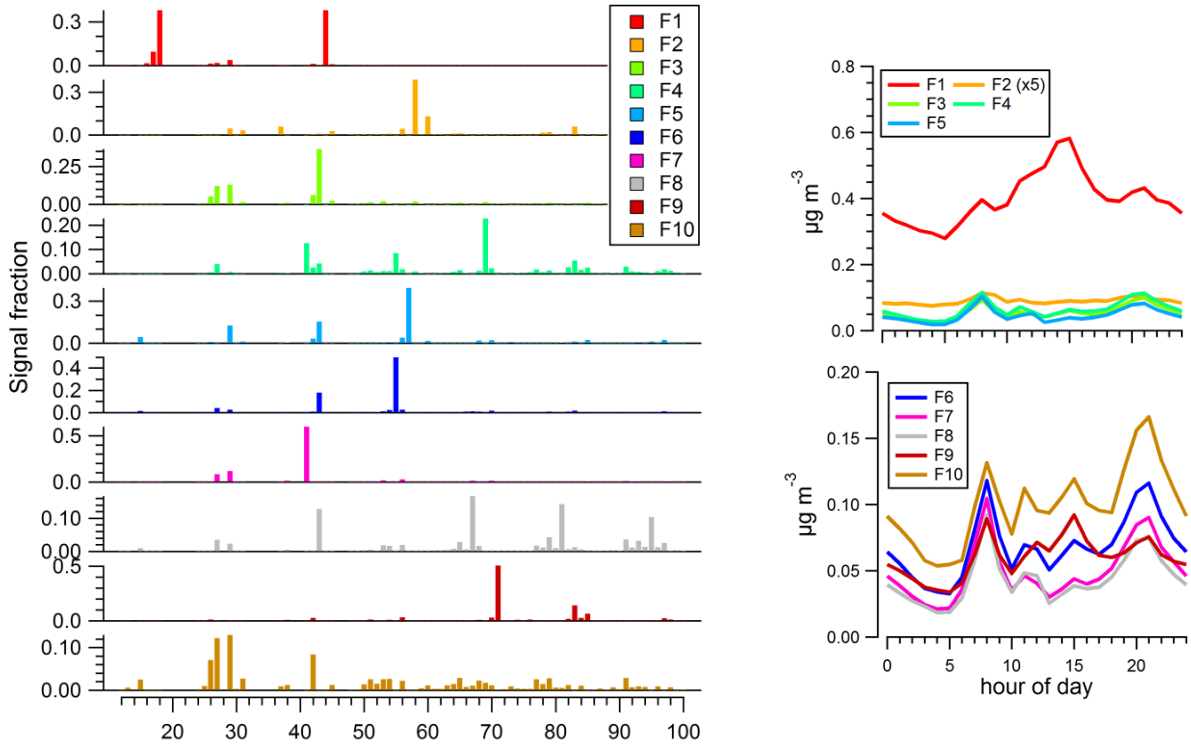

Figure S6.1. PMF unconstrained solutions from 3 to 10 factors, with (left) factors profiles and (right) corresponding daily cycles.

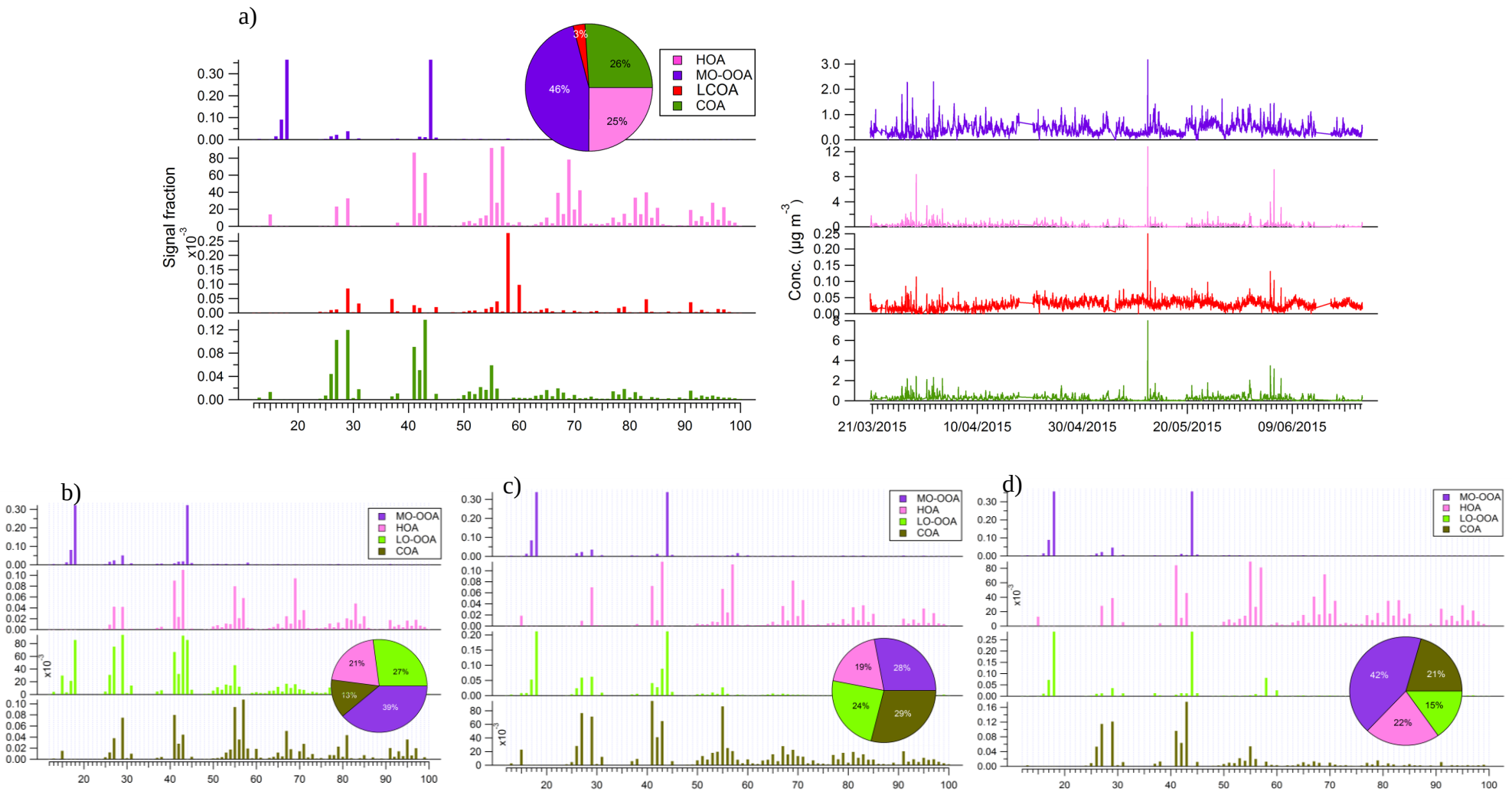

Figure ~~S4~~S6.~~12~~. 4-factor PMF unconstrained solutions with (a) factor profiles, pie chart and time series for IOP-1; and factor profiles and pie charts for (b) continental (Q/Qexp = 0.37), (c) sea breeze (Q/Qexp = 0.36) and (d) marine (Q/Qexp = 0.27) days ~~with corresponding pie charts~~.

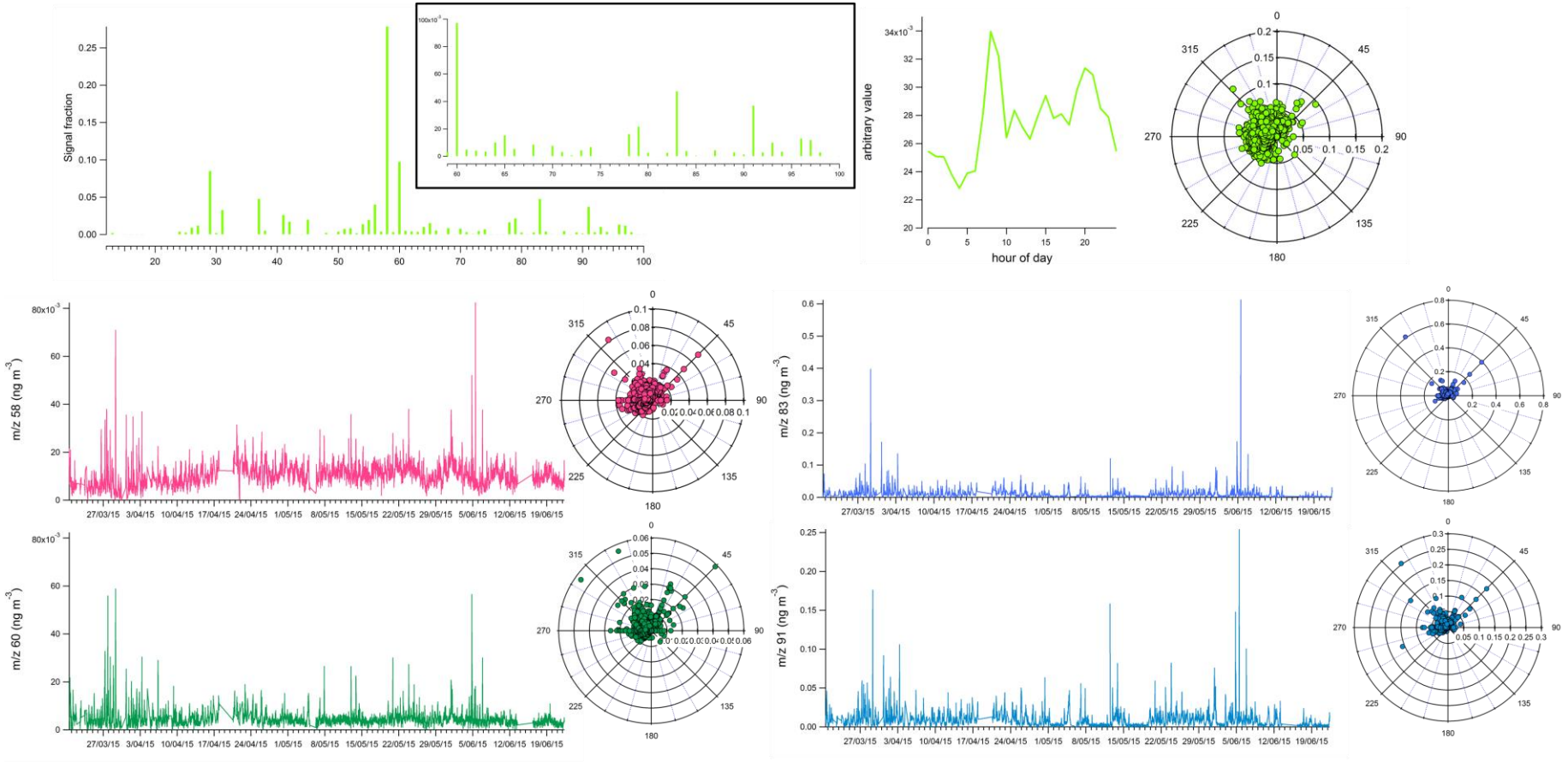

Figure ~~S4~~S6.~~2~~3. (top) Mass spectrum (inset: m/z ≥ 60), daily profile and rose plot of the LCOA factor from the unconstrained 4-factor solution; (bottom) Time series and rose plots of fragments at m/z 58, 60, 83 and 91

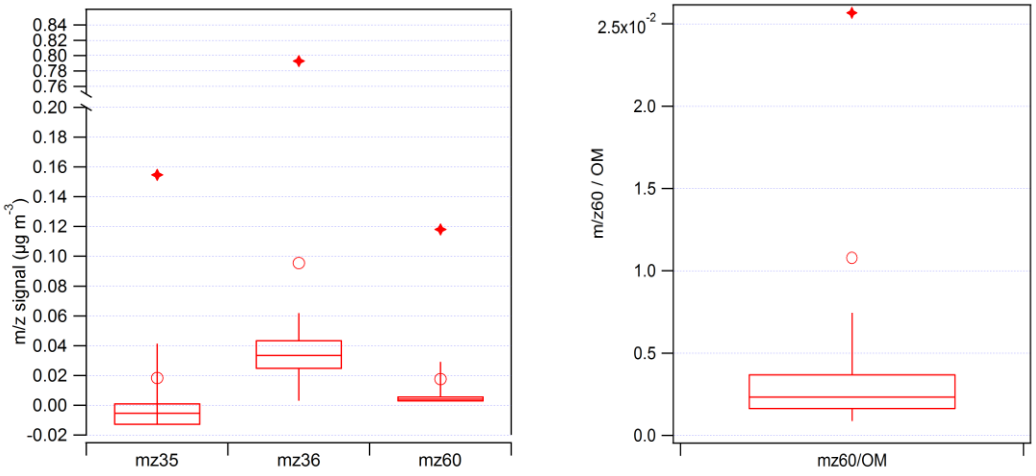

Figure ~~S5~~S7. Box plots of (left) -the m/z 35, 36 and 60 signals and (right) of themz 60/OM (f_{60}) ratio. For each box plot, top line: 75th percentile, bottom line: 25th percentile, middle line: 50th percentile (median); top whisker: 95th percentile, bottom whisker: 5th percentile. The open circle and the cross represent the 99th percentile and maximum value, respectively.

Appendix ~~S6~~S8. –PMF 5-factor solution including organics + m/z 36 as input data

Since the behavior of Chl had also been suspected to come from the same sources, m/z signals at 35 and 36 were investigated in order to possibly implement them in the model input. However the m/z 35 signal presented an important amount of slightly negative values (-3.0 ± 6.2 × 10-13, see Figure S~~5~~7) which likely resulted from a slow vaporization of refractory chloride species both during filter and non filter measurement as previously observed (Nuaaman et al., 2015). For this reason only m/z 36 was incorporated into the model without additional normalization since the signal intensity was close to organic ones. Uncertainties were estimated as followed.

The detection limits (DL_x) for these m/z were assumed to be equal to 3 times their respective signal-to-noise ratio for filtered air. The method to determine the uncertainties has already been used to carry out source apportionment studies based on filter data (Tauler et al., 2009; Jang et al., 2013). When the mass concentrations were below the detection limit, concentrations C_x were replaced by $DL_x/2$ and the uncertainties calculated by Equation 1:

$$S_x = 0.2 \times C_x + LD/3 \quad \text{(Eq. 1)}$$

If the concentrations were above the detection limit, Equation 2 was used:

$$S_x = 0.1 \times C_x + LD/3 \quad \text{(Eq. 2)}$$

New unconstrained runs of the PMF model using the combined dataset of OM plus HCl+ signal for IOP-1 led to the almost complete (95%) attribution of the m/z 36 signal to the Local Combustion OA (LCOA), where it represented 40% of the total factor mass. Besides, in order to refine the solutions, and due to the possible specificity of local emissions, the PMF model was run with constraints on the primary factor profiles, that is to say LCOA obtained from the IOP-1 solution, and COA and HOA from the sea breeze solution, using the a-value approach with 10% freedom (a = 0.1).

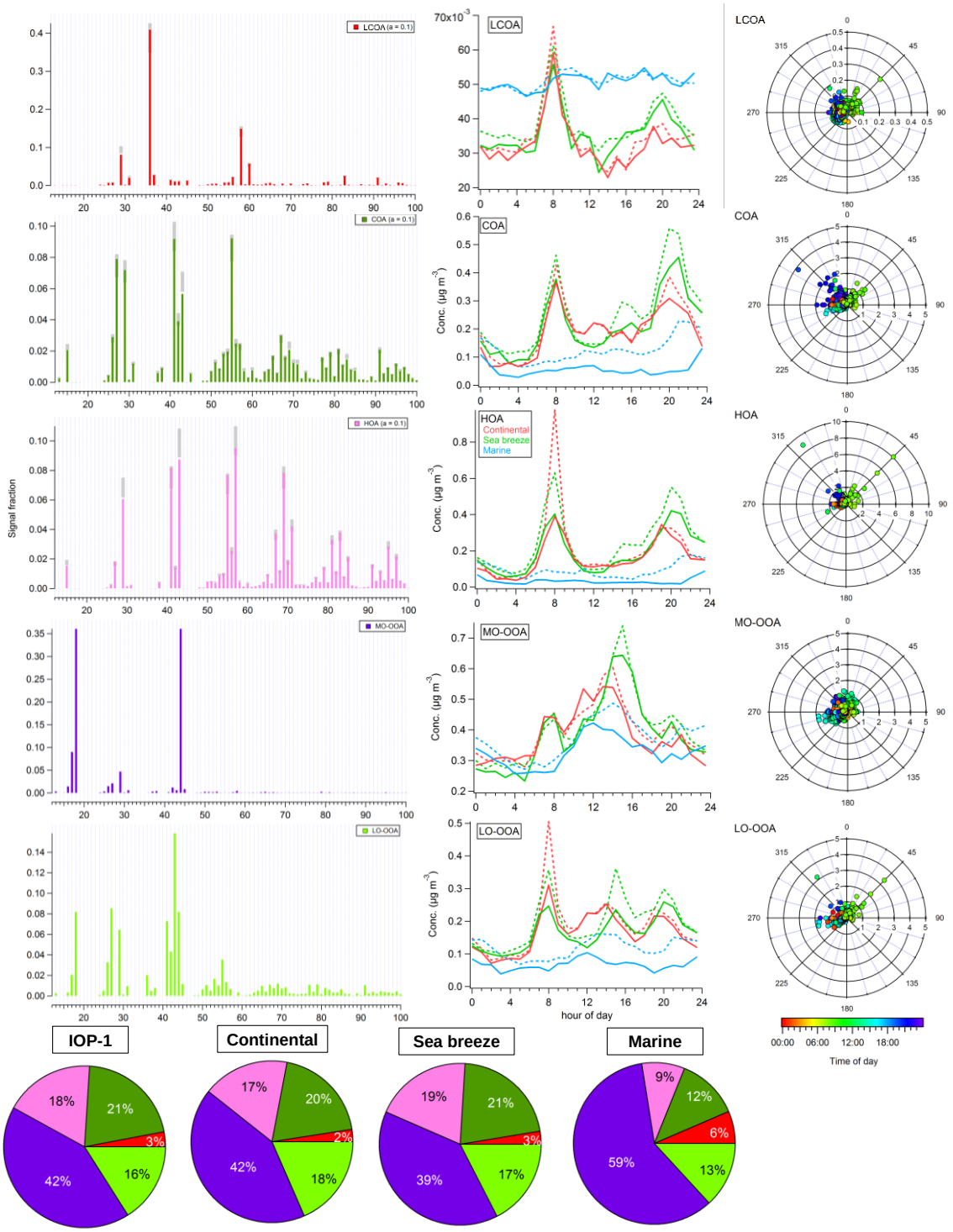

Figure~~.~~ ~~S6~~S8. PMF constrained 5-factor solution including the m/z 36 chloride peak: (left) factor profiles of LCOA, COA, HOA (all primary factors constrained), MO-OOA, LO-OOA; (middle) corresponding daily cycles according to day types (solid lines: median; dotted lines: average); and (right) pollution rose plots colored by hour of day. (bottom) Average pie charts of the contributions to the total organic fraction for IOP-1, continental, sea breeze and marine days

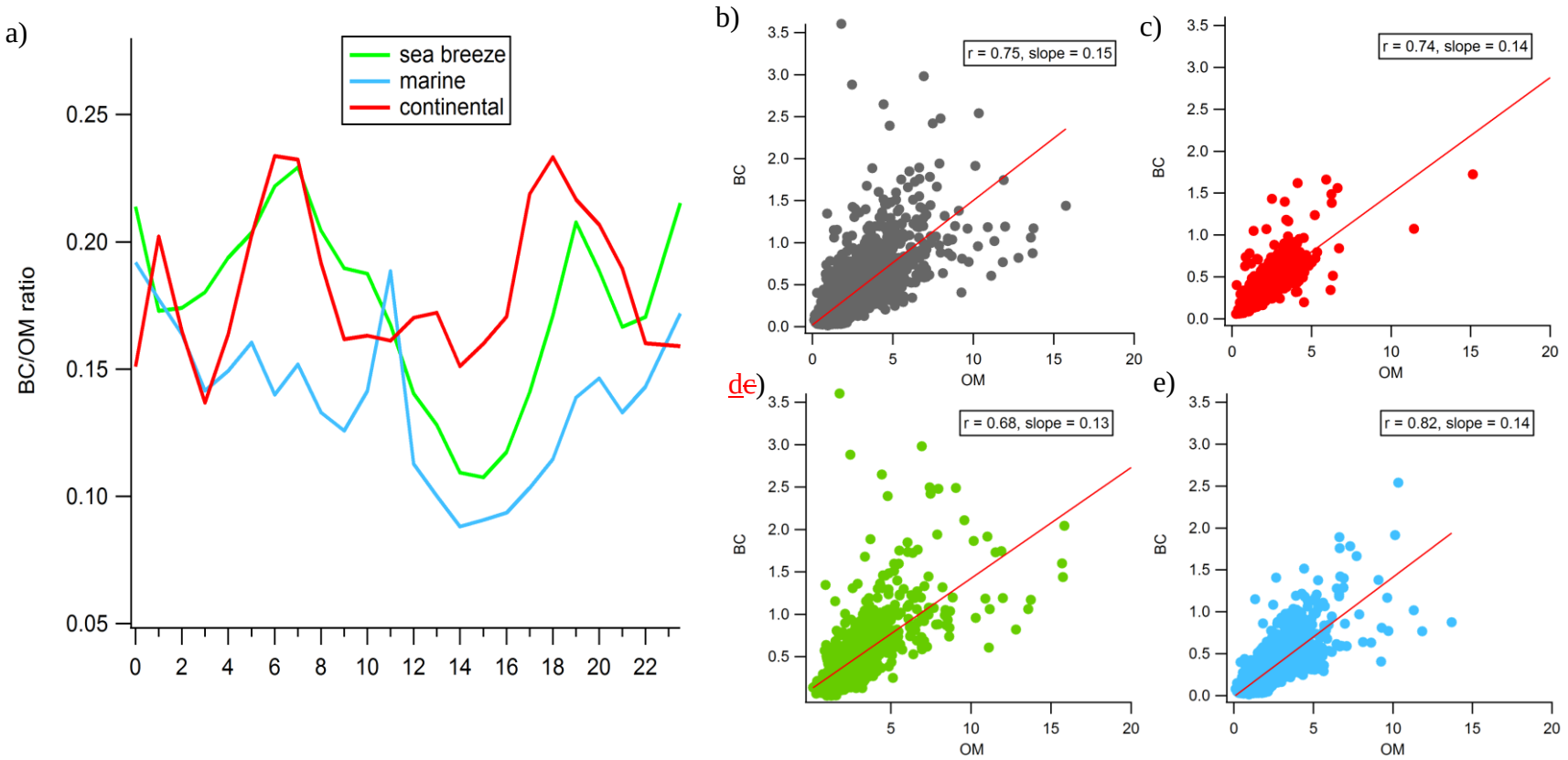

Fig. ~~S7~~S9. (a) Diurnal average profile of BC/OM ratio for continental, sea breeze and marine days and scatter plot of BC vs OM concentrations (in µg m^{-3}) for (b) IOP-1, (c) continental, (d) sea breeze and (e) marine days.

References:

Caponi, L., Formenti, P., Massabó, D., Di Biagio, C., Cazaunau, M., Pangui, E., Chevaillier, S., Landrot, G., Andreae, M. O., Kandler, K., Piketh, S., Saeed, T., Seibert, D., Williams, E., Balkanski, Y., Prati, P. and Doussin, J.-F.: Spectral- and size-resolved mass absorption efficiency of mineral dust aerosols in the shortwave: a simulation chamber study, Atmos Chem Phys Discuss, 2017, 1–39, doi:10.5194/acp-2017-5, 2017.

Fialho, P., Freitas, M. C., Barata, F., Vieira, B., Hansen, A. D. A. and Honrath, R. E.: The Aethalometer calibration and determination of iron concentration in dust aerosols, J. Aerosol Sci., 37(11), 1497–1506, doi:10.1016/j.jaerosci.2006.03.002, 2006.

Formenti, P., Rajot, J. L., Desboeufs, K., Caquineau, S., Chevaillier, S., Nava, S., Gaudichet, A., Journet, E., Triquet, S., Alfaro, S., Chiari, M., Haywood, J., Coe, H. and Highwood, E.: Regional variability of the composition of mineral dust from western Africa: Results from the AMMA SOP0/DABEX and DODO field campaigns, J. Geophys. Res. Atmospheres, 113(D23), D00C13, doi:10.1029/2008JD009903, 2008.

Hansen, A. D. A.: Aethalometer Operations Manual, Magee scientifique, Berkeley, CA, USA., 2005.

Joshi, N., Romanias, M., Riffault, V. and Thévenet, F.: Investigating water adsorption on natural mineral dust particles: A DRIFT and BET theory study, submitted to Aeolian Research, 2017.

Journet, E., Balkanski, Y. and Harrison, S. P.: A new data set of soil mineralogy for dust-cycle modeling, Atmos Chem Phys, 14(8), 3801–3816, doi:10.5194/acp-14-3801-2014, 2014.

Kandler, K., SchÜTz, L., Deutscher, C., Ebert, M., Hofmann, H., JÄCkel, S., Jaenicke, R., Knippertz, P., Lieke, K., Massling, A., Petzold, A., Schladitz, A., Weinzierl, B., Wiedensohler, A., Zorn, S. and Weinbruch, S.: Size distribution, mass concentration, chemical and mineralogical composition and derived optical parameters of the boundary layer aerosol at Tinfou, Morocco, during SAMUM 2006, Tellus B, 61(1), 32–50, doi:10.1111/j.1600-0889.2008.00385.x, 2009.

Lafon, S., Rajot, J.-L., Alfaro, S. C. and Gaudichet, A.: Quantification of iron oxides in desert aerosol, Atmos. Environ., 38(8), 1211–1218, doi:10.1016/j.atmosenv.2003.11.006, 2004.

Lafon, S., Sokolik, I. N., Rajot, J. L., Caquineau, S. and Gaudichet, A.: Characterization of iron oxides in mineral dust aerosols: Implications for light absorption, J. Geophys. Res. Atmospheres, 111(D21), D21207, doi:10.1029/2005JD007016, 2006.

Linke, C., Möhler, O., Veres, A., Mohácsi, Á., Bozóki, Z., Szabó, G. and Schnaiter, M.: Optical properties and mineralogical composition of different Saharan mineral dust samples: a laboratory study, Atmos Chem Phys, 6(11), 3315–3323, doi:10.5194/acp-6-3315-2006, 2006.

Moreno, T., Querol, X., Castillo, S., Alastuey, A., Cuevas, E., Herrmann, L., Mounkaila, M., Elvira, J. and Gibbons, W.: Geochemical variations in aeolian mineral particles from the Sahara–Sahel Dust Corridor, Chemosphere, 65(2), 261–270, doi:10.1016/j.chemosphere.2006.02.052, 2006.

Müller, T., Schladitz, A., Massling, A., Kaaden, N., Kandler, K. and Wiedensohler, A.: Spectral absorption coefficients and imaginary parts of refractive indices of Saharan dust during SAMUM-1, Tellus B, 61(1), 79–95, doi:10.1111/j.1600-0889.2008.00399.x, 2009.

Petzold, A., Rasp, K., Weinzierl, B., Esselborn, M., Hamburger, T., Dörnbrack, A., Kandler, K., Schütz, L., Knippertz, P., Fiebig, M. and Virkkula, A.: Saharan dust absorption and refractive index from aircraft-based observations during SAMUM 2006, Tellus B, 61(1), 118–130, doi:10.1111/j.1600-0889.2008.00383.x, 2009.

Schladitz, A., Müller, T., Kaaden, N., Massling, A., Kandler, K., Ebert, M., Weinbruch, S., Deutscher, C. and Wiedensohler, A.: In situ measurements of optical properties at Tinfou (Morocco) during the Saharan Mineral Dust Experiment SAMUM 2006, Tellus B, 61(1), 64–78, doi:10.1111/j.1600-0889.2008.00397.x, 2009.

Val, S., Liousse, C., Doumbia, E. H. T., Galy-Lacaux, C., Cachier, H., Marchand, N., Badel, A., Gardrat, E., Sylvestre, A. and Baeza-Squiban, A.: Physico-chemical characterization of African urban aerosols (Bamako in Mali and Dakar in Senegal) and their toxic effects in human bronchial epithelial cells: description of a worrying situation, Part Fibre Toxicol, 10(10), 2013.

Zotter, P., Herich, H., Gysel, M., El-Haddad, I., Zhang, Y., Močnik, G., Hüglin, C., Baltensperger, U., Szidat, S. and Prévôt, A. S. H.: Evaluation of the absorption Ångström exponents for traffic and wood burning in the Aethalometer-based source apportionment using radiocarbon measurements of ambient aerosol, Atmos Chem Phys, 17(6), 4229–4249, doi:10.5194/acp-17-4229-2017, 2017.